Functional and structural characterization of cytoplasmic poly(A) binding protein

Jingwei Xie
Department of Biochemsitry
McGill University, Montreal

April 2016

A thesis submitted to McGill University in partial fulfillment of the requirements of the degree of Doctor of Philosophy

Table of Contents

Table of Figures and Tables

Abstract

Cytoplasmic poly(A) binding protein (PABP) binds the 3' poly(A) tail of mRNA and plays an important role in translation of genetic information. Here, I review our knowledge of PABP with a focus on the C-terminal MLLE domain, and present the results of functional and structural studies of PABP. I elucidated the interactions between PABP and its binding partner Paip2. These interactions could regulate PABP and potentially affect PABP dissociation from mRNA. I found a link between PABP and formation of P-bodies, which suggests that PABP is important in mRNA decay and remodeling of mRNA-protein complexes. I also identified a new PAM2 motif in RNA-related LARP4. Structural characterization revealed a conserved pattern of residues in the PAM2 motif and enabled us to look for additional PAM2-containing proteins. Finally, I report a study of PABP isoform specific functions. The study utilized new genome editing technology and RNA-seq analysis to detect transcriptome changes that correlate with PABP isoform usage. In all, the thesis presents multidisciplinary studies of PABP function and structure.

Résumé

La protéine *poly(A) binding protein* (PABP) se lie à la queue poly(A) à l'extrêmité 3' et joue un rôle important dans la traduction de l'information génétique. Ici, je passe en revue notre connaissance de PABP en mettant l'accent sur le domaine C-terminal, appelé MLLE, et présente des études fonctionnelles et structurelles de PABP. J'élucidé les interactions entre PABP et son partenaire de liaison Paip2. Cette interaction pourrait contrôler PABP et affecter la dissociation du PABP de l'ARNm. J'ai trouvé un lien entre PABP et la formation de P-bodies. Cela suggère que PABP était important dans la dégradation des ARNm et le remodelage des complexes ARNm en protéines. J'également identifié un nouveau motif de PAM2 dans LARP4. La caractérisation structurale a raffiné la définition des acides aminés dans le motif PAM2. Cela nous a permis de chercher d'autres protéines contenant un motif PAM2. Enfin, j'ai étudié les fonctions spécifiques d'isofomes de PABP. L'étude a intégré des nouvelles technologies d'édition du génome et d'analyse de l'ARN-Seq pour détecter des changements du transcriptome dus á l'utilisation d'isoformes de PABP. En tout, la thèse rapporte des études multi-disciplinaires des fonctions et structures de la protéine PABP.

Acknowledgements

I'm grateful to Dr. Kalle Gehring for giving me opportunity to learn and explore science in his lab. I appreciate his patience and support all the way.

I am grateful for the advice and comments from members of my research advisory committee: Drs. Paul Lasko, Jerry Pelletier, Thomas Duchaine, and John Silvius. Their insights and discussions are invaluable.

Dr. Guennadi Kozlov worked with PABP for many years before me. He introduced me to X-ray crystallography and showed me the bread-and-butter of lab work. I appreciate his sharing of expertise in structural studies. Dr. Kozlov also read my manuscripts and provided me with valuable comments for improvement. Dr. Marie Menade made research possible by ensuring the logistics of materials. Her sharing of expertise in science and willingness to discuss facilitated the progress of all the research in the lab including mine.

Xiaoyu Wei and Yu Chen assisted me as undergraduates on work in the first two research chapters. A lot of Yu and Xiaoyu's work on the crystallization of PABP is not shown in this thesis. I was impressed by the problem solving skills and independence that they obtained during the work. Without them, I would not have had time to do many other experiments and analysis.

I thank Drs. Olivia Rissland and Beth Nicholson at SickKids Hospital and the University of Toronto for help with iCLIP experiment. I stayed in Toronto for a week, and Dr. Olivia Rissland spent most of the week working with me. I appreciate her patience and helpfulness.

Last but not least, I'm grateful to the company of my wife Danqi, and our boys, Anye and Anchu, through these years. This thesis won't exist without their support.

Contribution of Authors

I conceived, designed and carried out experiments of Chapter 2 (PABPC1 and Paip2), Chapter 3 (PABPC1 and P-bodies), and Chapter 5 (PABPC1, PABPC4 isoforms). Xiaoyu Wei and Yu Chen assisted me with some western blottings and protein purifications. Dr. Guennadi Kozlov did the NMR analysis of PABPC1's interaction with Paip2. Dr. Kozlov also designed the sequence of the super-PAM2 peptide. I went on to characterize it and use it in different scenarios.

Chapter 4 (LARP4) is a collaborative work with Dr. Richard Maraia's group at NIH. I identified the PAM2 motif in LARP4, and characterized its interaction with MLLE domain of PABPC1 by X-ray, NMR and ITC shown in Fig. 4.5 and Table 4.3. This work was published as (Yang et al., 2011).

I did all of the work presented in Chapter 5, except the library preparation for total RNA and sequencing. I conducted the analysis of mapped reads provided by the Genome Quebec Innovation Centre.

The above elements of the thesis are original scholarship and distinct contributions to knowledge.

Chapter 1. Introduction

1.1 Cytoplasmic poly(A) binding protein

Cytoplasmic poly(A) binding protein (PABP) has been known for four decades as a key component of the translational machinery (Blobel, 1973). PABP circularizes the mRNA and stimulates its translation into protein (Fig. 1.1) (Sonenberg and Hinnebusch, 2009, Kahvejian et al., 2005). PABP plays a direct role in 60S subunit joining and is integral to the formation of the translation initiation complex on the mRNA (Kahvejian et al., 2005).

Most structural and functional studies of PABP are based on PABPC1, the most abundant of several isoforms (Fig. 1.2) found in vertebrates. PABPC1 consists of four RNA-binding domains (RRM1-4) followed by a linker region and a conserved C-terminal MLLE domain (Fig. 1.1). The RRM domains mediate the circularization of mRNA through the binding of the 3’ poly(A) tail and eIF4F complex on the mRNA 5' cap (Safaee et al., 2012, Kahvejian et al., 2005, Deo et al., 1999, Imataka et al., 1998). The linker region appears to promote the self-association of PABPC1 on mRNA although the molecular details of the interaction are unknown (Melo et al., 2003, Simon and Seraphin, 2007). The C-terminal MLLE domain mediates binding of a peptide motif, PAM2, found in many PABP-binding proteins.

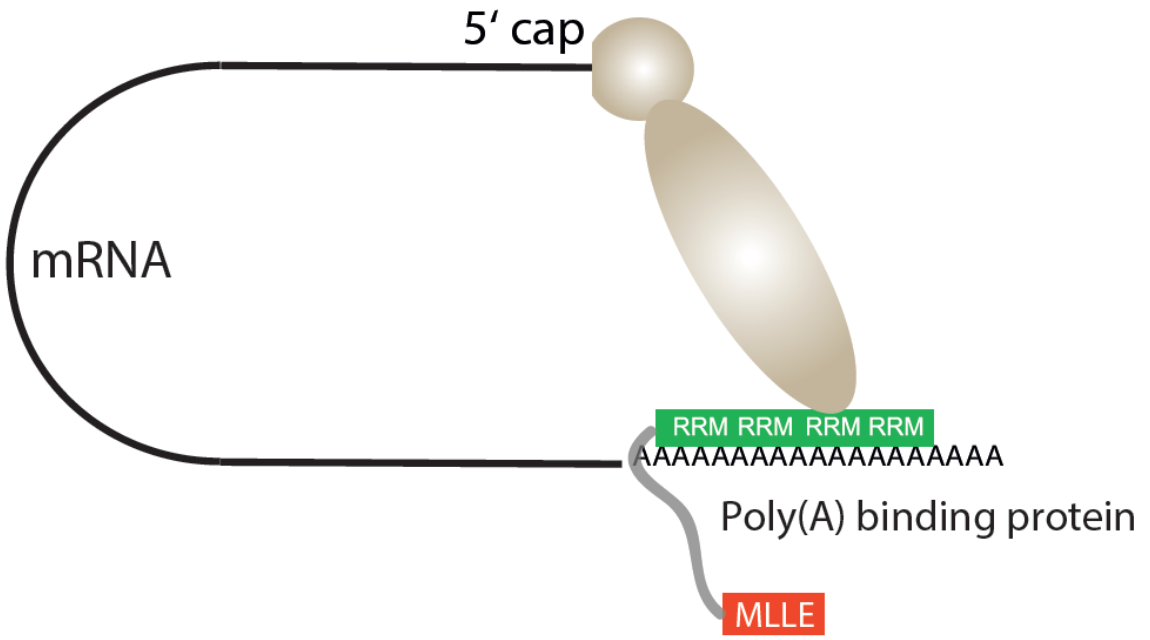

Figure 1.1 Cytoplasmic poly(A) binding protein and mRNA. PABPC1 consists of four RNA-binding domains (RRM1-4) followed by a linker region and a conserved C-terminal MLLE domain. The RRM domains mediate the circularization of mRNA through the binding of the 3’ poly(A) tail and eIF4F complex on the mRNA 5' cap. The C-terminus of all cytosolic PABPs contains a MLLE domain.

Five other less abundant cytoplasmic PABPs exist in higher vertebrates (Fig. 1.2). PABP isoforms are suggested to be functionally different in vertebrate development (Gorgoni et al., 2011). PABPC3 (tPABP or PABPC2 in mouse) is testis-specific (Kleene et al., 1998). PABPC4 (iPABP) is inducible in activated T cells (Yang et al., 1995) and serves a critical role in erythroid differentiation (Kini et al., 2014). PABPC1L (ePABP) functions in oocytes and early embryos (Seli et al., 2005, Guzeloglu-Kayisli et al., 2008, Voeltz et al., 2001). PABPC1L is substituted by PABPC1 later in development, but remains expressed in ovaries and testes of adult (Vasudevan et al., 2006). PABPC4L and PABPC5 (Blanco et al., 2001) lack the linker and MLLE region.

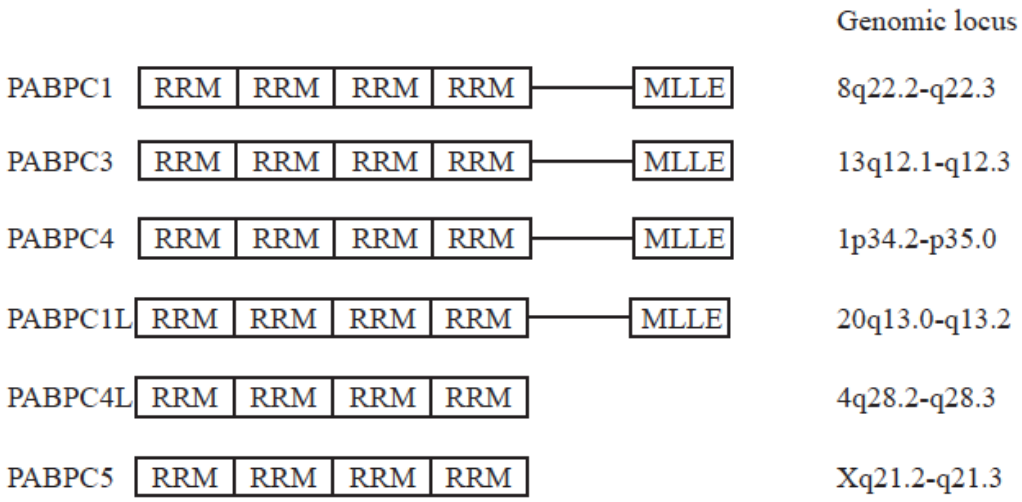

Figure 1.2 Isoforms of cytoplasmic poly(A) binding proteins in human. The genomic loci are shown on right for each of the isoforms.

1.2 PABPC1 and PABP-interacting protein 2 (Paip2)

PAM2-containing proteins, including PABP-interacting protein 2 (Paip2), can regulate translation and other mRNA related processes. Paip2 was identified based on its interaction with PABPC1 (Khaleghpour et al., 2001b). Paip2 inhibits translation *in vitro* through preventing PABPC1 from binding poly(A) RNA and destabilizing the closed mRNA loop (Khaleghpour et al., 2001a, Karim et al., 2006). By suppressing PABPC1, Paip2 contributes to control of synaptic plasticity and memory (Khoutorsky et al., 2013), spermatogenesis (Yanagiya et al., 2010), and serves as innate defense to restrict viral protein synthesis to counter the virus-induced increase in PABPC1 (McKinney et al., 2013).

Paip2 interacts with PABPC1 through two motifs: PAM1 and PAM2 (Fig. 1.3). PAM1 binds to the RRM domains of PABPC1, and is characterized by the presence of a large number of negatively charged residues (Khaleghpour et al., 2001a). The binding of PAM1 changes the conformation of PABPC1 and excludes poly(A) RNA binding (Lee et al., 2014). Interactions between Paip2 PAM2 and PABPC1 MLLE domain are well

characterized (Xie et al., 2014, Kozlov et al., 2004, Kozlov et al., 2010a). The PAM2 has a highly conserved pattern and a phenylalanine residue is critical for PAM2/MLLE interaction (Kozlov et al., 2004). Though the PAM1/RRM and PAM2/MLLE interactions are both observed *in vitro*, it is not clear how the two interaction sites of Paip2/PABPC1 work together in cells.

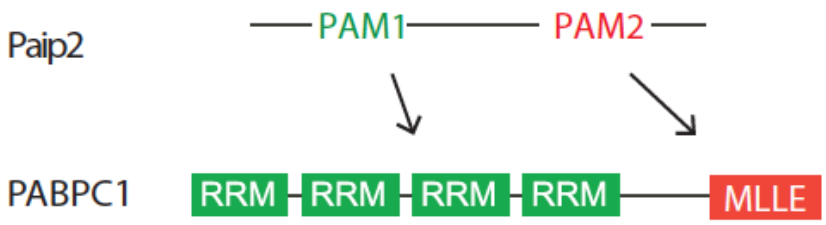

Figure 1.3 Dual interactions between Paip2 and PABPC1. Paip2 contains PAM1 and PAM2 motifs, which respectively bind the RRM domains and MLLE domain of PABPC1.

1.3 PABPC1 and RNA granules

Cytoplasmic messenger ribonucleoproteins (mRNPs) are suggested to cycle among polysomes, stress granules (SGs) and P-bodies (PBs) (Fig. 1.4). In this cycle, mRNAs exist in different functional states: translating, non-translating, and undergoing degradation. Polysomes consist of translating mRNAs and SGs of paused mRNAs with translation initiation components; PBs contain mRNA decay machineries (Decker and Parker, 2012).

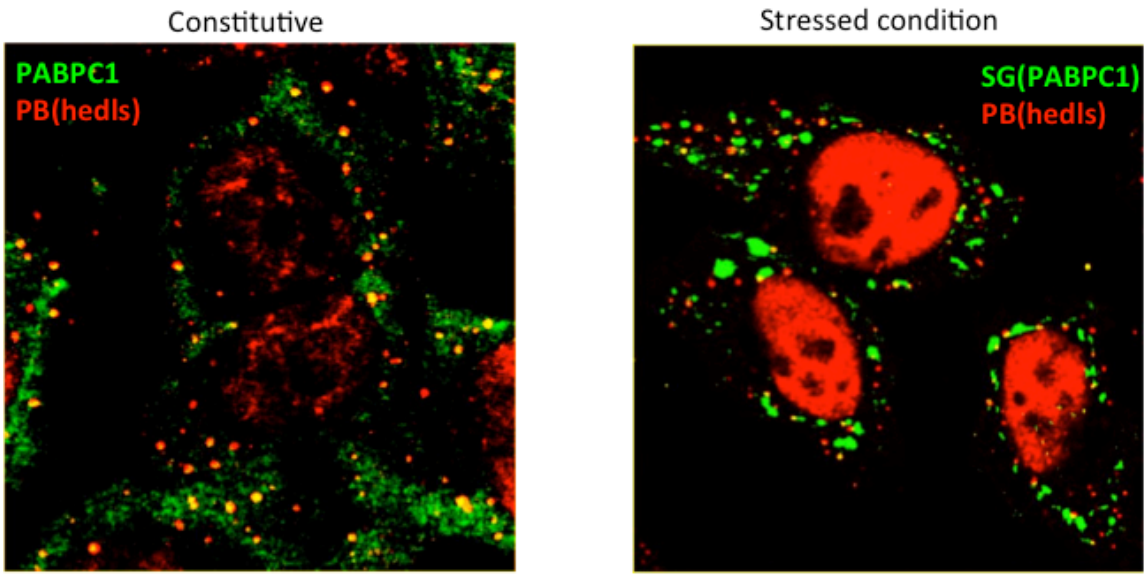

Figure 1.4 P-bodies and stress granules in HeLa cells. (Left) PBs, stained by anti-hedls, are present constitutively in HeLa cells. (Right) Separate SGs and PBs coexist in HeLa cells treated by Sodium Arsenite at 0.5 mM for 30 minutes. SGs were labeled by anti-PABPC1 antibody.

PBs are present constitutively in unstressed cells, and further induced upon inhibition of translation initiation (Teixeira et al., 2005, Kedersha et al., 2005). PBs are closely related to control of translation and mRNA degradation. Proteins present in PBs are involved in mRNA decay and translation repression and include the decapping enzyme complex Dcp1/Dcp2; the decapping activator hedls/GE-1; the translation repressor and decapping activator DDX6/RCK, and the CCR4/NOT deadenylase complex (Anderson and Kedersha, 2006, Eulalio et al., 2007a).

SGs can be juxtaposed with PBs in animal cells (Kedersha et al., 2005, Stoecklin and Kedersha, 2013), which suggests that they are close in origin. SGs share some common components with PBs, but distinctively contain translation initiation factors such as PABPC1, eIF4G, eIF4A, eIF3 and eIF2 etc. (Decker and Parker, 2012). The assembly of PBs and SGs is thought to start from non-translating mRNPs, which aggregate into microscopic granules through certain protein-protein interactions. In yeast, a self-interacting domain of the Edc3 protein and the prion-like glutamine/asparagine (Q/N)

rich region of Lsm4 can facilitate the aggregation (Reijns et al., 2008, Decker et al., 2007). However, in metazoans, Edc3 is not required for PB assembly (Eulalio et al., 2007b). Instead, depletion of GW182 or hedls/GE-1, two proteins containing low-complexity and Q/N rich regions, leads to decreased PBs in unstressed animal cells (Eulalio et al., 2007b, Liu et al., 2005a, Yu et al., 2005, Kato et al., 2012).

The absence of most translation initiation factors, including poly(A) binding protein cytoplasmic 1 (PABPC1), in PBs of mammalian cells, is intriguing. Components of RNA granules are in dynamic exchange with cytoplasmic proteins (Kedersha et al., 2005, Andrei et al., 2005). The association and dissociation of proteins, such as PABPC1, to and from the cap and tail of mRNA may be an important step in the transitions of mRNAs from translating to non-translating or decay states.

1.4 The MLLE domain and PAM2

The 70-residue MLLE domain was first identified as a peptide-motif binding domain in 2001 (Kozlov et al., 2001). The domain consists of a bundle of five a-helices and was named MLLE ("Mademoiselle") due to the presence of a conserved four amino acid sequence, MLLE, in the heart of the peptide recognition site (Fig. 1.5B). In the literature, the domain has also been referred to as PABC, C2, and H2. It is highly conserved and is present in all eukaryotic kingdoms (Fig. 1.5C) (Kuhn and Wahle, 2004, Mangus et al., 2003).

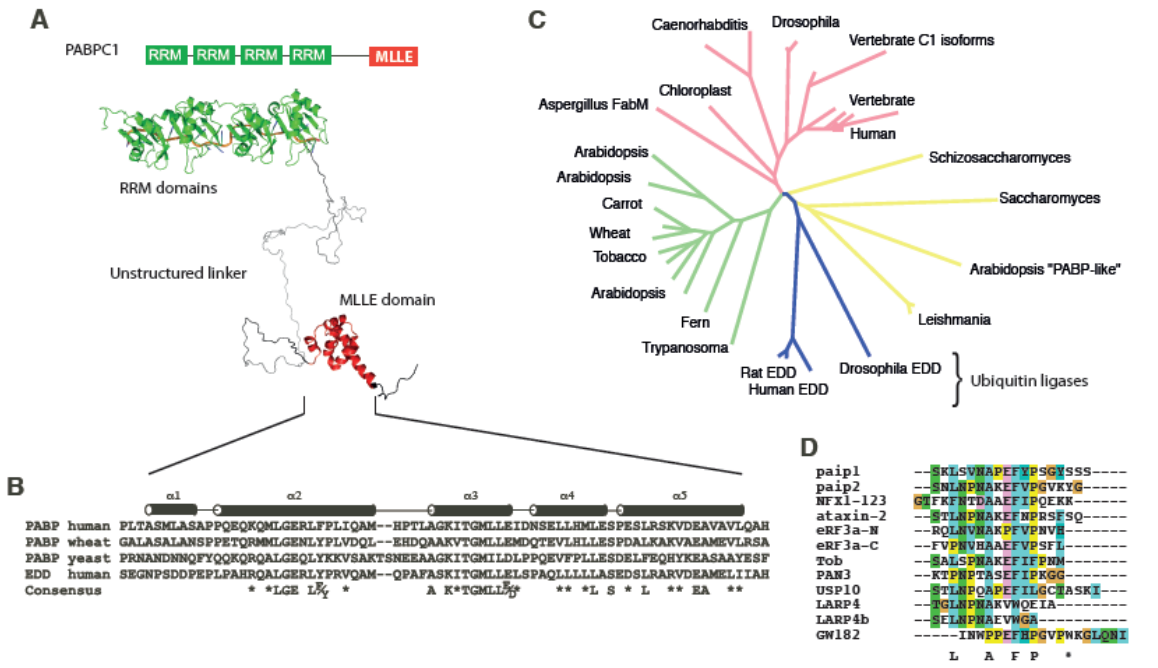

Figure 1.5 PABPC1, MLLE domain, and PAM2. (A) Domain structure and model of full-length PABPC1 based on structures of the first two RRM domains with polyA RNA, the fourth RRM domain and the MLLE domain (PDB ID: 1CVJ (Deo et al., 1999), 1G9L (Kozlov et al., 2001), 2D9P and 4F02 (Safaee et al., 2012)). (B) Sequence alignment of MLLE domains from human, wheat, and yeast PABPC1 and human EDD. The secondary structure and the helices are labeled according to the structure of human PABPC1. (C) Unrooted phylogenetic tree of MLLE domains showing the grouping of plant, vertebrate, and EDD sequences. Sequences labeled EDD are MLLE domains from HECT E3 ubiquitin ligases; all other sequences are poly(A)-binding proteins. The figure was generated with ClustalW (Thompson et al., 1994) and TreeViewPPC (Page, 1996). (D) Sequence of MLLE-binding PAM2s. The consensus of conserved residues that contribute to the MLLE-PAM2 interaction is shown. The asterisk labels a tryptophan in GW182 that interacts with MLLE.

The MLLE domain recognizes a conserved peptide sequence (L/P/F)X(P/V)XAXX(F/W)XP, which was named "PABP-interacting Motif 2" or PAM2 (Fig. 1.4D) (Roy et al., 2002, Kozlov et al., 2001). PAM2 sequences were first identified at the N- and C-termini of proteins that bind to PABPC1 (Kozlov et al., 2001);

subsequent studies confirmed their localization to unstructured regions of proteins (Albrecht and Lengauer, 2004, Huang et al., 2013). Evolutionally, the motif is well conserved across eukaryotes from humans to *S. pombe* (Albrecht and Lengauer, 2004). In *S. cerevisiae*, the motif may have diverged. While the yeast protein, Pab1p, contains a bonafide MLLE domain (Kozlov et al., 2002), no PAM2 motifs were found in Pab1p-interacting proteins identified in a yeast two-hybrid screen (Mangus et al., 1998) or by mass spectrometry (Richardson et al., 2012). Among the conserved residues, the two hydrophobic residues in the motif are the most critical (Fig. 1.4D). Mutation of either the leucine or the aromatic phenylalanine residues to alanine decreased the affinity binding by over 1000-fold (Kozlov et al., 2004).

1.5 PAM2-containing proteins (PACs)

Since their first identification, PAM2 motifs have been found in some twenty human proteins; the best studied are listed in Table 1.1 (Albrecht and Lengauer, 2004, Kozlov et al., 2001). The majority of studies have shown that PACs function in different mRNA-related processes by interacting with PABPC1 (Fig. 1.6).

Table 1. 1 List of PAM2-containing proteins (PACs)

Properties / **Protein**	Functions	Stress granule or P-body localization[a]	Affinity for PABPC1 (μM) [b]	Affinity for EDD (μM)
Paip1	Translation enhancement (Martineau et al., 2008b, Craig et al., 1998, Martineau et al., 2014)	-	1.4	3.4
Paip2	Translation inhibition (Yanagiya et al., 2010, Karim et al., 2006, Khaleghpour et al., 2001b, Khaleghpour et al., 2001a)	SG[c]	0.2	6
Ataxin-2	microRNA mediated gene silencing (McCann et al., 2011); neurodegenerative diseases (Elden et al., 2010, Lessing and Bonini, 2008, Kim et al., 2014); behavioral rhythm (Lim and Allada, 2013)	SG	0.7	10
eRF3	Deadenylation and mRNA decay (Osawa et al., 2012, Funakoshi et al., 2007, Hosoda et al., 2003)	-	1	5.2
GW182 proteins	Deadenylation (Braun et al., 2012); miRISC assembly (Moretti et al., 2012)	P-body	6	200[c]
Tob1/2	Deadenylation (Ezzeddine et al., 2012, Funakoshi et al., 2007, Ezzeddine et al., 2007)	P-body	16	12
PAN3	Deadenylation (Siddiqui et al., 2007)	P-body	40	No binding
LARP4	mRNA stability (Yang et al., 2011)	SG	22	-
NFX1	Increases mRNA level of telomerase catalytic subunit (Katzenellenbogen et al., 2007, Katzenellenbogen et al., 2010)	-	-	-
USP10	mRNA stability (Soncini et al., 2001)	SG	26	33
TTC3	Neurodegenerative Down syndrome (Tsukahara et al., 1998)	-	5.4	37

a. Based on data from human cells following heat shock or sodium arsenite treatment
b. For details of affinity studies, refer to (Kozlov et al., 2010b, Kozlov et al., 2010a, Lim et al., 2006, Kozlov et al., 2004, Yang et al., 2011, Siddiqui et al., 2007, Yoshida et al., 2006).
c. Unpublished data

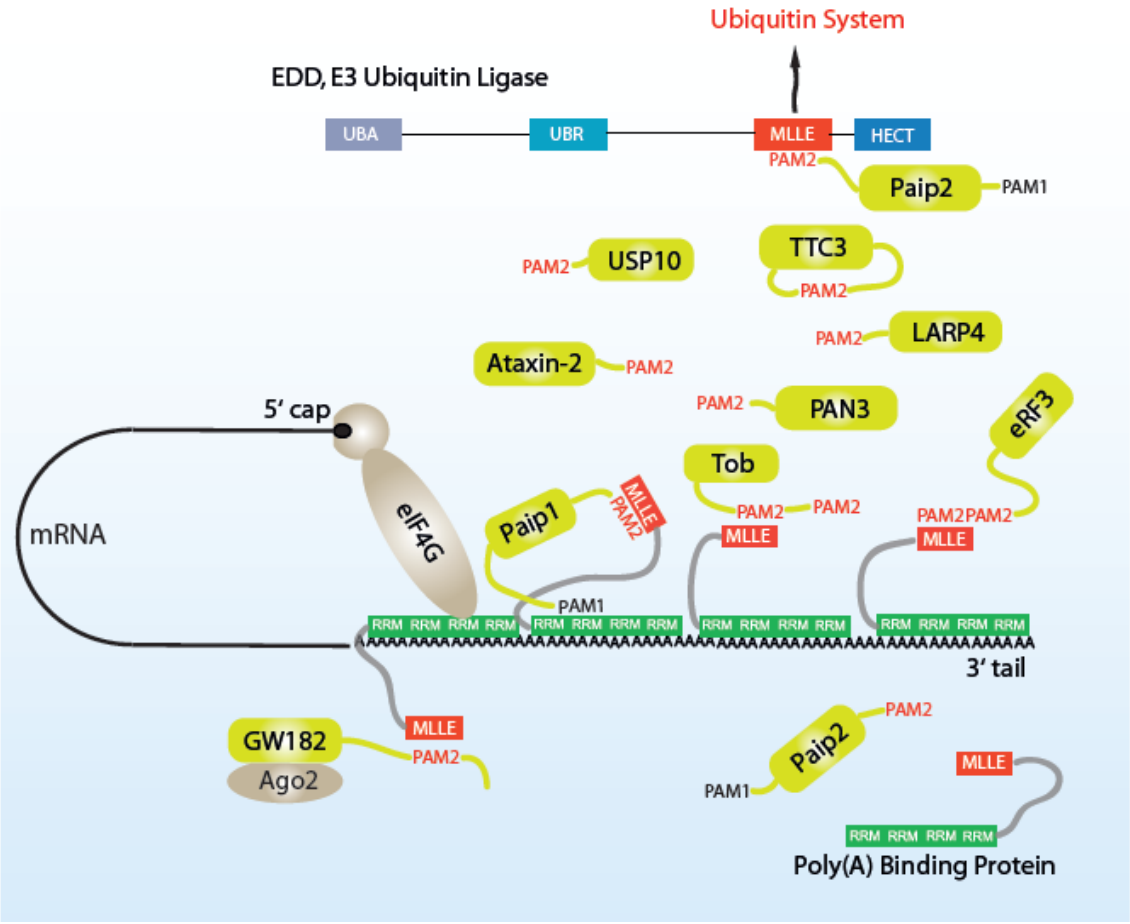

Figure 1.6 Network of interactions between MLLE domains and PACs. PACs interact with PABPC1 and EDD through the MLLE domain. PACs are illustrated in yellow-green. MLLE domain and PAM2 are highlighted red. More information about PAC functions, localizations, and binding affinities to MLLE is listed in Table 1.

1.5.1 PAN3, Tob1/2 and GW182 in mRNA decay

Deadenylation is an initial step for major mRNA decay pathways in higher eukaryotes. Several PACs regulate mRNA degradation via interactions with PABPC1. PAN3 is a PAC found in one of the two major cytoplasmic deadenylase complexes: PAN2-PAN3 and CCR4-NOT. The two complexes may function at different stages of deadenylation (Yamashita et al., 2005). PABPC1 directly recruits PAN2-PAN3 deadenylase complex to

mRNA through PAM2 of PAN3 (Siddiqui et al., 2007). The CCR4-NOT complex, however, can be brought to mRNA by multiple factors including PACs like Tob1, Tob2 and GW182. Tob1 and Tob2 are members of antiproliferative BTG family. They promote deadenylation by simultaneously binding PABPC1 and CAF1, a component of CCR4-NOT complex (Ezzeddine et al., 2012, Funakoshi et al., 2007, Ezzeddine et al., 2007).

GW182 family proteins (three paralogs in vertebrates: TNRC6A, TNRC6B and TNRC6C) are key components of miRISC (microRNA Induced Silencing Complex), which facilitates the cleavage of fully complementary targets or the translation repression and decay of partially complementary targets (Braun et al., 2012). The PAM2 of GW182 is critical for microRNA-mediated gene silencing in human and fly cells (Huntzinger et al., 2010), and also for deadenylation of mRNA *in vitro* (Fabian et al., 2009, Jinek et al., 2010, Kozlov et al., 2010b). Consistent with roles of PABPC1 in both translational repression and degradation of miRNA targets, the MLLE domain of PABPC1 serves to assemble miRISC complex by recruiting GW182 and bringing the deadenylase complexes close to mRNA (Moretti et al., 2012, Huntzinger et al., 2013). In this process, microRNA is loaded onto a complex of *Argonaute* proteins and the N-terminus of GW182 (Eulalio et al., 2008), while the C-terminus of GW182 recruits CCR4-NOT and PAN2-PAN3, the deadenylase complexes (Fabian et al., 2011, Chekulaeva et al., 2011, Braun et al., 2011). Meanwhile, GW182 proteins may promote the dissociation of PABPC1 from mRNA independent of deadenylation (Zekri et al., 2013), and thus facilitate deadenylation on exposed mRNA tails.

1.5.2 Ataxin-2 in neurodegeneration, microRNA silencing and behavioral rhythms

Ataxin-2 is attracting increasing attention in terms of its medical relevance and the recent discovery of a role in circadian rhythms. Ataxin-2 was one of the first PACs identified (Kozlov et al., 2001) and is associated with spinocerebellar ataxia type 2 (SCA2), a genetic neurodegenerative disease caused by an expansion of glutamine residues (34 or more) in the Ataxin-2 protein. The PAM2 of Ataxin-2 is critical for its toxicity in SCA2 and, the related disease, SCA3 (Lessing and Bonini, 2008). Ataxin-2 with intermediate-

length (27-33 residues) polyglutamine tracks was identified as the most common genetic risk factor for amyotrophic lateral sclerosis (ALS) (Van Damme et al., 2011, Lee et al., 2011). In ALS patients, an increase in Ataxin-2 (Elden et al., 2010) and PABPC1 (Kim et al., 2014) aggregates are observed in motor neurons. Such aggregates promoting degeneration may be related to endogenous stress granules (Ramaswami et al., 2013). Stress granules accumulate translationally silent mRNAs and are considered a cellular adaption to stress. PABPC1 is a component of stress granules, where it interacts with polyadenylated mRNAs. A recent study shows that PABPC1 modulates toxicity of TDP-43, a pathological protein associated with ALS, via its PAM-2 dependent association with Ataxin-2 (Kim et al., 2014). Encouragingly, pharmacological modulation of eIF2α phosphorylation, a stress granule-inducing factor, functionally affects TDP-43 toxicity (Kim et al., 2014). The mechanistic details of how higher-order mRNP structures affect neurodegeneration remain to be elucidated.

Many PACs are found associated with stress granules or P-bodies (Table 1.1). We could expect more PAM2-dependent roles of PACs in stress responses (Kim et al., 2014). High-affinity PAM2 can be fused to protein as stress granule deposition signal (unpublished data). This can be a useful tool in RNA granule studies.

Studies in fly show that Ataxin-2 is required for microRNA function and certain synapse-specific neuronal processes (McCann et al., 2011). Although molecular mechanisms of the action are not known, it is possible that Ataxin-2 functions to regulate gene expression by competing with deadenylation related PACs like GW182 and PAN3 etc. Additionally, Ataxin-2 may play part in translational control of certain genes. Two groups recently showed the association of Ataxin-2 and PABPC1 is critical for Ataxin-2's role in controlling behavioral rhythms and activating the rate-limiting clock protein PERIOD (Lim and Allada, 2013, Zhang et al., 2013).

1.5.3 Paip1, Paip2 and translation regulation

PABP-interacting protein 1 and 2 (Paip1 and Paip2) were identified based on their ability to bind to PABPC1 (Craig et al., 1998, Khaleghpour et al., 2001b). They have opposite

effects on translational activity: Paip1 enhances translation (Craig et al., 1998) while Paip2 inhibits translation (Khaleghpour et al., 2001b). In addition to PAM2 motifs, both Paip1 and Paip2 contain a second PABPC1-binding motif. This motif, PAM1, binds to the RRM domains of PABPC1, and is characterized by the presence of a large number of negatively charged residues. Paip2 is present in two isoforms: Paip2a and, a much less abundant form, Paip2b (Berlanga et al., 2006). The PABPC1-binding sites of Paip2a and Paip2b are conserved and the proteins are thought to act similarly to inhibit PABPC1 function. Paip2a inhibits translation through preventing PABPC1 from binding poly(A) RNA and destabilization of the circularization of the mRNA (Khaleghpour et al., 2001a, Karim et al., 2006). By suppressing PABPC1, Paip2a contributes to control of synaptic plasticity and memory (Khoutorsky et al., 2013), spermatogenesis in mice (Yanagiya et al., 2010), and serves as innate defense to restrict viral protein synthesis to counter virus-induced PABPC1 increase (McKinney et al., 2013). The mechanism underlying these effects is not known but one hypothesis is that Paip2a acts as a chaperone of PABPC1 by interacting with its RNA and PAM2-binding sites to alter PABPC1 specificity or promote other protein-protein associations. Still less is understood about how the PAM1 and PAM2 motifs of Paip1 stimulate translation (Roy et al., 2002, Martineau et al., 2008b, Martineau et al., 2014).

1.5.4 eRF3 and interplay with deadenylase complexes

eRF3 (eukaryotic Release Factor 3) binds MLLE domain with two overlapping PAM2 (Kozlov and Gehring, 2010). GTP hydrolysis by eRF3 facilitates nascent peptide release via coupling codon recognition with peptidyl-tRNA hydrolysis by eRF1(Taylor et al., 2012). PAM2 is important for eRF3 in translation termination-coupled deadenylation and mRNA decay, through competition with other PACs including PAN3, Tob1, Tob2 and GW182 (Osawa et al., 2012, Funakoshi et al., 2007, Hosoda et al., 2003).

1.5.5 LARP4, LARP4b and mRNA stability

La-related proteins (LARP) contain RNA-binding La motif and RRM domain and function in mRNA-related processes (Bayfield et al., 2010b). LARP4 and LARP4b, new members of PACs, use a variant PAM2 to bind PABPC1, and may help to maintain mRNA stability (Yang et al., 2011). It is suggested that during duplication in evolution, vertebrate LARP4 acquired PAM2 together with significantly remodeling of its RNA-binding module for neofunctionalization (Merret et al., 2013).

1.5.6 USP10, TTC3 and ubiquitin system

The ubiquitin hydrolase USP10 interacts with a stress granule protein G3BP (Ras-GTPase-activating protein SH3 domain-binding protein) and regulates mRNA stability (Gallouzi et al., 1998, Soncini et al., 2001, Tourriere et al., 2003, Kedersha et al., 2005). It remains to be seen to what extent ubiquitination is involved in mRNA-related processes and whether PAM2 of USP10 plays a specific role in those (Rybak et al., 2009, Gibbings et al., 2009, Lee et al., 2009).

Also, TTC3**,** an E3 ubiquitin ligase involved in the neurodegenerative Down syndrome (Tsukahara et al., 1998), contains a PAM2 motif. However, how TTC3's interaction with PABPC1 affects its function remains to be investigated.

1.6 Recognition of MLLE/PAM2

The molecular basis for the interaction between PACs and MLLE domains is highly conserved. High-resolution crystal structures of MLLE in complex with PAM2 peptides from Paip2a (Kozlov et al., 2010a), GW182 (Jinek et al., 2010, Kozlov et al., 2010b), Ataxin-2 (Kozlov et al., 2010b), eRF3 (Kozlov and Gehring, 2010) and LARP4 (Yang et al., 2011) provide a detailed picture of the hydrophobic interactions that are responsible for binding. MLLE does not undergo any significant conformational changes upon PAM2 binding, indicating that the binding site is fully preformed for PAM2 recognition (Kozlov et al., 2010a).

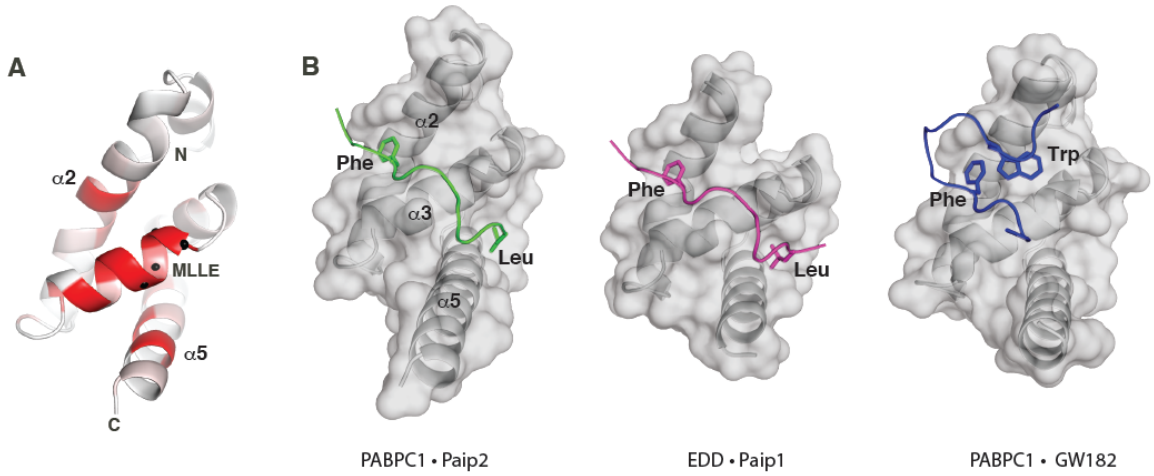

Figure 1.7 Structural basis of the MLLE/PAM2 interaction. (A) Schematic representation of the PABPC1 MLLE domain showing the conservation of residues that compose the PAM2 binding site (PDB ID: 3KUR). The most conserved residues, which includes the MLLE sequence in helix 3, are colored red (Kozlov et al., 2010a). (B) Comparison of three different MLLE-PAM2 complexes. In the complex of the MLLE domain from PABPC1 (PDB ID: 3KUS) and the PAM2 motif from Paip2a, the peptide motif wraps around helix α3 with key phenylalanine and leucine residues binding to pockets formed by helices a2 and a5. The PAM2 of Paip1 binds to the EDD MLLE domain in a similar fashion (PDB ID: 3NTW). In contrast, the PAM2 peptide from GW182 binds to the PABPC1 MLLE as a hairpin-like structure with a key tryptophan residue that inserts between helices a2 and a3 (PDB ID: 3KTP).

PAM2 motifs bind to MLLE by engaging two hydrophobic pockets located around a central helix (Fig. 1.7B). The two pockets provide the most important binding interactions and recognize the conserved leucine and phenylalanine residues in the PAM2 motif. The phenylalanine is found in all PACs except for LARP4/4b (Yang et al., 2011). In LARP4/4b, the phenylalanine is replaced by a tryptophan, whose aromatic side-chain reaches into the hydrophobic pocket. Our unpublished data show that this aromatic residue can also be substituted by a tyrosine.

To link the pockets, the PAM2 peptide runs over the central helix α3 through a gap in the conserved KITGMLLE sequence provided by the central glycine residue (Fig. 1.7B). This is matched by an invariant alanine residue in the PAM2 motif that contacts the glycine. This mode of peptide binding is conserved for the MLLE domains of PABPC1 and EDD and all PAM2 motifs with one exception.

GW182 contains an atypical PAM2 and binds the PABPC1 MLLE domain in a unique manner (Kozlov et al., 2010b, Jinek et al., 2010). While the conserved phenylalanine residue of the GW182 PAM2 makes typical contacts with the MLLE domain, the leucine residue present at the N-terminus of the PAM2 motif is absent. Instead, GW182 contains an extension of the C-terminus of its PAM2 motif that mediates additional contacts. Following the phenylalanine residue, the peptide from GW182 flips back to form a hairpin-like structure (Fig. 1.7B, right most panel). The tryptophan residue (W1395) at the C-terminus of GW182 PAM2 promotes binding by interacting with helices α2 and α3 in MLLE. This tryptophan-binding pocket may play a role in modulating the binding affinity of other PACs such as Paip2a which contains a tyrosine residue at the same position as the GW182 tryptophan. Truncating the tyrosine and surrounding residues decreased the affinity of a Paip2a PAM2 peptide by 18-fold (Kozlov et al., 2004).

The relatively recent discovery of atypical PAM2 motifs in GW182 and LARP4 raises the question of whether MLLE domains could bind other motifs. The strong bias in sequence conservation across MLLE domains suggests that the PAM2-binding site is a conserved function of the domain (Fig. 1.7A). There is an almost perfect correspondence between conservation of surface-exposed residues and residues involved in PAM2 binding. While novel MLLE-binding peptide motifs could exist, it seems likely that they will contain elements of known PAM2 motifs. The highest affinity peptides recognize the hydrophobic pockets on MLLE with appropriate spacers; loss of any of the elements leads to a progressive decrease in affinity. The function of the orphan MLLE domain in Pab1p in *S. cerevisiae* remains a mystery. In higher eukaryotes, other MLLE-binding proteins may exist but they likely interact with lower affinity or as part of larger complexes.

The discovery of PACs has significantly broadened our view of the role of PABPC1-dependent protein interactions in the regulation of mRNA translation and metabolism. The MLLE domain provides a highly conserved platform for the recruitment of PACs to polyadenylated mRNA. While PACs are expected to compete with each other for binding to MLLE of PABPC1, the length of the polyA tail allows for the binding of multiple PABPC1 proteins and the recruitment of multiple PACs. It is not known if there are differences between PABPC1 proteins bound at the polyA tail or which PABPC1-PAC interactions dominate in different physiological conditions and cell types. There is evidence that MLLE/PAM2 interactions might be regulated by post-translational modifications of PABPC1 (Brook et al., 2012) or phosphorylation in vicinity of PAM2s (Huang et al., 2013). This additional complexity likely serves to finely tune the affinities and function of the MLLE/PAM2 network around the mRNA.

Rationale and objectives of the research

My thesis research involves multidisciplinary studies of cytoplasmic poly(A) binding protein. I am interested in the structure and function of the MLLE domain of PABPC1. The MLLE domain is so highly conserved, but the related functions are not quite understood.

Chapter 2 describes the interplay between PABPC1 and Paip2, specifically the involving the PAM2/MLLE interaction. Chapter 3 addresses the novel function of PABPC1 in P-body formation. The MLLE mediated interactions may be one of the links between PABPC1 and P-bodies. Chapter 4 presents a new PAM2 motif, identified in LARP4. Chapter 5 was developed from initial efforts to characterize MLLE related functions. The induction of a minor PABP isoform upon the loss of PABPC1 offered a rare opportunity to study PABP isoform specific functions.

Chapter 2: Paip2 associates with PABPC1 on mRNA, and may facilitate PABPC1 dissociation from mRNA upon deadenylation

Jingwei Xie[1], Xiaoyu Wei[1], Guennadi Kozlov[1], Yu Chen[1], Kalle Gehring[1, 2]

[1] Department of Biochemistry and Groupe de Recherche Axé sur la Structure des Protéines, McGill University, Montreal, Quebec H3G 0B1, Canada

[2] To whom correspondence should be addressed: Dept. of Biochemistry, McGill University, 3649 Promenade Sir William Osler, Rm. 473, Montreal, QC H3G 0B1, Canada. Tel.: 514-398-7287; Fax: 514-398-2983; E-mail: kalle.gehring@mcgill.ca.

KEYWORDS

PABPC1, Paip2, poly(A) RNA, PABPC1 dissociation

SHORT TITLE: Characterization of Paip2 and PABPC1 interaction

Abstract

Poly(A) binding protein cytoplasmic 1 (PABPC1) is an important translational initiation factor. PABPC1 recognizes proteins through conserved PABPC1-interacting motifs 1 and 2 (PAM1 and PAM2). PABPC1-interacting protein-2 (Paip2) interacts with PABPC1 and modulates its activities. Here, we report that the formation of Paip2/PABPC1 complex protects Paip2 and PABPC1 from proteasome independent degradation. We also show that PAM2 is critical for Paip2/PABPC1 interaction *in vivo*, in agreement with the observation that Paip2 requires PAM2 to interact with PABPC1 on mRNA. Lastly, we propose a role for Paip2 in displacing PABPC1 at the final stage of mRNA deadenylation when the poly(A) tail is partly degraded.

Introduction

Translation regulation is a critical step in gene expression control. Poly(A) binding protein cytoplasmic 1 (PABPC1) is an essential translation initiation factor and the most

abundant cytoplasmic PABP isoform. PABPC1 and eIF4 translation factors prepare mRNA for its recruitment to the translation pre-initiation complex (Sonenberg and Hinnebusch, 2009). PABPC1 consists of four RNA-binding domains (RRM1-4) followed by an unstructured linker region and a conserved MLLE domain. The RRM domains mediate the formation of a closed loop of mRNA through the binding of the 3' poly(A) tail and eIF4F complex on the mRNA 5' cap (Kahvejian et al., 2005, Deo et al., 1999, Imataka et al., 1998, Safaee et al., 2012). The C-terminal MLLE domain binds a peptide motif, termed PAM2 for PABPC1-interacting motif 2 (Xie et al., 2014).

PAM2-containing proteins, including PABPC1-interacting protein 2 (Paip2), can regulate translation and other mRNA related processes. Paip2 was identified based on its interaction with PABPC1 (Khaleghpour et al., 2001b). Paip2 inhibits translation *in vitro* through preventing PABPC1 from binding poly(A) RNA and destabilizing the closed mRNA loop (Khaleghpour et al., 2001a, Karim et al., 2006). By suppressing PABPC1, Paip2 contributes to control of synaptic plasticity and memory (Khoutorsky et al., 2013), spermatogenesis (Yanagiya et al., 2010), and serves as innate defense to restrict viral protein synthesis to counter the virus-induced increase in PABPC1 (McKinney et al., 2013).

Paip2 interacts with PABPC1 through two motifs: PAM1 and PAM2. PAM1 binds to the RRM domains of PABPC1, and is characterized by the presence of a large number of negatively charged residues (Khaleghpour et al., 2001a). The binding of PAM1 changes the conformation of PABPC1 and excludes poly(A) RNA binding (Lee et al., 2014). Interactions between Paip2 PAM2 and PABPC1 MLLE domain are well characterized (Xie et al., 2014, Kozlov et al., 2004, Kozlov et al., 2010a). The PAM2 has a highly conserved pattern and a phenylalanine residue is critical for PAM2/MLLE interaction (Kozlov et al., 2004). Though the PAM1/RRM and PAM2/MLLE interactions are both observed *in vitro*, it is not clear how the two interaction sites of Paip2/PABPC1 work together in cells.

Here, we report that the PAM2/MLLE interaction is required for Paip2/PABPC1 association *in vivo* and for maintaining Paip2 and PABPC1 stability. Furthermore, we find that Paip2 interacts with PABPC1 on mRNA through PAM2 and could function to displace PABPC1 after shortening of poly(A) tail by deadenylation.

Results

Overexpression of PAM2-GFP lowers Paip2 level

To block the Paip2/PABPC1 interaction at the PAM2/MLLE site, we overexpressed in HeLa cells a PAM2 motif of Paip2 (109-125) or a high affinity chimeric superPAM2 (sequence in Materials and Methods, affinity measured in Fig. S2.1). Cells expressing PAM2-GFP fusion proteins had decreased Paip2 protein levels compared with GFP controls (Fig. 2.1). This was unexpected, as the two PAM2 motifs also inhibit binding of Paip2 to EDD, a MLLE-containing protein that is involved in ubiquitination and degradation of Paip2 (Yoshida et al., 2006). It was observed but not understood that deletion of PAM2 destabilizes Paip2 due to loss of the interaction with EDD (Yoshida et al., 2006). Our results demonstrate that interaction of Paip2 with the MLLE domain of PABPC1 is important for Paip2 stability.

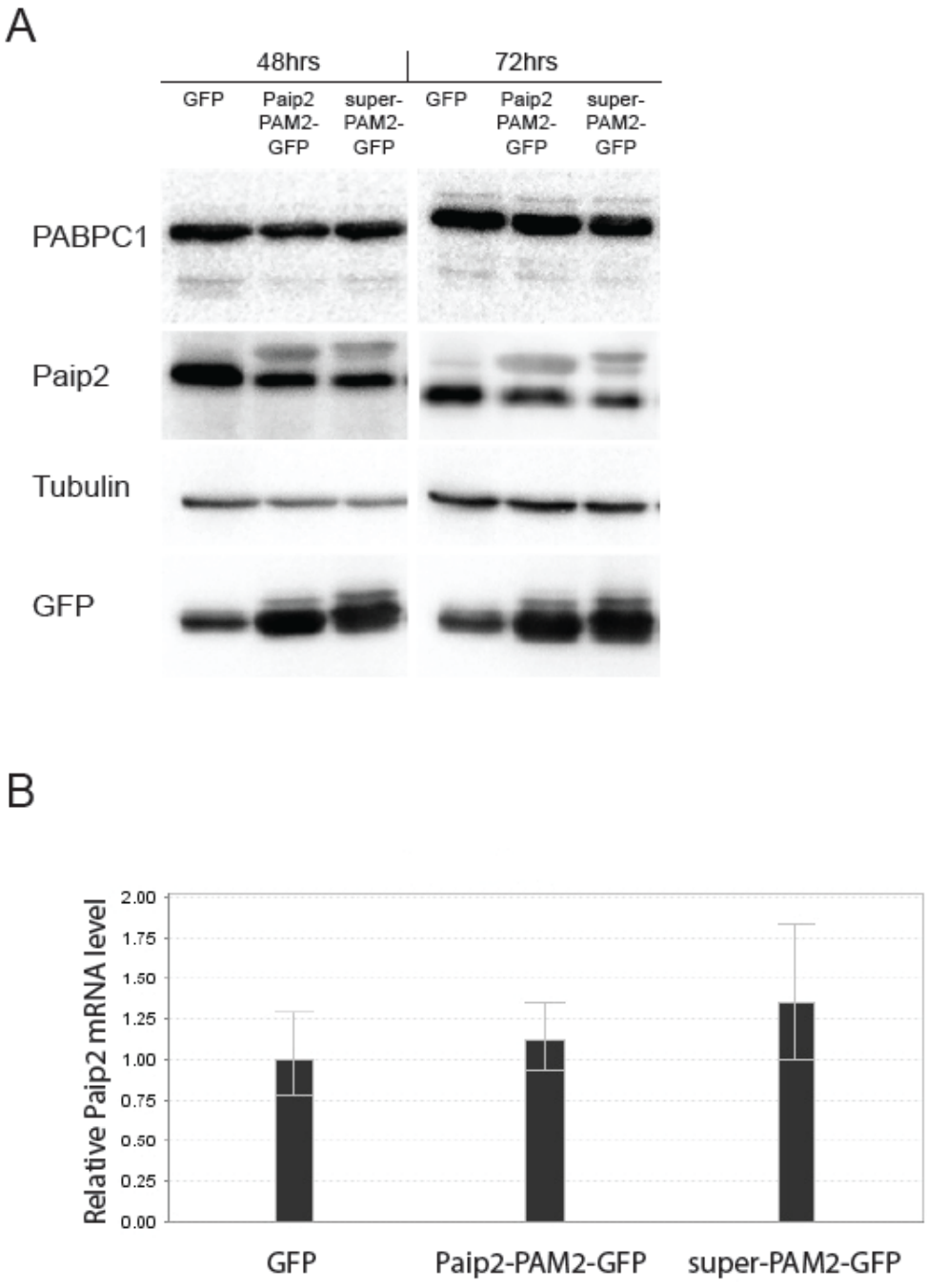

Figure 2.1 Expression of PAM2-GFP down-regulates Paip2 levels. (A) HeLa cells were transfected with empty vector or constructs expressing GFP tagged Paip2-PAM2 or super-PAM2. Cells were harvested for western blotting after 48 or 72 hours. Reduction of Paip2 levels was observed. (B) Total RNA was extracted with Trizol from cells 72 hours after transfection. qRT-PCR was performed to examine Paip2 mRNA level. mRNA levels were normalized using GAPDH as control.

Formation of the Paip2/PABPC1 complex protects components from degradation by calpain

Paip2 is subject to calpain-mediated degradation in stimulated neurons independently of the proteasome (Khoutorsky et al., 2013). To investigate the influence of complex formation on its stability, we treated the complex of full-length, recombinant Paip2 and PABPC1 proteins with calpain I. We found that formation of the complex protected both Paip2 (Fig. 2.2A) and PABPC1 (Fig. 2.2B) from degradation by calpain I. Competition from recombinant GST-super-PAM2 added into the reaction mix accelerated Paip2 degradation (Fig. 2.2). Similarly, PAM2 mutant of Paip2 was degraded faster than wild-type Paip2 (Fig. S2.2). Interaction with RRM1-4 domains of PABPC1 also protected Paip2 from calpain I digestion. (Fig. S2.2B). Thus, the protection depended on both PABPC1-binding sites of Paip2. We conclude that the Paip2/PABPC1 interaction prevents protease-mediated degradation of free Paip2 and PABPC1. However, the majority of PABPC1 *in vivo* associates with mRNA (Moretti et al., 2012) and is likely stabilized by this interaction. This explains why PABPC1 protein is not significantly affected by overexpression of GST-PAM2 (Fig. 2.1).

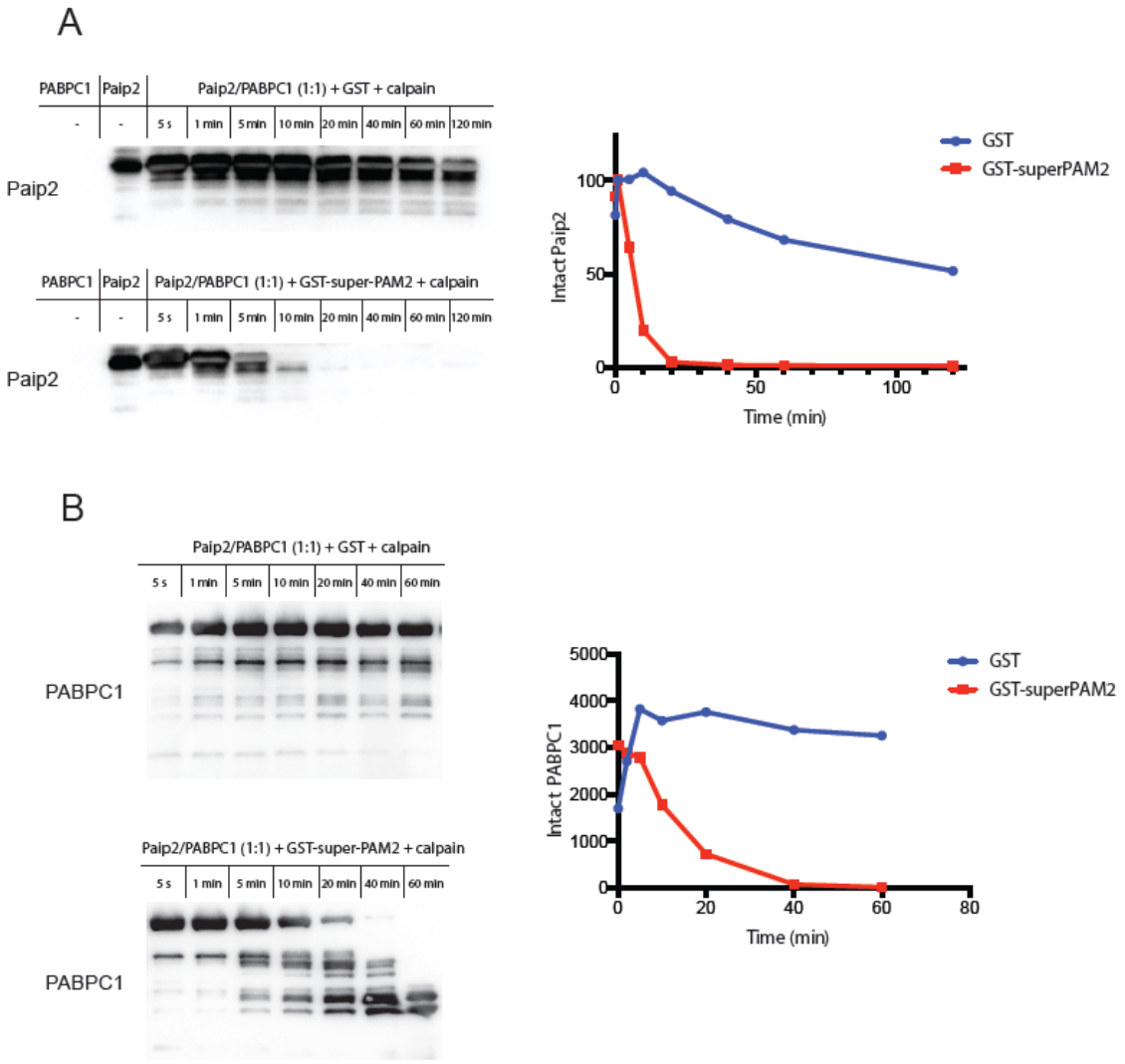

Figure 2.2 Formation of the Paip2/PABPC1 complex protects components from calpain I degradation. (A) Interaction of Paip2 with PABPC1 through PAM2 binding is important for stability. Paip2 levels decrease following challenge of the Paip2/PABPC1 complex by calpain and GST-super-PAM2. Samples of different time points were collected and the amount of Paip2 analyzed by western blotting and quantified for plotting. (B) PABPC1 levels decrease following challenge of the Paip2/PABPC1 complex by calpain and GST-super-PAM2.

PAM2/MLLE interaction is critical for Paip2/PABPC1 association in vivo

When the RRM domains of PABPC1 bind mRNA, the MLLE domain is available for binding PAM2-containing proteins, including Paip2 (Xie et al., 2014). Despite the lower affinity of the PAM2/MLLE interaction compared to the PAM1/RRM interaction, we found that the PAM2 motif was required for binding PABPC1 *in vivo*. We transfected cells with GFP-tagged Paip2 or the F118A mutant of Paip2 which does not bind MLLE (Kozlov et al., 2004). Overexpressed wild-type or mutant Paip2-GFP was immunoprecipitated by anti-GFP antibody to detect associated endogenous PABPC1. Recombinant GST or GST-super-PAM2 proteins were added to the lysate to test the requirement for the PAM2/MLLE interaction. We found that both the PAM2 mutation and competition by GST-superPAM2 significantly decreased the levels of endogenous PABPC1 bound to Paip2 (Fig. 2.3). This suggests that majority of Paip2 binds PABPC1 in a PAM2-dependent manner *in vivo*. This likely reflects the fact that most PABPC1 is bound to mRNA and, thus, only the PAM2 binding site is available for binding Paip2.

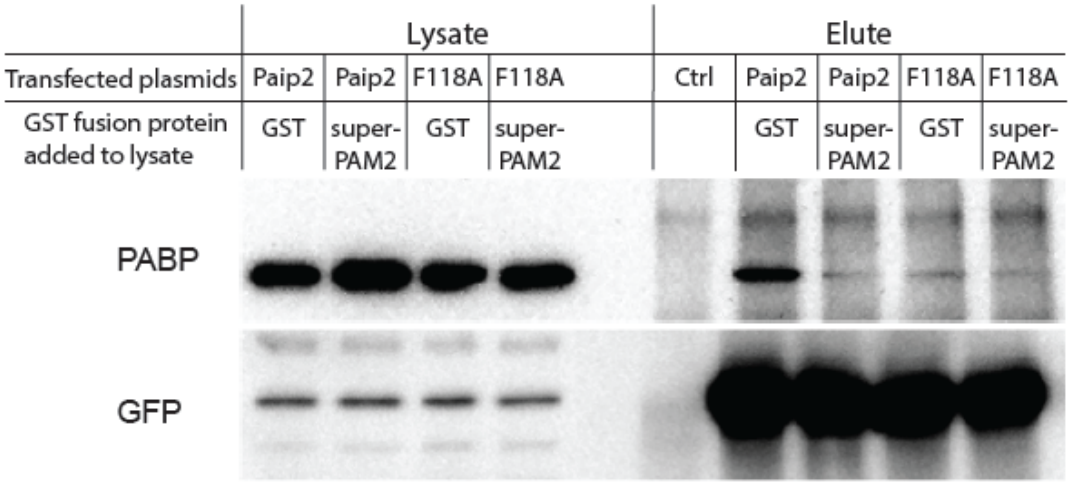

Figure 2.3 PAM2 is critical for the Paip2/PABPC1 interaction *in vivo*. Paip2-GFP or Paip2(F118A)-GFP were overexpressed in HeLa cells and cell lysates were cleared by centrifugation. GFP antibodies were added to lysate, in presence of GST or GST-super-PAM2 protein. Less PABPC1 was co-immunoprecipitated when the PAM2/MLLE interaction was blocked by mutation of F118 or addition of competing GST-PAM2 protein.

PABPC1 colocalizes with Paip2 and mRNA simultaneously

In arsenite-stressed mammalian cells, PABPC1 is enriched in stress granules containing mRNA-protein complexes (Kedersha et al., 2005). This provides a way to examine whether Paip2 colocaizes with PABPC1 on mRNA. Paip2 and PABPC1 proteins strongly co-localized at arsenite-induced stress granules (Fig. 2.4A). To investigate the role of PAM2 in the localization, we transfected cells with Paip2-GFP or Paip2 (F118A)-GFP and induced formation of stress granules. Paip2(F118A) was no longer enriched at stress granules, while wild-type Paip2 (Fig. 2.4B) and Paip2-GFP were. Thus, Paip2 colocalizes with PABPC1 on mRNA likely through MLLE domain of PABPC1. To visualize the ternary Paip2/PABPC1/RNA complex, we challenged the Paip2/PABPC1 (1:1) complex in vitro with increasing amounts of an RNA oligomer, $r(A)_{25}$. The Paip2/PABPC1/RNA complex displayed a unique migration pattern on native gel. $r(A)_{25}$ readily formed a complex with Paip2/PABPC1 at low molar ratios (Fig. 2.5A). This implies that RRM domains of PABPC1 prefer binding RNA over Paip2. This agrees with our previous observations that Paip2 needs a functional PAM2 motif to interact with PABPC1 *in vivo* and that PABPC1 is predominantly in complex with mRNA *in vivo*.

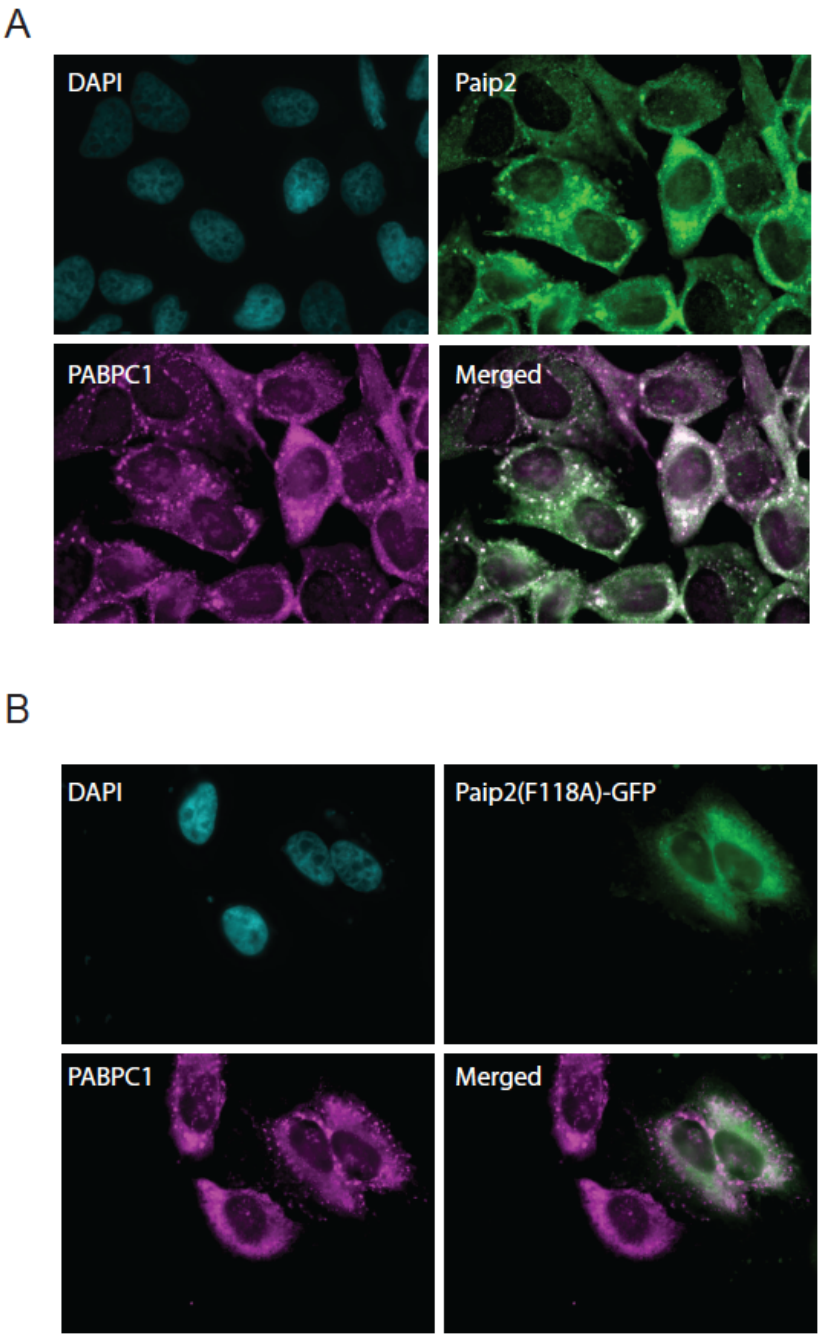

Figure 2.4 Paip2 colocalizes to stress granules. (A) HeLa cells were grown on cover slides and fixed after treatment in 0.5 mM sodium arsenite for half an hour. PABPC1 (*magenta*) and Paip2 (*green*) colocalize at stress granules. (B) PAM2 is required for Paip2 localization to stress granules. Cells were transfected with Paip2(F118A)-GFP. The mutant Paip2 does not colocalize with PABPC1.

PABPC1 uses similar interface on RRM domains to bind Paip2 or poly(A) RNA

Full-length PABPC1 can form a ternary complex with Paip2 and poly(A) RNA as shown in the native gel of Fig. 2.5A. We then asked how the Paip2 and poly(A) RNA compete with each other for binding to the RRM domains. The N-terminal 75-residue fragment of Paip2A was previously shown to bind to PABPC1 RRM2/3 (Khaleghpour et al., 2001a). NMR experiments with ^{15}N-labeled Paip2A (1-75) showed that the N-terminal residues of Paip2A did not participate in the interaction, so a smaller Paip2 (22-75) fragment was cloned and used to study the binding site on PABPC1 (Fig. S2.3).

Pull-down experiments have shown that, while RRM23 provides full affinity for Paip2, PABPC1 residues R166-Q267 were sufficient to detect binding (Khaleghpour et al., 2001a). This shorter fragment containing RRM3 and the preceding linker sequence gave excellent NMR spectra (Fig. S2.4). Addition of unlabeled Paip2 (22-75) to ^{15}N-labeled PABPC1 (166-267) resulted in specific chemical shift changes for a number of amides indicating binding of the proteins (Fig. S2.4). The backbone NMR assignments for this PABPC1 fragment alone and in complex with Paip2 (22-75) identified the binding site on the RRM3 domain (Fig. 2.5B & C). Residues in the β-sheet surface and the RRM2-RRM3 linker showed the largest spectral changes upon Paip2 binding. This same interface is used for recognition of poly(A) RNA (Deo et al., 1999), which explains why the RRM domains of PABPC1 cannot interact with Paip2-PAM1 and poly(A) RNA simultaneously. Thus, when PABPC1 is in complex with mRNA, only the MLLE domain is available for the interaction with Paip2.

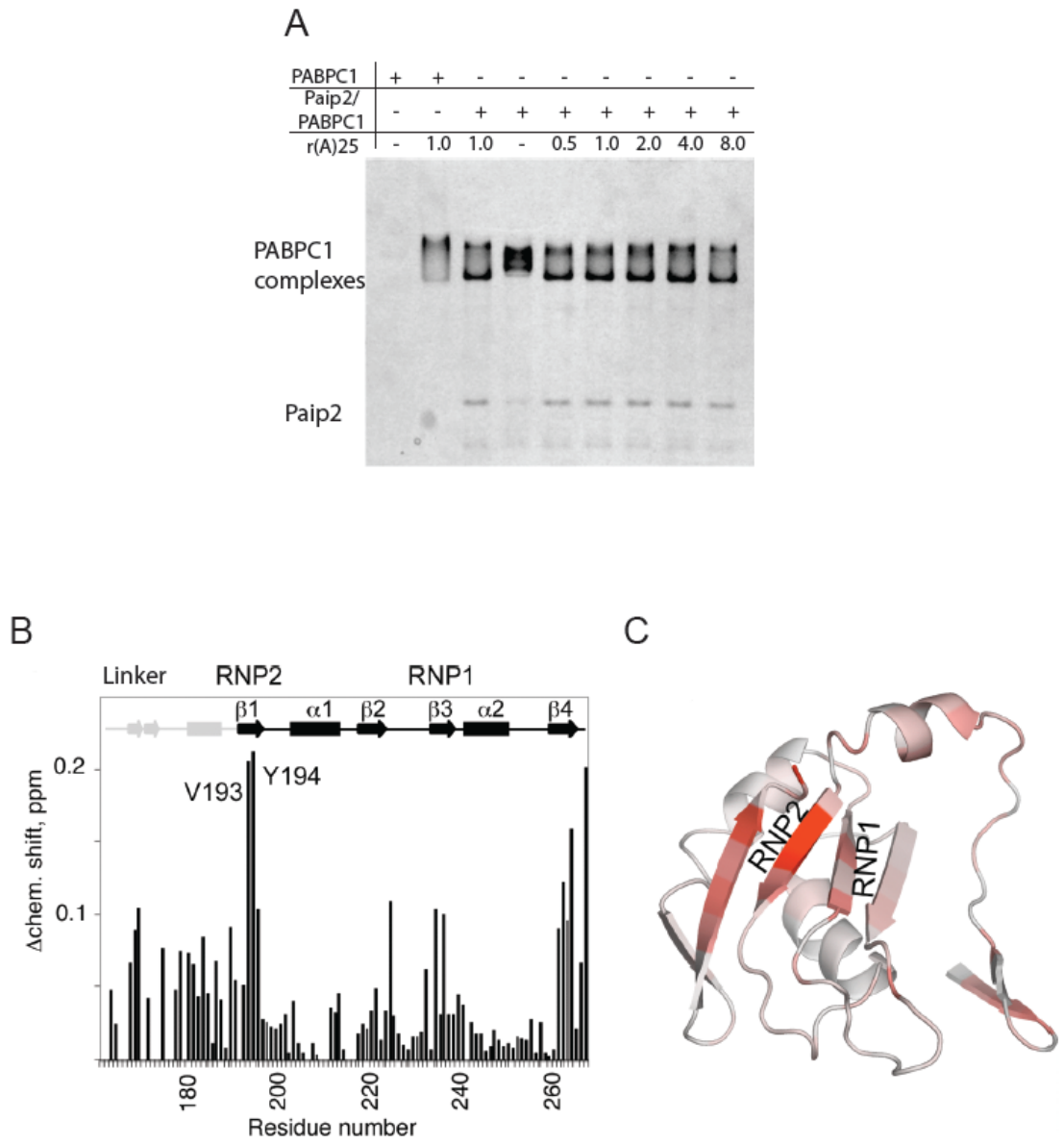

Figure 2.5 Analysis of Paip2, PABPC1 and poly(A) interplay. (A) Paip2/PABPC1/RNA tertiary complex on native gel. Full-length Paip2/PABPC1 complex were run in native gel. Different molar ratios of $r(A)_{25}$ was added to the protein complex. RNA formed a new complex with Paip2/PABPC1 and gave a new migration pattern. (B) Identification of the Paip2 PAM1 binding site on RRM3 of PABPC1 (166-267). Plot of chemical shift changes in RRM3 upon addition of Paip2 (22-75) identifies regions involved in binding. (C) Color-coded homology model of RRM3 based on the X-ray structure of RRM1-2 (Deo et al, 1999). Residues with large chemical shift changes upon PAM1 addition (panel

A) are colored red. The major chemical shift changes are in the RNP2 motif and overlap with the residues predicted to bind RNA.

PABPC1 can interact with one or two Paip2 molecules

We have shown that majority of Paip2 interacts with PABPC1 which is binding mRNA through its RRM domains. This suggests that Paip2 does not necessarily bind PABPC1 using both of its binding sites. To characterize the stoichiometry of Paip2/PABPC1 protein complex, we mixed recombinant full-length PABPC1 and Paip2, and analyzed protein complex formation by size exclusion chromatography-coupled multi-angle light scattering (SEC-MALS). Paip2 and PABPC1 at 1:1 or 2:1 molar ratio both formed mono-dispersed peaks with difference in molecular weight of about 14 kDa, which corresponded to one Paip2 molecule (Fig. 2.6 A & B). This suggests that PABPC1 can bind either one or two Paip2 proteins. By comparing the root mean square radius (Rg) and the hydrodynamic radius (Rh), we can learn about the compactness of the complex (S. E. Harding, 1992, W. Burchard, 1980). A higher Rg/Rh ratio indicates an extended conformation. From the Rg/Rh ratio, the Paip2/PABPC1 (2:1) complex was more extended, as PABPC1 was open to bind two Paip2, with one Paip2 at each end (Fig. 2.6B). Thus Paip2 interacts with PABPC1 at different ratios, depending on the relative abundance of Paip2 and PABPC1 (Fig. 2.9).

A

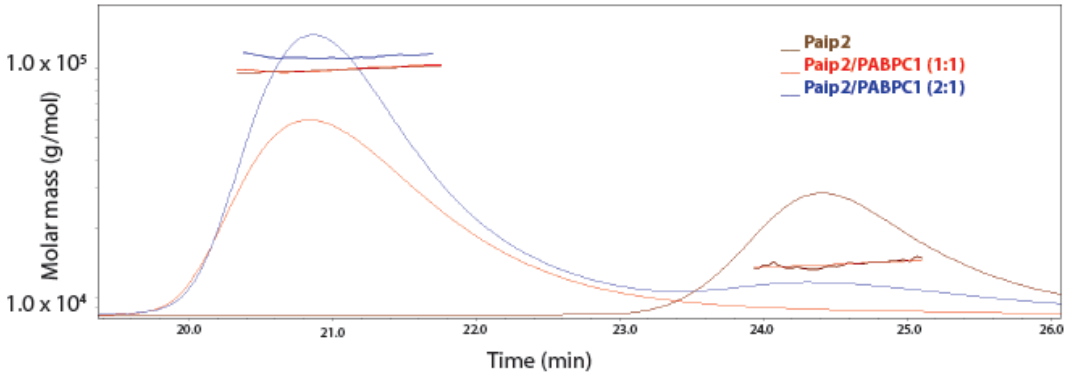

B

Protein	Molecular weight (KDa)	RMS radius (Rg)	Hydrodynamic radius (Rh)	Rg/Rh
Paip2/PABPC1 (1:1)	98.6	10.7	4.7	2.3
Paip2/PABPC1 (2:1)	112.4	20.5	5.9	3.5
Paip2	14.1	- *	1.5	-

** RMS radius has a lower limit of about 10 nm according to Wyatt Technology.*

Figure 2.6 Paip2 and PABPC1 interact with two different ratios. (A) Full-length Paip2/PABPC1 complex was analyzed by SEC-MALS. The molecular weight difference suggested a second Paip2 bound to PABPC1 at ratio 2:1. (B) The calculated molecular weight, root mean square radius and hydrodynamic radius corresponding to Paip2/PABPC1 ratios are listed in the table.

Paip2 may displace PABPC1 from shortened poly(A) tail of mRNA

The above experiments showed that the RRM domains of PABPC1 prefer to bind to $r(A)_{25}$ over Paip2. To study the interplay of Paip2, PABPC1, and poly(A) RNA, we purified RRM1234 (1-372) of PABPC1 and Paip2-PAM1 (22-75). The two proteins were mixed at 1:1 molar ratio and purified by gel filtration chromatography. The resulting RRM1234/PAM1 complex migrated in a sharp band on non-denaturing PAGE (Fig. 2.7A). We added increasing $r(A)_{25}$ or $r(A)_{11}$ to the complex. Although the $r(A)_{25}$ (Sladic et al., 2004) or $r(A)_{11}$ (unpublished results) has similar affinity for PABPC1, RRM1234/PAM1 was disrupted by $r(A)_{25}$, but remained stable even in the presence of high $r(A)_{11}$ levels (Fig. 2.7A). This suggested that the length of RNA was critical for competing with Paip2. To further understand the competition, we assembled a complex of RRM23 (98-293) and Paip2 (22-75), and tested whether different RNAs could disrupt the protein complex (Fig. 2.7B & C). We found $r(A)_{16}$ disrupted the RRM23/Paip2 complex, while $r(A)_{11}$, $(AUUU)_3$, and $(AUUU)_4$ did not. Although PABPC1 binds all these RNA oligos *in vitro*, the length and sequence requirements of RNA in disassembly of RRM23/Paip2 indicate that longer poly(A) RNAs induce a unique conformation of PABPC1 that disfavors Paip2.

A

RRM1-4	+	+	-	-	-	-	-	-	+	-	-	-	-	-	-
Paip2/RRM1-4	-	-	+	+	+	+	+	+	-	+	+	+	+	+	+
r(A)25	-	1.0	-	0.5	1.0	2.0	4.0	8.0	-	-	-	-	-	-	-
r(A)11	-	-	-	-	-	-	-	-	1.0	-	0.5	1.0	2.0	4.0	8.0

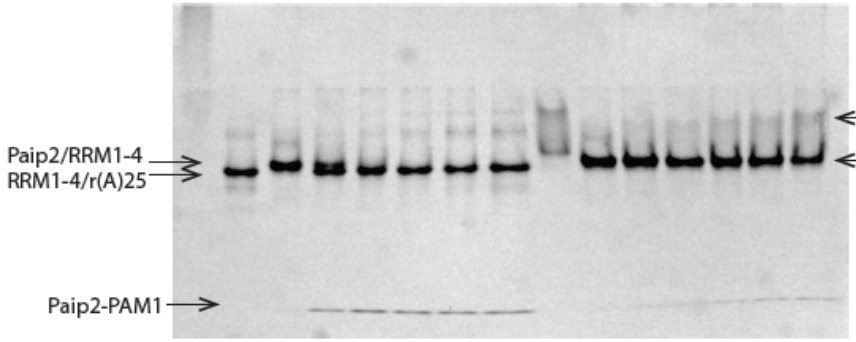

B

RRM23	+	+	-	-	-	-	-	-	+	-	-	-	-	-	-
Paip2/RRM23	-	-	+	+	+	+	+	+	-	+	+	+	+	+	+
r(A)11	-	1.0	-	0.5	1.0	2.0	4.0	8.0	-	-	-	-	-	-	-
(AUUU)3	-	-	-	-	-	-	-	-	1.0	-	0.5	1.0	2.0	4.0	8.0

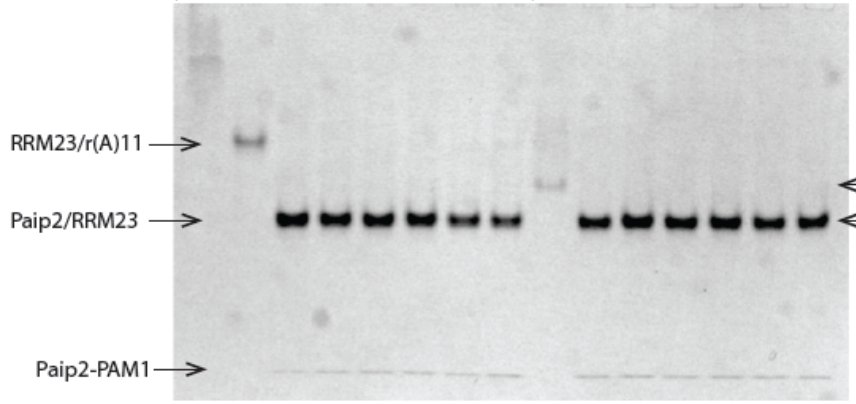

C

RRM23	+	+	-	-	-	-	-	-	+	-	-	-	-	-	-
Paip2/RRM23	-	-	+	+	+	+	+	+	-	+	+	+	+	+	+
r(A)16	-	1.0	-	0.25	0.5	1.0	2.0	4.0	-	-	-	-	-	-	-
(AUUU)4	-	-	-	-	-	-	-	-	1.0	0.25	0.5	1.0	2.0	4.0	

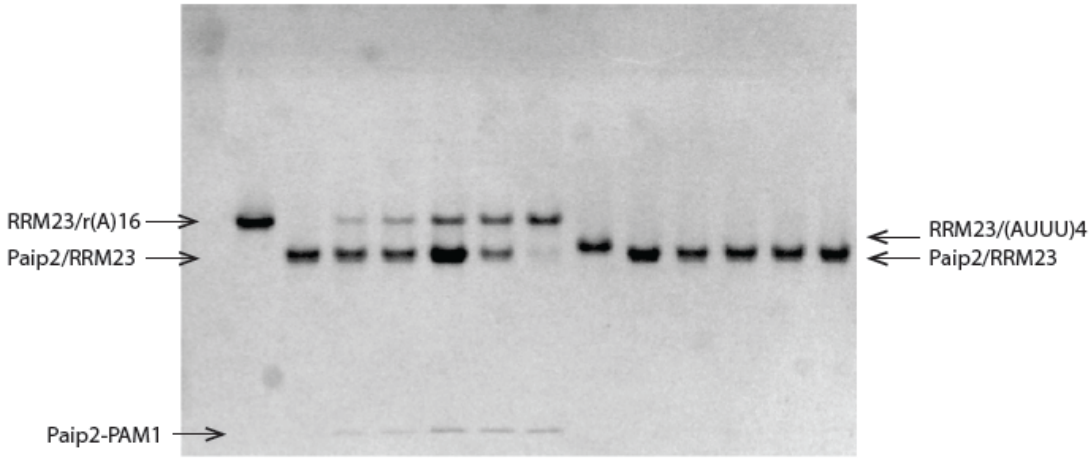

Figure 2.7 PABPC1 prefers binding to Paip2 over short poly(A) or (AUUU) repeats. (A) $r(A)_{25}$ disrupts RRM1234/Paip2 complex. 60 pmol of PABPC1 (1-372) (or RRM1234)/Paip2 (22-75) complex were challenged with increasing amounts of $r(A)_{25}$ or $r(A)_{11}$. The molar ratios of RNA compared to PABPC1/Paip2 complex are indicated above the gel. (B) $r(A)_{11}$ or $(AUUU)_3$ could not disrupt RRM23/Paip2 complex. (C) $r(A)_{16}$ disrupted RRM23/Paip2 complex, while $(AUUU)_4$ did not.

Depletion of Paip2 reduced microRNA-mediated gene silencing

The change of PABPC1's preference towards Paip2 with the shortening of RNA can be of great significance in the displacement of PABPC1 during mRNA deadenylation (Fig. 2.9). We examined the effects of Paip2 depletion in a Renilla and firefly dual luciferase reporter assay (Pillai et al., 2005). Presence of let-7 microRNA binding sites silenced the reporter by about 10 times, and the silencing was significantly attenuated after Paip2 knockdown (Fig. 2.8A & B). Consistent with our results, it was reported by two groups that Paip2 knockdown diminished microRNA-mediated silencing activity (Walters et al., 2010, Yoshikawa et al., 2015). Given the fact that very high concentration of Paip2 is required to disrupt the PABPC1/poly(A) RNA interaction *in vitro* (Khaleghpour et al., 2001b), we hypothesize that Paip2 does not actively compete with poly(A) for PABPC1, but instead enhances deadenylation at a later stage by promoting dissociation of PABPC1 from the shortened mRNA. Knockdown of Paip2 reduced microRNA-mediated silencing in luciferase reporter assay, likely through inhibition of late steps in the deadenylation process.

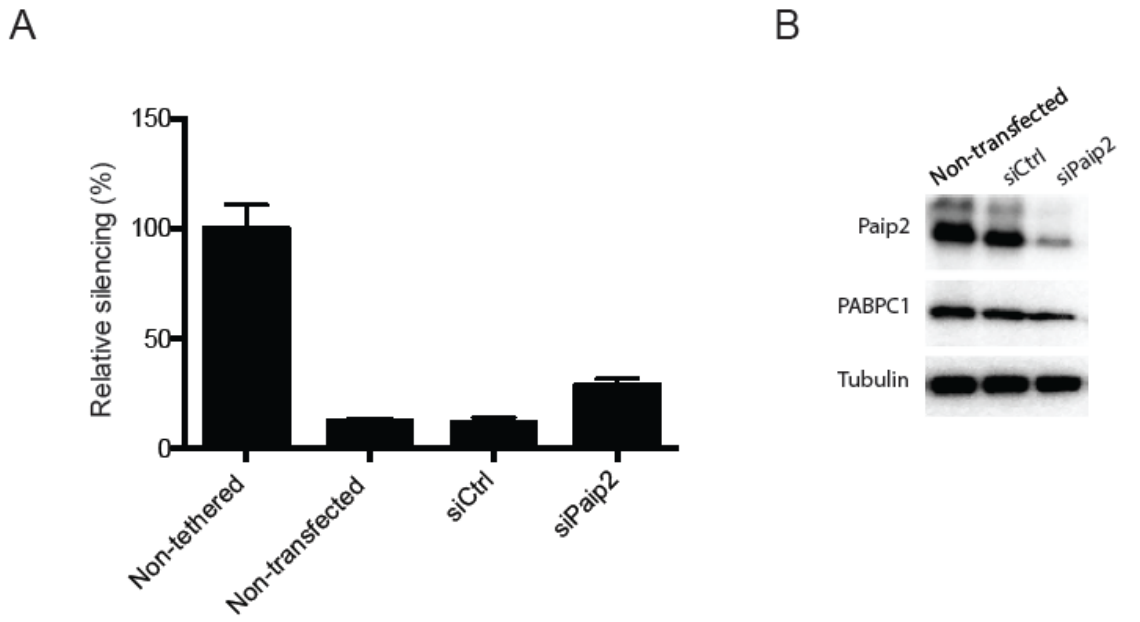

Figure 2.8 Knockdown of Paip2 reduced microRNA-mediated gene silencing. (A) HEK 293T cells were co-transfected with siRNA control or siPaip2 and firefly luciferase (FL) and Renilla luciferase (RL) plasmids. Luciferase activities from plasmids with three let-7 binding sites or mutated binding sites were normalized to firefly luciferase activities. The reduction of silencing activity by siPaip2 was significant at confidence level of 0.05, by two-tail t-test for two samples with unequal variances. (B) Paip2, PABPC1 and tubulin levels were probed by western blotting in cells after the same treatment as in (A).

Discussion

In this study, we illustrate a novel role of Paip2 in mRNA metabolism. Our results demonstrate that Paip2 interacts with PABPC1 on mRNA and can exclusively bind PABPC1 when the poly(A) tail is shortened. This supports the model that Paip2 enhances mRNA deadenylation through facilitating PABPC1 dissociation.

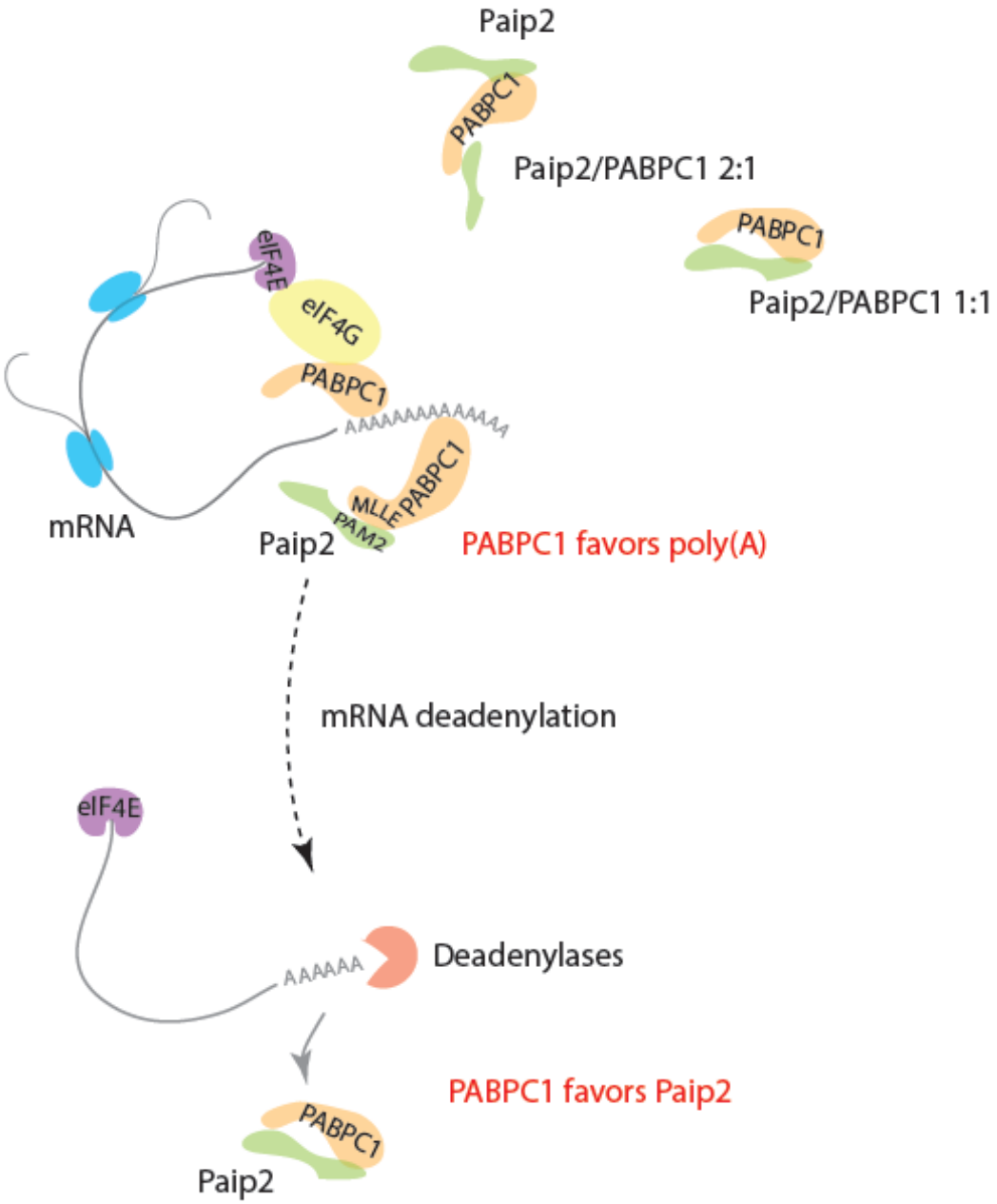

Figure 2.9 Model of the Paip2 and PABPC1 interaction in cells. Paip2 associates with PABPC1 on mRNA. In the cytoplasm, Paip2 may interaction with PABPC1 with stoichiometries of 1:1 or 2:1. When mRNA poly(A) tail is shortened by deadenylation, Paip2 may actively displace PABPC1 from the mRNA and protect PABPC1 by formation of a protein complex.

PABPC1 is required for deadenylation of mRNA by Pan2/Pan3 deadenylases to a short length of about 10-25 nucleotides (Lowell et al., 1992; Zheng et al., 2008). At that point, the mRNA is stabilized and protected by PABPC1 from further deadenylation by Ccr4/Not deadenylases (Tucker et al., 2002). The last PABPC1 molecule needs to be displaced at this stage to finish deadenylation. However, the displacement of PABPC1 from mRNA is not well understood. Paip2 has been known to act as a competitor of RNA for PABPC1, but high concentrations of Paip2 are needed to disrupt the PABP/r$(A)_{25}$ complex (Khaleghpour et al., 2001b). Such disruption can take place *in vivo* when local concentration of Paip2 is high enough, or when other factors alter interaction of PABP/r$(A)_{25}$. Here, we show that Paip2 associates with PABPC1 on mRNA and out-competes shortened poly(A) RNA for binding to PABPC1, which renders Paip2 a good candidate as a mediator of the final displacement (Fig. 2.9). Nonetheless, other mechanisms for dissociate PABPC1 off mRNA remain possible. In microRNA-mediated gene silencing, PABPC1 facilitates recruitment of GW182-containing silencing complex and later appears to be displaced prior to deadenylation (Moretti et al., 2012, Zekri et al., 2013). Multiple mechanisms may come into play for different scenarios in cells.

PABPC1 has a flexible linker in its middle region, which is targeted by a number of proteases (Smith and Gray, 2010). Immediate binding of PABPC1 to Paip2 after dissociation from mRNA offers protection to mRNA-free PABPC1 in cytoplasm. Indeed, addition of Paip2 slows down PABPC1 cleavage by protease 3C and 2A (Rivera and Lloyd, 2008). The interaction between Paip2 and PABPC1 on mRNA makes the immediate protection possible.

Less than 10% of PABPC1 can be depleted by GST-Paip2 without micrococcal nuclease treatment (Moretti et al., 2012), which suggests that over 90% of PABPC1 in cells is bound to mRNA. According to our data, the levels of PABPC1 are 2 to 4 times higher than Paip2 in HeLa, HEK293 or MEF cells (Fig. S2.5). Thus, there is an excess of Paip2 in cytoplasm relative to free PABPC1 not associated with mRNA. This is supported by the co-localization of Paip2 with PABPC1 at stress granules (Fig. 2.4).

Paip2 is subjected to extensive proteasome-dependent (Yoshida et al., 2006) and proteasome-independent (Khoutorsky et al., 2013) degradation. It is conceivable that regulation of Paip2 levels is used by host to restrict viral protein synthesis (McKinney et al., 2013). An optimal level of Paip2 is important for spermatogenesis (Yanagiya et al., 2010) and microRNA-mediated gene silencing (Yoshikawa et al., 2015, Walters et al., 2010).

In conclusion, we have shown that Paip2 uses its dual interaction sites to interact with PABPC1 in cells. Paip2 protects free PABPC1 and may actively function through PABPC1 on mRNA. More studies are needed to elucidate the upstream and downstream pathways of this Paip2 and PABPC1 interplay.

Materials and methods

Plasmids and RNA oligos

pET-28B-PABPC1 (NM_002568.3) plasmid was a gift from Drs. Svitkin and Sonenberg at McGill University. Firefly luciferase and renilla luciferase reporter plasmids were kindly provided by Dr. Filipowicz at the Friedrich Miescher Institute for Biomedical Research. PABPC1 (1-372), Paip2a (NM_001033112.2), Paip2a-PAM2 (109-125), Paip2a-PAM1 (22-75) were cloned into pGEX-6p1 for protein expression in *E. coli*. Paip2a-PAM2 (109-125) and super-PAM2 (SNLNPNAPEFHPGVPWKGLQNI) were cloned into pCDNA3.1–EGFP. Paip2a was subcloned into pCDNA3.1-EGFP and mutated to express Paip2aPhe118Ala-GFP, with QuikChange site-directed mutagenesis kit (Agilent). siPaip2 (5'- GAGUACAUGUGGAUGGAAAUU-3'), RNA oligo $r(A)_{25}$ and $r(A)_{11}$ were synthesized, desalted and gel purified at Dharmacon. Control siRNA was purchased from Qiagen (SI03650318).

Protein purification

BL21 (DE3) *E. coli* was transformed with related plasmids and induced with 1 mM IPTG at an OD of 0.7. Bacteria were grown for 3 hours at 30 degrees before being harvested.

Pelleted cells were resuspended in 1x PBS buffer (pH 7.4) with 5 mM BME and proteinase inhibitor cocktail (Roche). For purification of PABPC1-His, 10 mM imidazole, 10 μg/ml RNase A and 10 μg/ml DNase I were added to lysate. PABPC1-His was bound to Ni-NTA resin (Qiagen), washed by 1x PBS (10 mM imidazole added) and eluted with 200 mM imidazole. PABPC1 (1-372) was purified using GST resin (GE) and cleaved on the column by 3C PreScission protease. Eluted PABPC1-His or PABPC1 (1-372) was run through anion-exchange and cation-exchange columns (Biosuite Q and Biosuite SP, 13 μm, 21.5 x 150 mm column, Waters), before it was finally applied to Superdex 200 Hiload 16/60 size-exclusion column (GE). The buffer for gel filtration was 20 mM HEPES pH 7.0, 150 mM NaCl, 2 mM DTT. Paip2 was purified using Superdex 75 after affinity purification by GST tag and cleavage on the column. The PABPC1 (1-372)/PAM1 complex was obtained by incubation of purified RRM1234 and 1.5 fold molar excess of GST-Paip2 (22-75) in 1x PBS supplemented with 3C protease and 2 mM DTT. The protein complex was further purified using Superdex 75 Hiload 16/60 column (GE).

Cell culture and transfection

HeLa cells were cultured in DMEM supplemented with antibiotics and 10% fetal bovine serum. 10^5 cells per well were plated in 24-well plate the day before transfection. 0.8 μg DNA plasmid was mixed with 2 μl Lipofectamine 2000 in Opti-MEM and then added to cells. After 24 hours, cells were trypsin digested and split onto cover slides. Cells were treated with 0.5 mM sodium arsenite for 0.5 hour and fixed on the second day.

Immunofluorescence and confocal microscopy

Cells were fixed with 4% PFA in 1x PBS, and penetrated by cold methanol (-20°C) or 0.1% Triton X-100 in 1x PBS for 10 minutes. Cells were blocked with 5% normal goat serum (Millipore S26) in PBS for 1 hour. Then cells were incubated in 1x PBS, supplemented with anti-PABPC1 (Abcam ab21060; Santa Cruz sc32318)(1:200) or anti-Paip2 (Sigma-Aldrich P10087). Cells were washed in PBS 3 times, before being incubated with corresponding second antibodies conjugated with Dylight550 (Bethyl A120-101D3) or Rhodamine (Millipore 12-509, 12-510) at 1:200 – 1:500 dilutions.

DAPI (Roche) was added to washing buffer at 0.5 μg/ml to treat cells for 10 minutes. Cover slides were finally mounted in ProLong Gold antifade reagent (Life Technology P36930). Images were collected on Zeiss LSM 310 confocal microscope in the McGill University Life Sciences Complex Advanced BioImaging Facility (ABIF).

Quantitative RT-PCR

Total RNA was extracted from cells with Trizol (Life Technology). cDNA libraries were prepared using SuperScript First-Strand Synthesis System for RT-PCR (Life Technology). Validated Taqman assays were purchased for quantification of GAPDH (Applied Biosystems Hs 99999905) and Paip2 (Applied Biosystems Hs00212868). qRT-PCR reactions were run in Stepone Plus PCR system (Applied Biosystems).

Immunoprecipitation

Cells were lysed in 20 mM HEPES (pH 7.4), 150 mM NaCl, 0.5% NP-40, 2 mM DTT, 2 mM $MgCl_2$, 1 mM $CaCl_2$ and protease inhibitor tablet (Roche), and cleared by centrifugation. 2 μg antibodies were added per 1 mg cleared lysate for 2 hours. Dynabeads conjugated with protein A or protein G (Life Technology) were washed and added to lysate for 0.5 hour. Dynabeads were then washed with 1x PBS and boiled in SDS loading buffer for further analysis.

Western blotting

Protein samples were heated at 95°C and separated by SDS-PAGE. Proteins were then transferred to PVDF membrane (Millipore) in Tris/Glycine buffer with 20% methanol in cold room. PVDF membrane was blocked in 1x TBST (pH 7.5), containing 0.05% Tween-20 and 5% skim milk powder or bovine serum albumin. The membrane was then incubated with primary antibodies, including anti-PABPC1 (Abcam ab21060 1:1000), anti-Paip2 (Sigma-Aldrich P10087 1:2000), anti-tubulin (Sigma-Aldrich T9028 1:5000) and anti-GFP (Clontech 632381 1:2000). Membrane was then washed three times in 1x TBST and incubated with goat-anti-rabbit (Jackson ImmunoResearch 111-035-046 1:5000) or goat-anti-mouse (Jackson ImmunoResearch 115-035-071 1:5000) for 0.5

hour. After wash, membrane was developed with Amersham ECL prime kit (GE healthcare RPN2236) and imaged with Alpha Innotech imaging system.

NMR spectroscopy

NMR samples were prepared in 90% NMR buffer (10 mM HEPES pH 7.0 and 50 mM NaCl) and 10% D_2O. NMR resonance assignments of the RRM3 domain were carried out using standard heteronuclear 3D-experiments HNCACB and CBCA(CO)NH on ^{13}C,^{15}N-labeled protein. For NMR titrations, unlabeled Paip2 (22-75) was added stepwise to 0.2 mM ^{15}N-labeled RRM3 to a final molar ratio of approximately 3 to 1. Chemical shift changes were calculated according to the formula $\sqrt{(\Delta H)^2 + (0.2 \times \Delta NH)^2}$. All NMR experiments were performed at 301 K on a Bruker 600 MHz spectrometer. NMR spectra were processed using NMRPipe(Delaglio et al., 1995) and analyzed with XEASY(Bartels et al., 1995).

Size Exclusion Chromatography-coupled Multi-Angle Light Scattering

200 μg of recombinant PABPC1 protein was mixed with Paip2 at indicated molar ratios. Protein mixture was injected into Superdex 200 10/300 GL column and analyzed by a MiniDAWN TREOS light-scattering detector (Wyatt Technology Corporation) and a Optilab rEX (Wyatt) refractive index detector. All analysis was done in 20 mM HEPES pH 7.0, 150 mM NaCl, 2 mM DTT. Data processing was performed using Astra software (Wyatt).

Fluorescence polarization assay

Peptides SNLNPNAPEFHPGVPWKGLQNI-FITC (super-PAM2) and SNLNPNAPEAHPGVPWKGLQNI-FITC (super-PAM2-F10A) were synthesized at EZBiolab. 5 nM of fluorophore-labeled peptide was mixed with serial dilutions of GST-PABPC1-MLLE or GST-EDD-MLLE. Fluorescence polarization signals of each well were recorded on a SpectraMax M5e Microplate Reader at excitation wavelength of 495 nM and emission wavelength of 519 nM. Fluorescence polarization signals as milli-polarization units (mP) were plotted against a log scale of protein concentration (μM).

Calpain digestion of proteins

40 μg Paip2 was mixed with equal molar amount of PABPC1 and then incubated with Calpain I. Samples were collected at indicated time points. GST or GST-super-PAM2 was added as a control or to compete with Paip2 for interaction with PABPC1. Degradation of Paip2 was examined by western blotting using anti-Paip2 or anti-PABPC1 antibodies. Bands were quantified in Alphaview software (AlphaInnotech), and plotted against digestion time.

Dual luciferase reporter assay for microRNA-mediated silencing activity

Renilla and firefly luciferase reporters were described before(Pillai et al., 2005). For overexpression assays, human HeLa cells were seeded in 24-well plates and transfected using Lipofectamine 2000 (Life Technology). The transfection mixtures contained 10 ng of R-Luc-3xlet-7 reporter plasmid (RL-3xlet-7) or the corresponding reporter carrying mutations in the let-7-binding sites (RLuc-Mut), 100 ng of the pEGFP-N3-F-Luc transfection control and 60 pmol of siRNA control or siPaip2. R-Luc and F-Luc activities were measured 48 h after transfection using the Dual-Luciferase Reporter Assay System (Promega). Renilla luciferase activity was normalized to firefly luciferase.

Acknowledgements

We are grateful for suggestions and help from colleagues during the project.

Competing interests

No competing interests declared.

Author contributions

J. X. and G. K. designed the experiments. J. X., W. X., G. K., and Y. C. carried out the experiments. J. X., G. K., and K. G. wrote the manuscript.

Funding

This study was supported by Canadian Institutes of Health Research grant MOP-14219. J. X. was supported by the CIHR Strategic Training Initiative in Chemical Biology, the

CIHR Strategic Training Initiative in Systems Biology, Graduate Student Scholarship of the Quebec Network for Research on Protein Function, Engineering, and Applications (PROTEO), and the Recruitment Award of the Groupe de Recherche Axé sur la Structure des Protéines (GRASP).

Supplemental materials

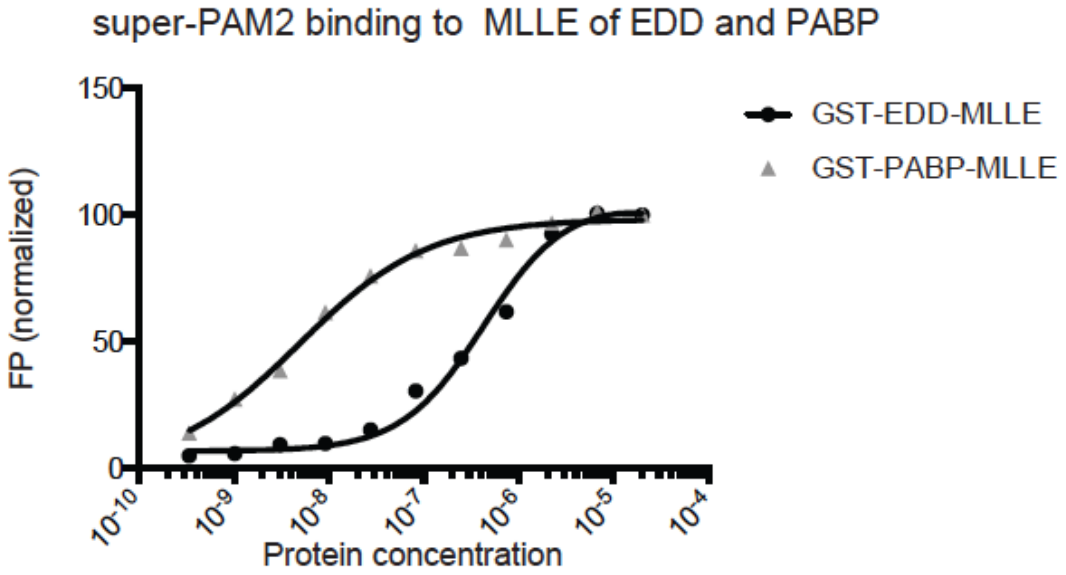

Affinities of PAM2s to MLLE domains

	PABPC1-MLLE	EDD-MLLE
PAM2 (Paip2)	0.12 µM	6 µM
super-PAM2	0.03 µM	0.2 µM

Figure S2.1 Affinities of super-PAM2 to MLLE domain of PABPC1 and EDD measured by fluorescence polarization. Peptides were labeled with FITC and fluorescence measured in the presence of the MLLE domains of PABPC1 or EDD.

A

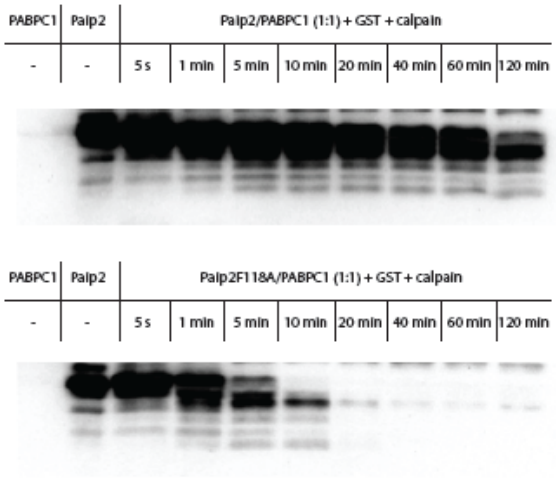

B

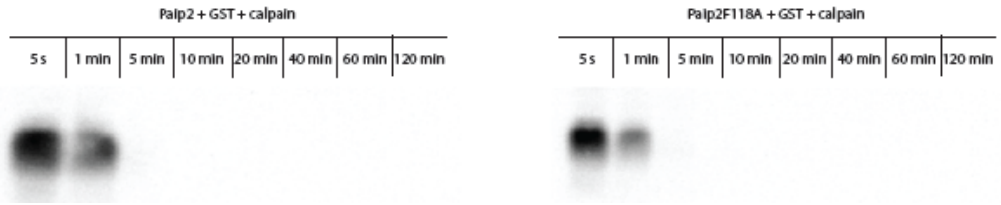

Figure S2.2 Paip2 degradation by calpain I. (A) Paip2-PAM2 mutant (F118A) was degraded faster compared to wild-type Paip2 in presence of PABPC1. (B) Paip2 or Paip2F118A were rapidly degraded with equal rates by calpain I.

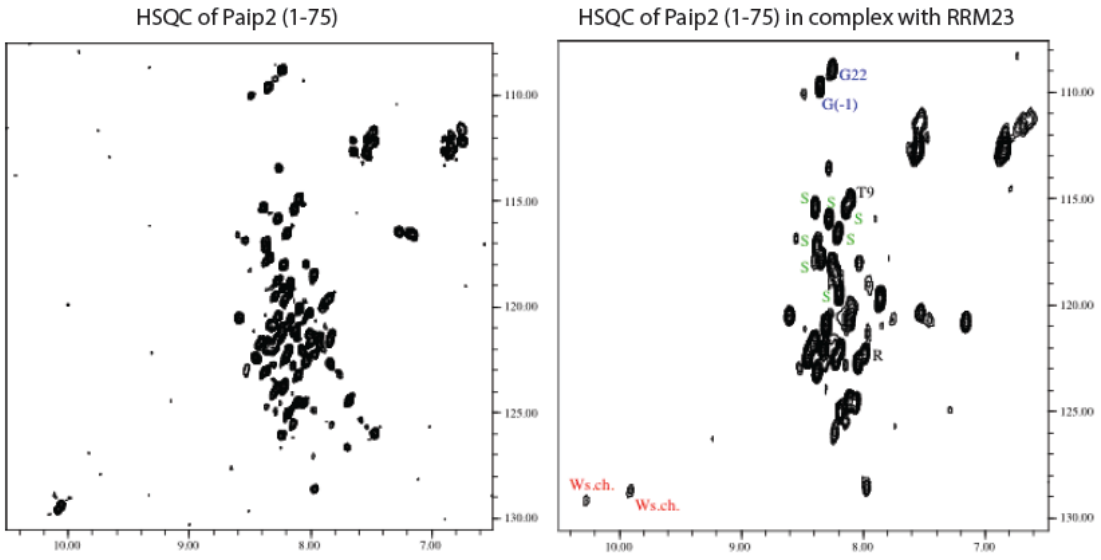

Figure S2.3 Mapping of PAM1 region of Paip2 to residues 22-75. 15N-HSQC spectra of Paip2 (1-75) before and after addition of RRM23 are shown side by side. Upon addition of RRM23 fragment of PABPC1 to ^{15}N-labeled Paip2 (1-75), signals of the residues involved in PABPC1 interactions undergo broadening, which results in weak or disappearing signals. In contrast, residues that do not bind to PABPC1 produce sharp signals and can be identified using 3D ^{15}N-TOCSY experiment. In particular, all serine and glycine residues (labeled as S and G, respectively) reside in the N-terminal 22-residue fragment of Paip2 (1-75) and do not interact with PABPC1 RRM23, while side chains (Ws.ch.) of all three tryptophans (W36, W52, W73) are in the bound region of Paip2.

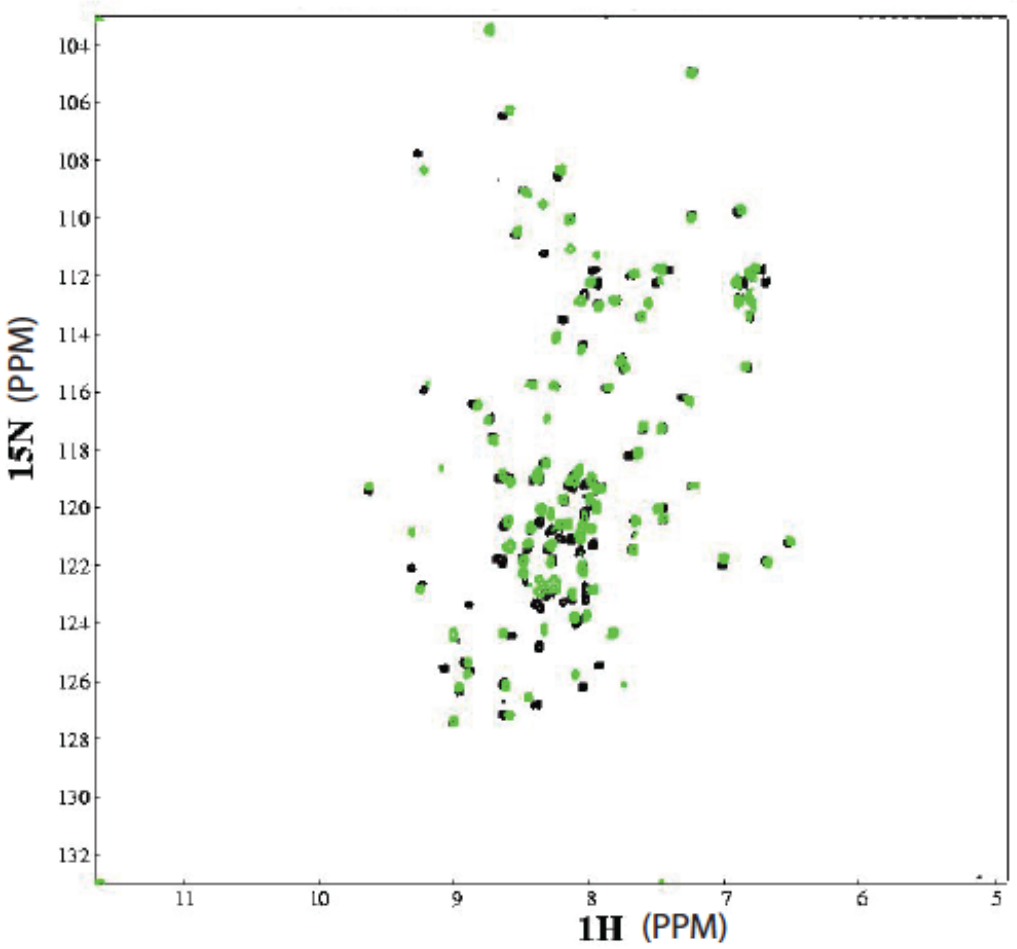

Figure S2.4 Overlay of the ^{1}H-^{15}N correlation NMR spectra of the ^{15}N-labeled PABPC1 RRM3 domain (residues 166-277) alone (in black) and in the presence of equimolar amount of unlabeled Paip2 (22-75) (in green). NMR titration resulted in specific chemical shift changes indicating binding between the proteins.

A

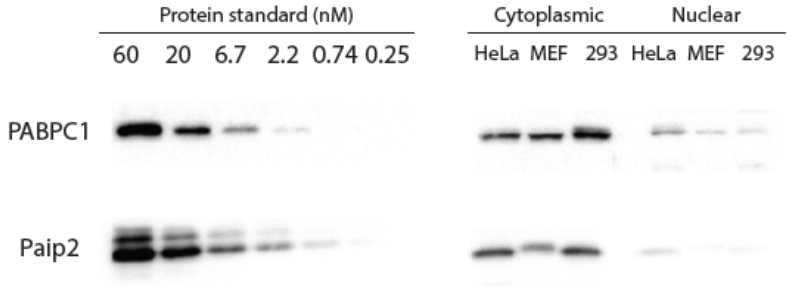

B

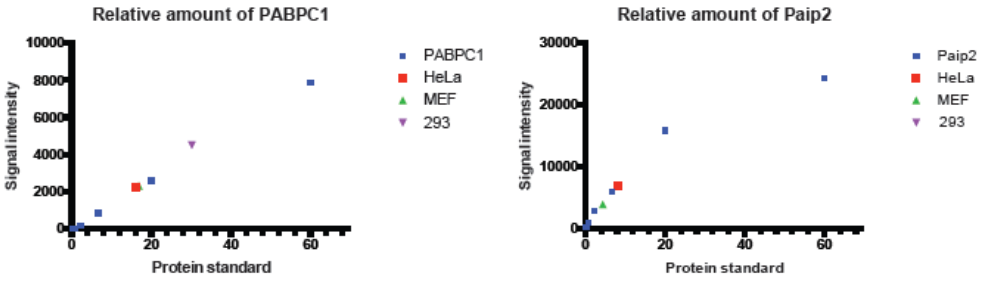

Relative amount of PABPC1 and Paip2 in cells (nM)

	Hela CE	MEF CE	293 CE	Hela NE	MEF NE	293 NE
PABPC1	16.3	16.9	30.2	6	1.5	1
Paip2	8.2	4.4	8.3	0.5	-0.5	-0.3
PABPC1/Paip2	2	3.9	3.6	-	-	-

C

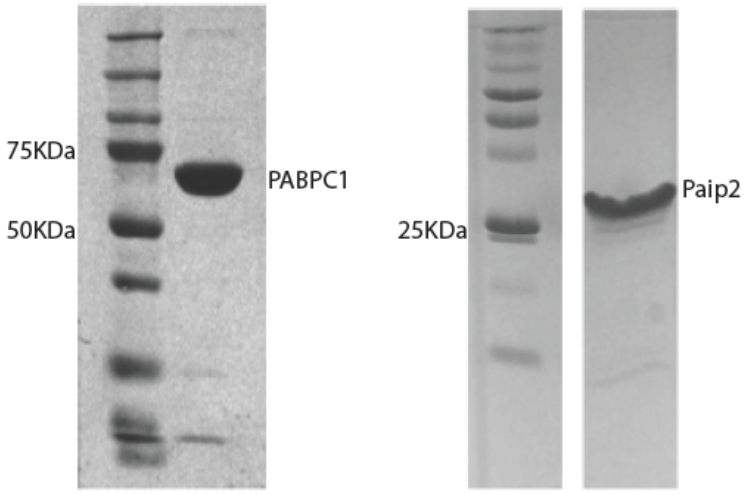

Figure S2.5 Quantification of amounts of PABPC1 and Paip2 in cells. (A) Dilutions of recombinant PABPC1 or Paip2 protein were analyzed in SDS-PAGE together with

cytoplasmic extract (CE) or nuclear extract (NE) of HeLa, MEF, and HEK 293T cells. Proteins were detected by western blotting using anti-PABPC1 or anti-Paip2 antibodies. (B) Signals of purified PABPC1 or Paip2 were plotted against loaded concentrations to make standard curves. Relative amounts of PABPC1 and Paip2 were determined by fitting signal intensities into the curve. All the cytoplasmic extract signals fell into the linear ranges of standard curves. PABPC1/Paip2 ratios were calculated as in the table. (C) Coomassie blue staining of purified PABPC1 and Paip2 proteins. PABPC1 and Paip2 were run in SDS-PAGE. Paip2 shows retarded migration in SDS-PAGE, due to the high content of acidic amino acids.

Connecting text 1

PABPC1 is closely related to RNA metabolism. The level of PABPC1 is critical for cellular activities and regulated by factors including Paip2. In the following chapter, I investigated the impact of PABPC1 depletion on formation of P-bodies, a high-order RNA structure in cells. In human cells, P-bodies do not contain PABPC1. The link between PABPC1 and P-body formation reveals a novel role of PABPC1 in mRNA remodeling into high-order structures.

Chapter 3: Cytoplasmic poly(A) binding protein 1 is required for P-body formation in mammalian cells

Jingwei Xie[1,2], Yu Chen[1], Xiaoyu Wei[1], Guennadi Kozlov[1], Kalle Gehring[1, 2]

[1] Department of Biochemistry and Groupe de Recherche Axé sur la Structure des Protéines, McGill University, Montreal, Quebec H3G 0B1, Canada

[2] To whom correspondence should be addressed: Dept. of Biochemistry, McGill University, 3649 Promenade Sir William Osler, Rm. 473, Montreal, QC H3G 0B1, Canada. Tel.: 514-398-7287; E-mail: jingwei.xie@mail.mcgill.ca, E-mail: kalle.gehring@mcgill.ca.

Running title

PABPC1 and P-body formation

Keywords

PABPC1, P-bodies, stress granules, GW182

Abstract

Compartmentalization of mRNA through formation of RNA granules is involved in many cellular processes, yet it is not well understood. mRNP complexes undergo dramatic changes in protein compositions, reflected by markers of P-bodies and stress granules. Here, we show that PABPC1, albeit absent in P-bodies, plays important role in P-body formation. Depletion of PABPC1 decreases constitutive P-bodies in unstressed cells. Upon stress in PABPC1 depleted cells, individual P-bodies fail to form and instead reform in a merged manner with PABPC1-containing stress granules. Further, we propose interplay of PABPC1 and GW182 in P-body formation, and demonstrate that increased interaction of GW182 with PABPC1 can cause merged P-bodies and stress granules. These findings help us understand mRNP remodeling and P-body formation.

Introduction

Cytoplasmic messenger ribonucleoproteins (mRNPs) are suggested to cycle among polysomes, stress granules (SGs) and P-bodies (PBs). In this cycle, mRNAs exist in different functional states from translating, non-translating to degradation. While polysomes consist of translating mRNAs and SGs paused mRNAs with translation initiation components, PBs contain mRNA decay machineries (Decker and Parker, 2012).

PBs are present constitutively in unstressed cells, and further induced upon inhibition of translation initiation (Teixeira et al., 2005, Kedersha et al., 2005). PBs are closely related to control of translation and mRNA degradation. Proteins at PBs are involved in mRNA decay and translation repression, including decapping enzyme complex Dcp1/Dcp2; decapping activator hedls/GE-1; translation repressor and decapping activator DDX6/RCK, and the CCR4/NOT deadenylase complex (Anderson and Kedersha, 2006, Eulalio et al., 2007a).

SGs can be juxtaposed with PBs in animal cells(Kedersha et al., 2005, Stoecklin and Kedersha, 2013), which suggests that they are close in origin. SGs share some common

components with PBs, but distinctively contain translation initiation factors like PABPC1, eIF4G, eIF4A, eIF3 and eIF2 etc. (Decker and Parker, 2012). Assembly of PBs and SGs may start from non-translating mRNPs, which aggregate into microscopic granules through certain protein-protein interactions. In yeast, a self-interacting domain of Edc3 protein and prion-like glutamine/asparagine (Q/N) rich region of Lsm4 can facilitate the aggregation (Reijns et al., 2008, Decker et al., 2007). However, in metazoans, Edc3 is not required for PB assembly (Eulalio et al., 2007b). Instead, depletion of GW182 or hedls/GE-1, two proteins containing low-complexity and Q/N rich regions, leads to decreased PBs in unstressed animal cells (Eulalio et al., 2007b, Liu et al., 2005a, Yu et al., 2005, Kato et al., 2012).

One interesting issue is the absence of most translation initiation factors, including poly(A) binding protein cytoplasmic 1 (PABPC1), in P-bodies of mammalian cells. Components of RNA granules are in dynamic exchange with cytoplasmic proteins (Kedersha et al., 2005, Andrei et al., 2005). The association and dissociation of proteins, such as PABPC1, to and from the cap and tail of mRNA may be an important step in the transitions of mRNAs from translating to non-translating or decay states.

mRNAs have poly(A) tails at median sizes of about 50-100 nucleotides in mammalian cells (Chang et al., 2014, Subtelny et al., 2014). PABPC1 occupies around 27-residues on the poly(A) tail and forms repeating structures (Baer and Kornberg, 1983). PABPC1 is the major isoform out of four known in mammals. PABPC1 consists of four RNA binding domains (RRM 1-4) followed by a poorly conserved linker region and a protein-protein interaction (MLLE) domain at the C-terminus. The RRM domains are pivotal for closed loop formation of mRNA through the binding of the poly(A) tail and eIF4G (Kahvejian et al., 2005, Deo et al., 1999, Imataka et al., 1998, Safaee et al., 2012). The MLLE domain recognizes a conserved PAM2 peptide motif, found in a number of proteins including PB components GW182, Pan3 and Tob1/2 (Xie et al., 2014).

PABPC1 plays a double role regarding poly(A) tail of mRNA. mRNA is stabilized and protected by PABPC1 from deadenylation by Ccr4/Not deadenylases in yeast (Tucker et

al., 2002), possibly due to association with and protection of Pab1 to the poly(A) tail. Meanwhile, PABPC1 is required for deadenylation by Pan2/Pan3 deadenylase (Lowell et al., 1992, Zheng et al., 2008). The absence of PABPC1 in PBs is likely due to shortening of poly(A) in remodeling, as suggested by the absence of a signal for poly(A) RNA in PBs (Cougot et al., 2004). Nonetheless, active displacement of PABPC1 prior to deadenylation may exist. It was recently shown that PABPC1 helps recruiting microRNA-induced silencing complex (miRISC) through GW182, a major component of miRISC (Moretti et al., 2012). GW182, in turn, facilitates PABPC1 dissociation from silenced mRNA without deadenylation (Zekri et al., 2013).

Although PABPC1 displacement is a critical step in mRNA decay and can act as a scaffold protein on mRNA to recruit PB proteins GW182 and Pan3 etc. through PAM2 motifs, it is not known what role PABPC1 plays in assembling PBs. Here, we report that depletion of PABPC1 affects constitutive PB numbers in unstressed cells and causes merge of PB and SG components upon cell stress. By engineering GW182 to strengthen its binding to PABPC1, we simulated the merge of SGs and PBs. Overall, we conclude that PABPC1 may affect PB formation through interaction with GW182.

Results

PABPC1 protein depletion decreases constitutive PBs in unstressed cells

We were able to knock-down PABPC1 using two siRNAs previously characterized (Yoshida et al., 2006). The number of visible PBs decreased significantly upon PABPC1 knock-down in unstressed HeLa and MEF cells (Fig. 3.1A, and Fig. S3.2). PABPC1 depletion doesn't perturb the levels of the major translation factors (Yoshida et al., 2006). However, Paip2, a PABPC1-interacting protein, decreases in cells following PABPC1 depletion (Yoshida et al., 2006). To exclude a role of Paip2 in PB formation, we knocked down both isoforms, Paip2a and Paip2b, by siRNAs and found little effect on the number of PBs (Fig. 3.1B). It was reported that depletion of hedls or GW182 decreased PBs in cells (Eulalio et al., 2007b, Liu et al., 2005b, Yu et al., 2005). However, PABPC1 depletion does not lower hedls or GW182 protein levels (Fig. 3.1C), which suggests that PABPC1 is affecting PBs independently of changes in protein levels of hedls or GW182.

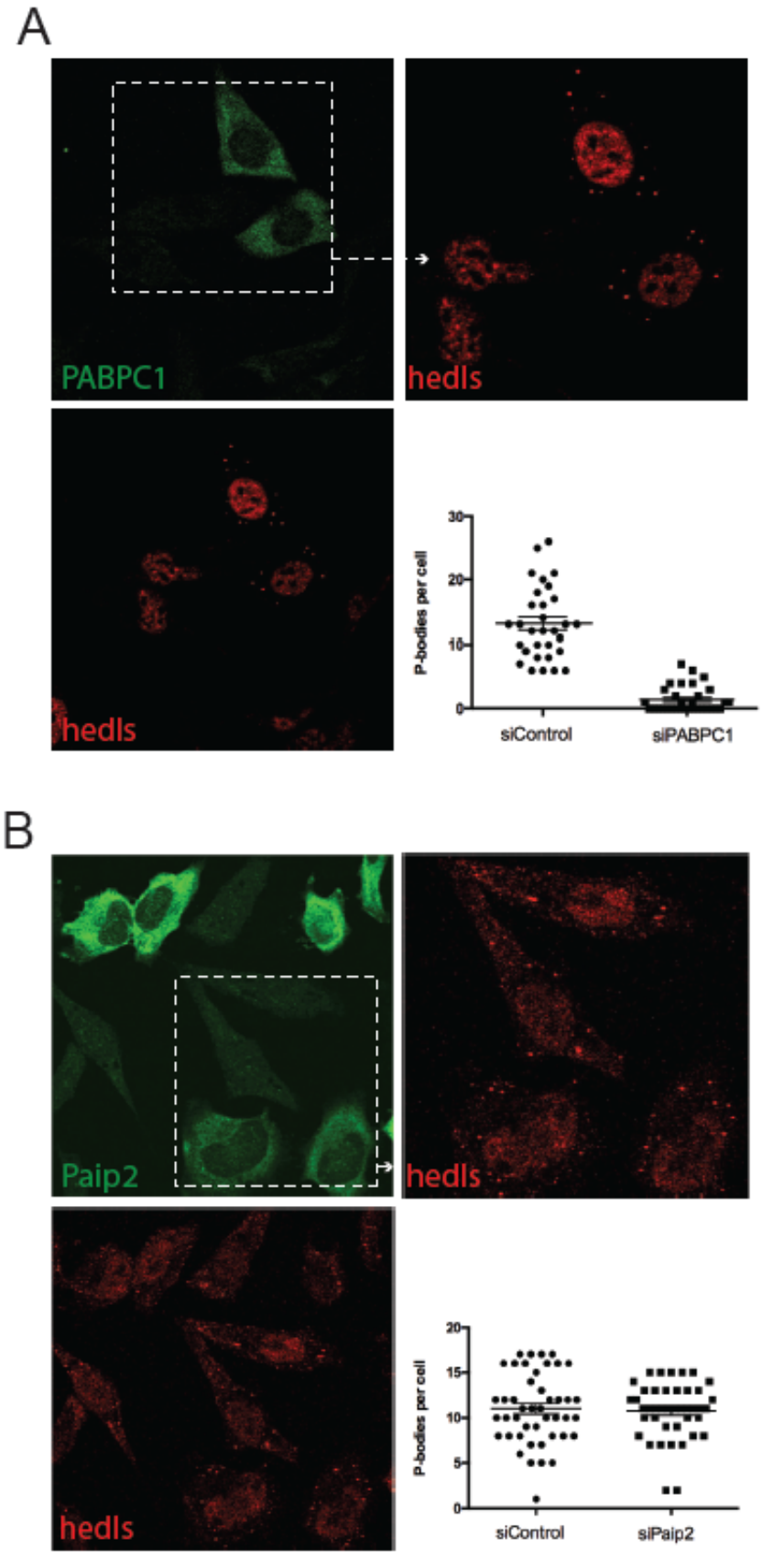
A
PABPC1
hedls
hedls
P-bodies per cell
30
20
10
0
siControl
siPABPC1
B
Paip2
hedls
hedls
P-bodies per cell
20
15
10
5
0
siControl
siPaip2

C

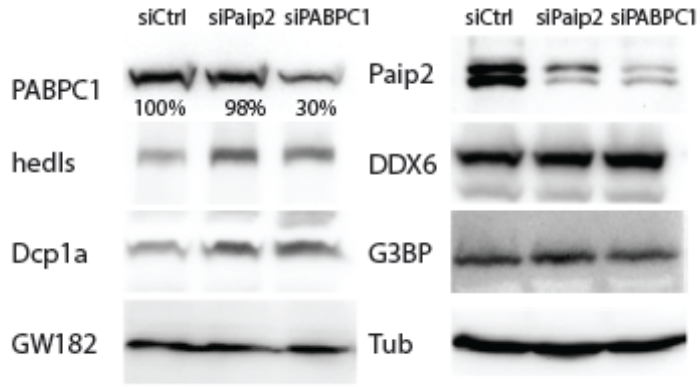

Figure 3.1 Constitutive P-body population, and protein levels after PABPC1 or Paip2 depletion. (A-B) HeLa cells transfected with scrambled siRNA were mixed with siPaip2 or siPABPC1 treated cells, to highlight knockdown effects and compare cells in the same environment. Staining of PABPC1 or Paip2 (*green*) indicated knockdown effects in cells. PB number was monitored by hedls (*red*). The anti-hedls antibody crossreacts with nuclear S6 kinase. Visible P-bodies of 50 cells were counted manually and sample deviation was calculated. The PB number in siPABP cells was significantly lower at 0.01 significance level using two-tailed t-test for two samples with unequal variance. (C) Western blot analysis of cell extracts showed that PABPC1 depletion did not significantly affect protein levels of hedls, DDX6, Dcp1a, G3BP, GW182 and tubulin compared to control or siPaip2 cells. Extracts were prepared 72 hours after siRNA knockdown, The Paip2 antibody recognized both Paip2a and Paip2b.

PBs can reform in a merged manner with stress granules in PABPC1 depleted cells

The approach of quantifying individual PB after siRNA treatment may be limited in some cases. PB population can be reduced by siRNAs unrelated to their silencing activities and individual PBs can often be re-induced by stress (Serman et al., 2007). Therefore, we checked whether individual PBs could be re-induced upon cell stress. In mammalian cells, PBs and SGs can be clearly distinguished. PBs are relatively compact and dense, while SGs are bigger, loose and more irregular (Stoecklin and Kedersha, 2013, Souquere

et al., 2009, Kedersha et al., 2005). When we treated PABPC1-depleted cells with arsenite to induce PBs and SGs, we found that individual compact dense PBs failed to form. Instead, PBs marked by hedls or Dcp1a merged with SGs marked by PABPC1 (Fig. 3.2). The colocalization was observed across the cytoplasm by 3D confocal microscopy. To our knowledge, DDX6, a RNA helicase also known as RCK/p54, can trigger merged PB/SG and prevent PB formation when depleted (Mollet et al., 2008, Serman et al., 2007, Ayache et al., 2015). However, DDX6 protein levels remained unchanged after PABPC1 depletion (Fig. 3.1C). Thus, PABPC1 affects PB formation independently of DDX6.

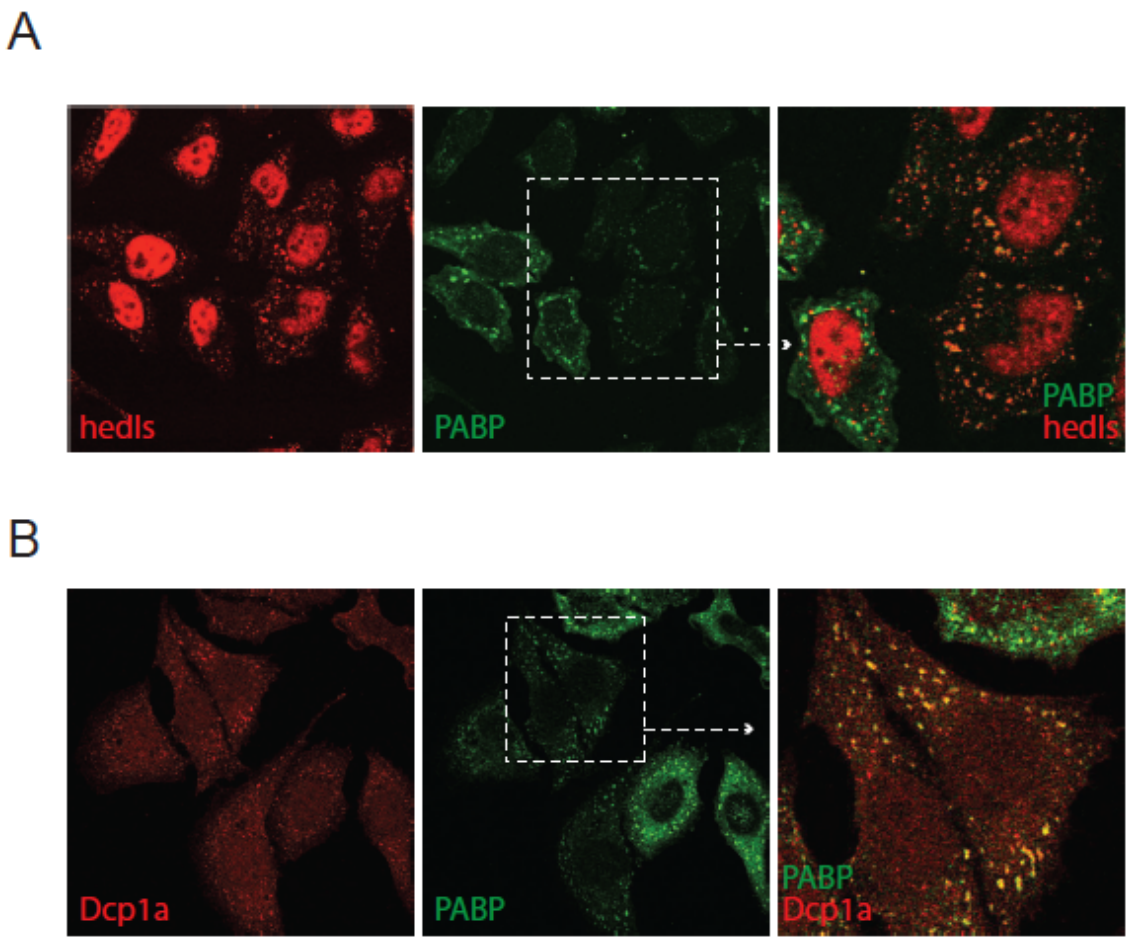

Figure 3.2 Merging of P-bodies and stress granules in PABPC1-depleted cells. HeLa cells were treated with 0.5 mM sodium arsenite for 0.5 hour before fixation. The PB labeled (*red*) by hedls (A) or Dcp1a (B) formed loose and irregular granules, colocalized with SGs labeled by PABPC1 (*green*).

SG is independent of PB assembly and can assemble in depletion of PABPC1

We checked SG assembly in stressed cells, and found SGs marked by G3BP, HuR (Fig. S3.1A & B) or Ago2 could assemble after PABPC1 depletion. This implies that SGs can form in the presence of low levels of PABPC1 protein. The assembly of PBs and SGs are independent processes (Kedersha et al., 2005, Kedersha et al., 2016). PBs exist in unstressed cells in the absence of SGs. Meanwhile, PBs can be increased by arsenite stress in MEF cells expressing non-phosphorylatable eIF2α mutant, which prevents SG formation (Kedersha et al., 2005). We treated HeLa cell overnight with 10 μM PP242, an mTOR inhibitor of SG assembly (Fournier et al., 2013, Feldman et al., 2009), and found PBs were increased by arsenite without SG formation (Fig. S3.1C). This implies that PBs do not require SGs to form, in agreement with previous studies (Kedersha et al., 2005).

Separate PBs can be induced after SG inhibition in PABPC1 depleted cells

PBs assembly is closely related to PABPC1-containing SGs at low PABPC1 levels. We then asked whether formation of SG structures were required or not in such process. After treatment of 10 μM PP242 overnight to inhibit SG assembly, we stressed PABPC1-depleted cells with arsenite and individual PBs began to form (Fig. S3.1D). It indicates that in depletion of PABPC1, PBs tend to merge with SGs following certain component(s) enriched at stress granules.

How could PABPC1, absent from PBs, affect PB formation? One hypothesis is that PB assembly may initiate on PABPC1-containing mRNPs. When the residual PABPC1 after depletion is packed into SGs, PB components are recruited there and thus merged PB/SG emerges. We speculated that certain PB proteins interacting with PABPC1 might mediate the processes. GW182 proteins (including isoforms TNRC6A, TNRC6B, and TNRC6C in human) interact with PABPC1 through the MLLE domain and are required for PB assembly (Eulalio et al., 2007b; Liu et al., 2005a). Besides, the interaction of GW182 with PABPC1 through PAM2 is modulated by phosphorylation, which takes place

extensively under stresses (Huang et al., 2013). Depletion of PABPC1 leads to less competition for GW182 by reduction of Paip2, a competitor of GW182 to bind PABPC1. Therefore, PABPC1/GW182 interaction may become more stable, resulting in merging of PBs and SGs.

Creating merged PB/SG without PABPC1 depletion

We used a protein engineering approach to test our hypothesis. We modified the PAM2 sequence of TNRC6A, an isoform of human GW182 proteins. The natural affinity of the GW182 PAM2 motif for MLLE of PABPC1 is about 6 μM (Kozlov et al., 2010b, Jinek et al., 2010). PAM2 motifs of TNRC6A or Paip2 both contain a phenylalanine critical for binding MLLE, but extend in different directions as shown in right panel of Fig. 3.3A. We designed a super-PAM2, including features of TNRC6A and Paip2 PAM2s to bind an extended surface on MLLE (Fig. 3.3A). The super-PAM2 peptide binds PABPC1 about 300 times tighter than PAM2 of TNRC6A (Fig. 3.3A). Fusion of the super-PAM2 peptide to green fluorescent protein (GFP) can target GFP to stress granules (Fig. 3.3B). Thus, super-PAM2 peptide can be a targeting signal to SGs when fused to protein, through interaction with PABPC1. Replacement of the wild-type PAM2 sequence of TNRC6A by the super-PAM2 sequence greatly strengthened association of TNRC6A and endogenous PABPC1 as shown by immunoprecipitation (Fig. 3.3C, construct information in Materials and Methods). When we stressed cells overexpressing super-TNRC6A-GFP, the super-TNRC6A along with other PB components located to SGs to make merged PB/SG (Fig. 3.4). The same results were observed using engineered super-TNRC6B (Data not shown). It indicates that PABPC1 interacting proteins, like GW182, could play an important role in PB assembly through interaction with PABPC1.

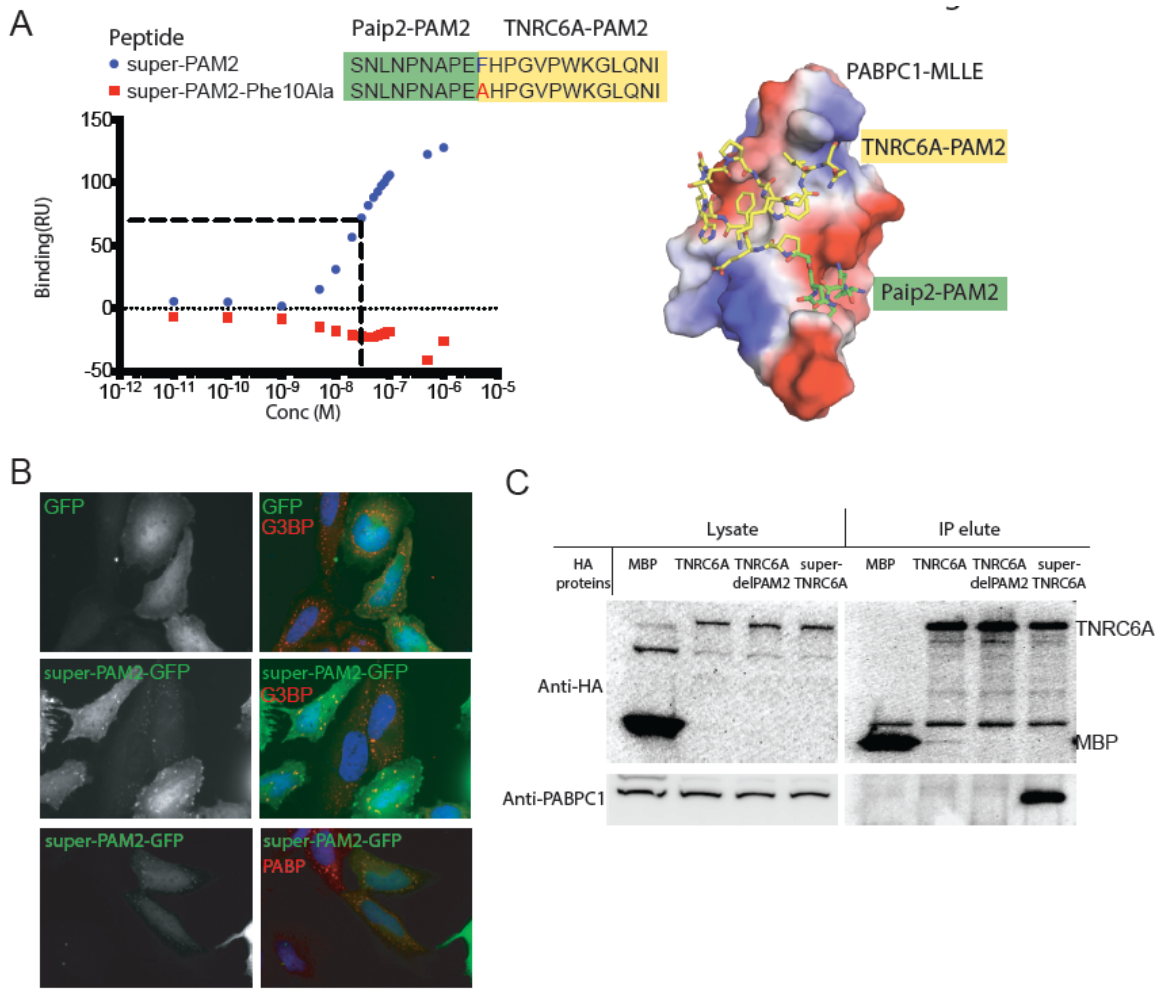

Figure 3.3 Characterization of super-PAM2 peptide and super-TNRC6A. (A) The super-PAM2 motif combines the PAM2 motifs from Paip2 and TNRC6A and binds an extended surface on the PABPC1 MLLE domain (PDB: 3KUS and 3KTP). Surface plasmon resonance measured an affinity of 20 nM for super-PAM2 peptide binding to the MLLE of PABPC1. The Phe10Ala mutant does not bind and is used as negative control. (B) Super-PAM2 serves as targeting signal to SGs. Overexpressed super-PAM2-GFP (*green*) fusion protein localized to PABP or G3BP (*red*) marked SGs upon sodium arsenite treatment. (C) HA-tagged MBP, TNRC6A, TNRC6AΔPAM2 or TNRC6A containing the super-PAM2 motif (super-TNRC6A) were transfected in HeLa cells. Immunoprecipitation with anti-HA antibodies showed stronger interaction of super-TNRC6A with endogenous PABPC1. The weak association between TNRC6A with its normal PAM2 motif and PABPC1 was not detected due to harsh washings.

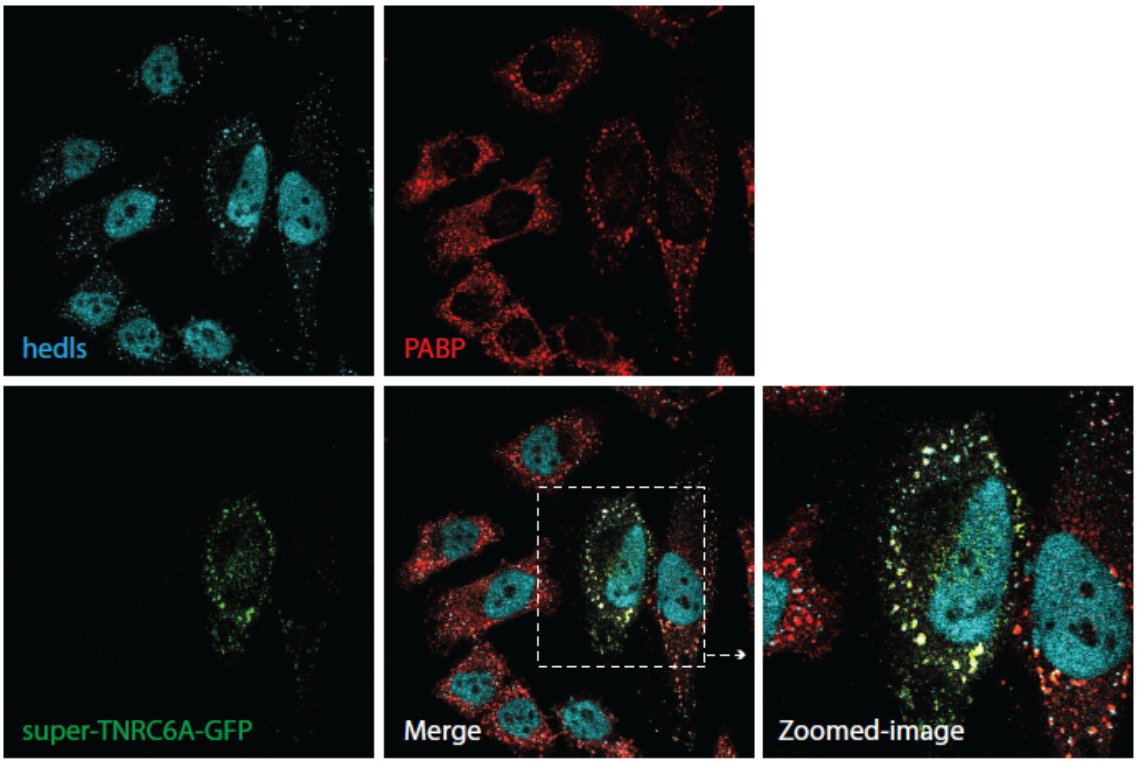

Figure 3.4 Simulation of merged P-body/Stress granule using super-TNRC6A. HeLa cells overexpressing super-TNRC6A-GFP (*green*) were stressed by sodium arsenite and stained with anti-hedls (*cyan*) for P-bodies and anti-PABPC1 (*red*) for SGs.

Discussion

PABPC1 recognizes poly(A) tail of mRNA and plays important role in mRNA metabolism. Here, we have shown that PABPC1 protein level is critical to PB assembly. Depletion of PABPC1 decreases the number of constitutive PBs. When the PABPC1-depleted cells are stressed, PBs reform in a merged manner with SGs. We have demonstrated that GW182 could be one factor linking PABPC1 level and PB formation.

There can be at least two different explanations for the effects of PABPC1 on PBs. The first explanation is structural (Fig. S3.3). PB assembly may initiate on PABPC1-containing mRNPs. PABPC1 might be required in mRNP remodeling into P-bodies, thus PABPC1 depletion decreases PB numbers in unstressed conditions. The requirement of

PABPC1 for PB formation drives PB components to certain SGs, where the residual PABPC1 is enriched after depletion. The decrease of Paip2 protein level, and the possibly increased interaction of GW182 PAM2 with PABPC1 by stress related phosphorylated (Huang et al., 2013), could contribute to increased GW182/PABPC1 association and formation of merged PB/SG. Meanwhile, the displacement of PABPC1 from microscope-visible PBs may be a critical step in PB assembly as was proposed by other colleagues (Chen and Shyu, 2013). We assume that the displacement of PABPC1 at SG is difficult so individual PBs fail to form. When SG formation is inhibited by PP242, the same residual amount of PABPC1 in cytoplasm can support normal PB formation. It implies that the ability of PABPC1 to disassociate from mRNPs is required for formation of individual PBs. However, the mechanisms regarding how and when PABPC1 disassociates from mRNP are still to be investigated.

A second explanation is that depletion of PABPC1 may reduce the pool of translationally repressed mRNAs and thus the constitutive PB population. In higher eukaryotes, PABPC1 functions in translation and miRNA silencing. It is reasonable that PABPC1 level relates to pool of repressed mRNAs. Interestingly, effects of PABPC1 depletion on PBs in human are different from those of yeast where Pab1 depletion leads to an increase in PBs (Brengues and Parker, 2007). This is likely because there is no miRNA silencing in yeast. Further, when stress is applied, the pool of repressed mRNAs grows, to support PB formation. The merge of PB and SG can be due to decrease of Paip2, a competitor of GW182 in binding PABPC1, which makes interaction of GW182 and PABPC1 more stable. However, knockdown of Paip2 does not lead to merge of PB/SG (Data not shown). Most likely, the effect of PABPC1 on PB formation is a mixture of structural impact and changes in pool of repressed mRNAs. Although strengthening the binding of GW182 to PABPC1 can simulate merge of PBs and SGs, there can be other mediators between PABPC1 and PB formation. Mechanistic details need further studying. We look forward to future studies on roles of PABPC1 in mRNA metabolism.

Materials and methods

Plasmids and siRNA

pT7-EGFP-C1-HsTNRC6A, pT7-EGFP-C1-HsTNRC6B, pT7-EGFP-C1-HsRCK (DDX6), pT7-EGFP-C1-HsDcp1a, and pT7-EGFP-C1-HsDCP2 were gifts from Elisa Izaurralde (Addgene plasmid # 25030, 25031, 25033, 25034, 25035)(Tritschler et al., 2009). Sequence (agcaatctgaatccaaatgca) encoding amino acids SNLNPNA was inserted between nucleotides 4827A and 4828C of TNRC6A, or 4431T and 4432C of TNRC6B to create super-GW182. Reverse-PCR was used for constructing TNRC6AΔAgo (Δ7-300) and TNRC6AΔQ/N (Δ360-402). Plasmids expressing HA-MBP, HA-TNTC6A and HA-TNRC6AΔPAM2 were generous gifts from Drs. Eric Huntzinger and Elisa Izaurralde (Huntzinger et al., 2010). PABPC1 was inserted between BamH I and Not1 of pCDNA3-EGFP. siRNAs were synthesized at Dharmacon. The siRNA sequences used were siPABPC1 (5'-AAGGUGGUUUGUGAUGAAAAU-3', 5'-AAUCGCUCCUGAACCAGAAUC-3'), siPABPC1_2 (5'-AACUAAGACCAAGUCCUCGCU-3'), siPaip2 (5'-GAGUACAUGUGGAUGGAAAUU-3', 5'- UGGAAGAUCUUGUGGUCAAUU-3'). Control siRNA was purchased from Qiagen (SI03650318).

Cell culture and transfections

HeLa S3 or MEF cells were cultured in DMEM supplemented with 10% fetal bovine serum. 10^5 cells were plated per well in 24-well plate the day before transfection. 60-90 pmol siRNA or 0.8 μg DNA plasmid was mixed with 2 μl Lipofectamine 2000 in Opti-MEM and then added to cells. After 48 hours, cells were trypsin digested and split onto cover slides. Cells were treated and fixed after another 24 hours. For western analysis, cells were harvested after 72 hours after transfection in SDS loading buffer.

Immunofluorescence and confocal microscopy

Cells were fixed with cold methanol (-20°C) for 10 minutes and then treated with 0.1% Triton X-100 in 1x PBS. Cells were blocked with 5% normal goat serum (Millipore S26) in PBS. Cells were incubated in 1x PBS, supplemented with anti-PABPC1 (Abcam ab21060; Santa Cruz sc32318)(1:200), anti-hedls (Santa Cruz sc8418)(1:1000), anti-Paip2 (Sigma-Aldrich P0087)(1:500), anti-eIF4G1 (Sigma-Aldrich AB-1232)(1:200),

anti-Ataxin-2 (BD Biosciences 611378)(1:200), anti-HA (Covance MMS-101P)(1:200), anti-Dcp1a (Abcam ab47811)(1:200), anti-DDX6 (Abcam ab40684)(1:200), anti-EDC4 (hedls)(Abcam ab72408)(1:200), anti-Ago1 (Santa Cruz sc53521)(1:200), anti-G3BP (gift of Dr. Imed Gallouzi)(1:500) or anti-HuR (gift of Dr. Imed Gallouzi)(1:200). Cells were washed in PBS 3 times, before incubated with corresponding second antibodies conjugated with Alexa488 or Alexa647 (Sigma-Aldrich A31620, A31628, A31571) or Dylight550 (Bethyl A120-101D3) or Rhodamine (Millipore 12-509, 12-510) at 1:200 – 1:500 dilutions. DAPI (Roche) was added to washing buffer at 0.5μg/ml to treat cells for 10 minutes. Cover slides were finally mounted in ProLong Gold antifade reagent (Life technology P36930). Images were collected on Zeiss LSM 310 confocal microscope in the McGill University Life Sciences Complex Advanced BioImaging Facility (ABIF). PBs were counted manually in a sample size of 50 cells for each group. Sample deviation was calculated within group.

Western blotting

Protein samples were heated at 95°C and separated in SDS-PAGE. Proteins were then transferred to PVDF membrane in Tris/glycine buffer, with 20% methanol in cold room. PVDF membrane was blocked in 1x TBS (pH 7.5), containing 0.05% Tween-20 and 5% skim milk powder or bovine serum albumin. Besides antibodies above, anti-GW182 (Novus NBP1-88232)(1:200) and anti-tubulin (Sigma-Aldrich T9028) were also used for detection of related proteins.

Immunoprecipitation

Cells were lysed in 20 mM Hepes (pH 7.4), 150 mM NaCl, 0.5% NP-40, 2 mM DTT, 2 mM $MgCl_2$, 1 mM $CaCl_2$ and protease inhibitor tablet (Roche), and cleared by centrifugation. Optimized amount of antibodies were added to cleared lysate for 2 hours. Dynabeads protein A or protein G were washed and added to lysate for 0.5 hour. Dynabeads were then washed with 1x PBS and boiled in SDS loading buffer for further analysis.

Surface plasmon resonance

GST-MLLE protein was applied to Series S sensor chip CM5 bound with anti-GST antibodies (GE Healthcare BR100223) in a Biacore T100. After washing, various concentrations of super-PAM2 (SNLNPNAPEFHPGVPWKGLQ) or super-PAM2-Phe10Ala (SNLNPNAPEAHPGVPWKGLQ) were added to GST-MLLE captured on chip. The corresponding steady states measured in relative units (RU) were plotted versus concentrations of peptides in the flow system to estimate dissociate constants.

Acknowledgements

We acknowledge Drs. Elisa Izaurralde, Witold Filipowicz and Imed Gallouzi for generously sharing plasmids or antibodies. We are grateful for suggestions and help from colleagues during the project.

Competing interests

No competing interests declared.

Author contributions

J.X. designed the experiments. Y.C. and X.W. assisted J.X. in carrying out the experiments. G.K. designed the super-PAM2 sequence. J.X. and K.G. prepared the manuscript.

Funding

This study was supported by Canadian Institutes of Health Research grant MOP-14219. J. X. was supported by the CIHR Strategic Training Initiative in Chemical Biology, the CIHR Strategic Training Initiative in Systems Biology, Graduate Student Scholarship of the Quebec Network for Research on Protein Function, Engineering, and Applications (PROTEO), and Award of the Groupe de Recherche Axé sur la Structure des Protéines (GRASP).

Supplemental materials

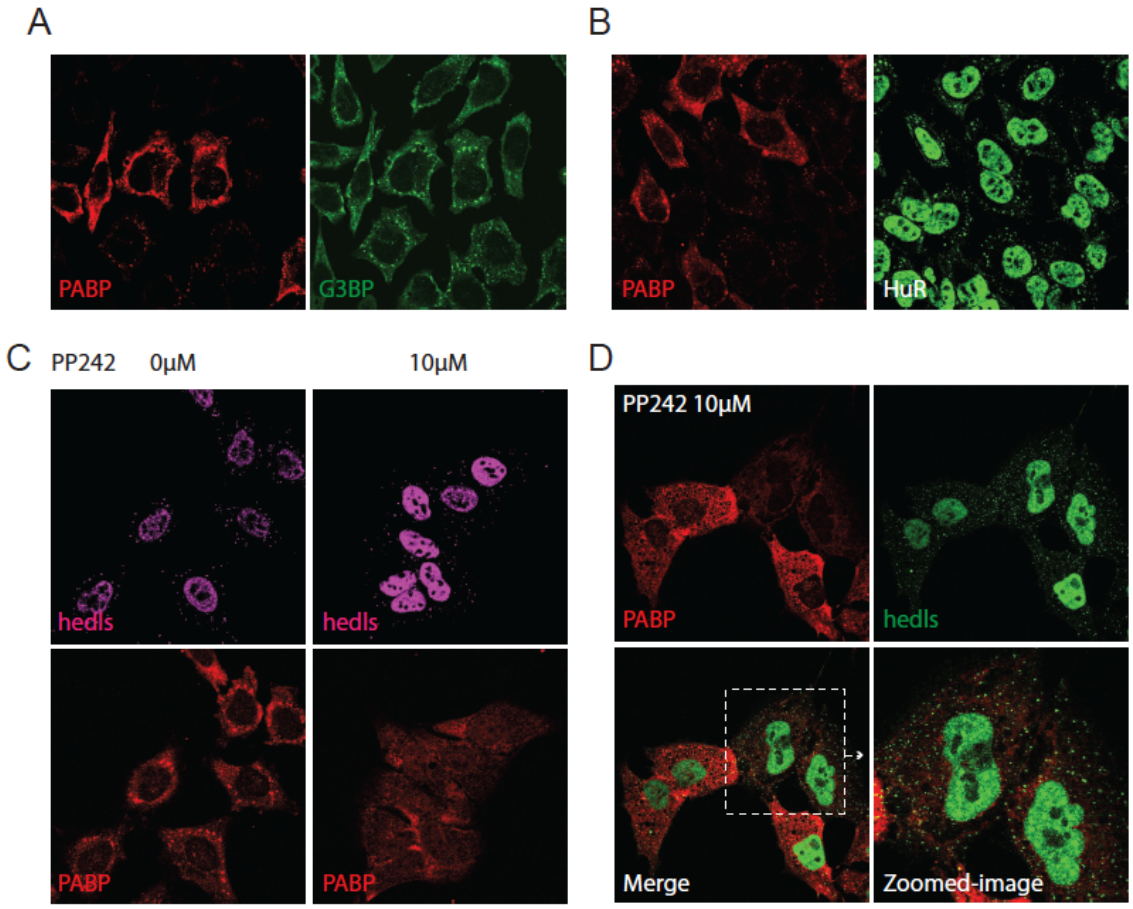

Figure S3.1 (A-B) Stress granule can assemble after PABPC1 depletion. PABPC1 depleted cells (Red) displayed similar SG pattern to control cells, stained by anti-G3BP or anti-HuR (*green*). (C) P-bodies form independent of SGs. HeLa cells treated by PP242 overnight failed to form SGs (*red*), but had normal PBs present. (D) Separate PBs can be induced after SG inhibition in depletion of PABPC1. HeLa cells were treated with 10μM PP242 overnight before stressed in 0.5 mM sodium arsenite for 0.5 hour. Individual PBs (*green*) formed in PABPC1 depleted cells (*red*).

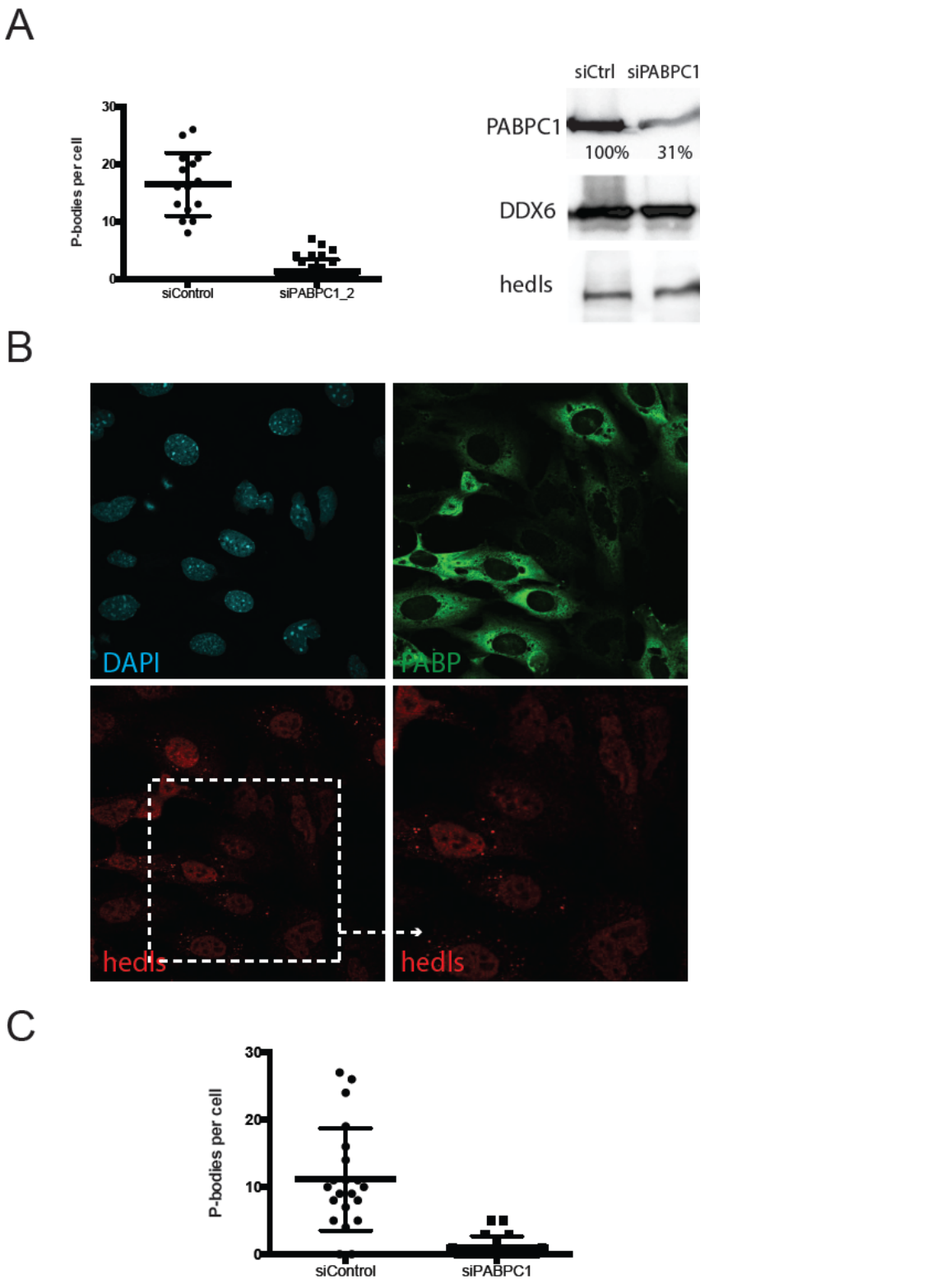

Figure S3.2 Constitutive P-body population, and protein levels after PABPC1 depletion in MEF cells or with a second siRNA in HEK293. (A) HeLa cells transfected with

scrambled siRNA were mixed with cells treated by a second siPABPC1, to highlight knockdown effects and compare cells in the same environment. Visible P-bodies of 30-50 cells were counted manually and sample deviation was calculated. The PB number in siPABP cells was significantly lower at 0.01 significance level using two-tailed t-test for two samples with unequal variance. Western blot analysis of cell extracts showed knockdown of PABPC1 did not significantly affect protein levels of hedls or DDX6. (B-C) MEF cells transfected with scramble siRNA were mixed with siPABPC1 treated cells, to highlight knockdown effects and compare cells in the same environment. Staining of PABPC1 (*green*) indicated knockdown effects in cells. PB number was monitored by hedls (*red*). The anti-hedls antibody crossreacts with nuclear S6 kinase. Visible P-bodies of about 50 cells were counted manually and sample deviation was calculated. The PB number in siPABP cells was significantly lower at 0.01 significance level using two-tailed t-test for two samples with unequal variance.

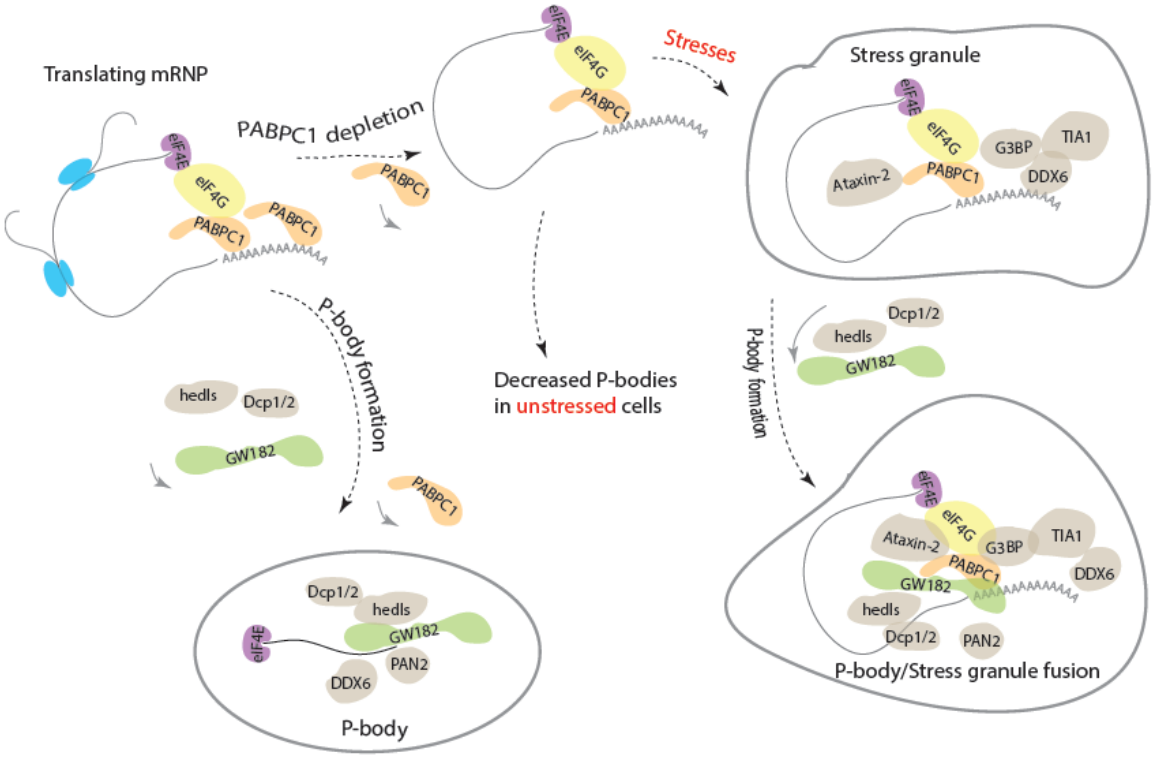

Figure S3.3 P-body formation. PB assembly may initiate on PABPC1-containing mRNPs. The requirement of PABPC1 in PB formation drives PB components to stress

granules, where the residual PABPC1 is enriched after depletion. However, the displacement of PABPC1 is difficult in SG and then individual PBs fail to form.

Connecting text 2

In the previous two chapters, I have shown functional studies regarding the MLLE domain of PABPC1. Meanwhile, my colleagues and I are continuing our search for PAM2 containing proteins, which recognize MLLE domain. Structural studies show that PAM2 motifs bind MLLE in a very conserved pattern. Here, I report that LARP4, a RNA binding protein, contains a novel PAM2 motif, which harbors a variant residue critical for interaction. Identification of the variant form of PAM2 expands our knowledge of the protein interaction network recognizing MLLE domain found in PABPC1 and EDD. This facilitates future identification of more PAM2-containing proteins and our understanding of PABP.

Chapter 4: LARP4 binds poly(A), interacts with poly(A)-binding protein MLLE domain via a variant PAM2w motif and can promote mRNA stability

Ruiqing Yang[1], Sergei A. Gaidamakov[1], Jingwei Xie[3], Joowon Lee[1], Luigi Martino[2], Guennadi Kozlov [3], Amanda K. Crawford[1], Amy N. Russo[1], Maria R. Conte[2], Kalle Gehring[3], Richard J. Maraia[1,4]

[1]Intramural Research Program on Genomics of Differentiation, *Eunice Kennedy Shriver* National Institute of Child Health and Human Development, National Institutes of Health, Bethesda, MD. , USA

[2]Randall Division of Cell and Molecular Biophysics, King's College London, UK.

[3]Department of Biochemistry, McGill University, Montreal, QC, Canada

[4]Commissioned Corps, U.S. Public Health Service.

Running Title: LARP4 is a polysome-associated mRNA factor

Abbreviations: PABP, poly-A binding protein, LaM, La motif, RRM, RNA recognition motif, PAM2, PABP interaction motif-2, ITC, isothermal titration calorimetry.

*To whom correspondence should be directed at:
31 Center Drive,
Bld. 31, Rm 2A25
Bethesda, MD 20892-2426
Phone: 301-402-3567
Fax: 301-480-6863
E-mail: maraiar@mail.nih.gov

Published in Molecular and Cellular Biology, volume 31, issue 3, pages 542-256.

doi: 10.1128/MCB.01162-10

ABSTRACT

The conserved RNA binding protein La recognizes UUU-3'OH on its small nuclear RNA ligands and stabilizes them from 3' end-mediated decay. We report that La-related protein-4 (LARP4) is a newly described factor that can bind poly(A) RNA and interact with poly(A) binding protein (PABP). Yeast two-hybrid analysis and reciprocal IPs from HeLa cells reveal that LARP4 interacts with RACK1, a 40S ribosome- and mRNA-associated protein. LARP4 cosediments with 40S ribosome subunits and polyribosomes, and its knockdown decreases translation. Mutagenesis of the RNA binding or PABP interaction motifs decrease LARP4 association with polysomes. Several translation and mRNA metabolism-related proteins use a PAM2 sequence containing a critical invariant phenylalanine to make direct contact with the MLLE domain of PABP, and their competition for the MLLE is thought to regulate mRNA homeostasis. Unlike all ~150 previously analyzed PAM2 sequences, LARP4 contains a variant PAM2 with tryptophan (PAM2w) in place of the phenylalanine. Binding and NMR studies show that a peptide representing LARP4 PAM2w interacts with the MLLE of PABP within the affinity range measured for other PAM2 motif peptides. A cocrystal of PABC bound to LARP4 PAM2w shows tryptophan in the pocket in PABC-MLLE otherwise occupied by phenylalanine. We present evidence that LARP4 expression stimulates luciferase reporter activity by promoting mRNA stability, as shown by mRNA decay analysis of luciferase and cellular mRNAs. We propose that LARP4 activity is integrated with other PAM2-protein activities by PABP as part of mRNA homeostasis.

INTRODUCTION

The RNA binding domain of the conserved La protein consists of a La motif (LaM) and RNA recognition motif (RRM) that work together to recognize UUU-3'OH on small nascent transcripts and protect them from 3' exonucleases (Bayfield and Maraia, 2009, Maraia and Bayfield, 2006). In addition to this, La proteins can modulate mRNA translation (Svitkin et al., 1994, Holcik and Sonenberg, 2005, Svitkin et al., 1996, Svitkin et al., 2009). The LaM-RRM arrangement has been found in La-related proteins (LARPs) 1, 1b, 4, 4b, 6 & 7 that have been separately conserved during evolution (Bousquet-Antonelli and Deragon, 2009, Bayfield et al., 2010a) (LARP4b is also referred to as LARP5 in multiple databases and will be designated hereafter as LARP5/4b). LARP7 is specific for 7SK snRNA which it recognizes in part via UUU-3'OH (He et al., 2008, Markert et al., 2008). LARP6 binds to a stem-loop in the 5' UTRs of collagen mRNAs in a Uracil-dependent manner (Cai et al., 2009) and LARP1 was shown to bind poly(U) and to a lesser extent poly(G) but not (A) or (C) (Nykamp et al., 2008). Consistent with these specificities, LARPs 1, 6 & 7 have conserved all of the amino acids involved in UUU-3'OH recognition in La-RNA crystals (Kotik-Kogan et al., 2008, Teplova et al., 2006), while LARPs 4 and 5/4b have diverged, suggesting alternative RNA binding (Bayfield et al., 2010a). Moreover, an invariant divergence in all of the LARP4 and 5/4b sequences available occurs in a most critical residue involved in base-specific recognition seen in La-RNA crystals, corresponding to human La Q20, suggesting a conserved difference in RNA recognition (Bayfield et al., 2010a). Although the LaM-RRM in La protein recognizes RNA in a unique way (Bayfield et al., 2010a, Maraia and Bayfield, 2006) whether LARPs share this or have adopted alternative modes of RNA recognition is unknown.

Of the LARP families studied for function, LARPs 1, 5/4b and 6 appear to be involved in mRNA metabolism and/or translation (Blagden et al., 2009, Cai et al., 2009, Nykamp et al., 2008, Schaffler et al., 2010, Burrows et al., 2010). Of these, LARPs 1 and 5/4b interact with poly(A) binding protein (PABP) although the precise mechanisms were not reported (Blagden et al., 2009, Burrows et al., 2010, Schaffler et al., 2010), whereas LARP6 appears to block assembly of its associated mRNAs with initiating ribosomes (Cai et al., 2009).

Translation is facilitated by interactions of the 5' cap and 3' poly(A) of the mRNA by eukaryotic initiation factors 4E (eIF4E) and PABP (Martineau et al., 2008a). The translation initiation activity of PABP can be regulated by PABP-interacting protein-1 (Paip1) which stabilizes initiation complexes via interactions with the 40S ribosome (Craig et al., 1998, Martineau et al., 2008a). Multiple molecules of PABP can bind poly(A) tails (Baer and Kornberg, 1980, Mangus et al., 2003) and some data suggest that at least two molecules of poly(A)-associated PABP are required for efficient translation initiation (Amrani et al., 2008). PABP can engage a variety of protein partners via their common PABP interaction motif-2 (PAM2) sequences, including Paip1, Paip2, eRF3, GW182 (TNRC6C), Ataxin-2, Tob2, and poly(A) nuclease, representing different mechanisms of control involving translation initiation and termination as well as mRNA stability (Roy et al., 2002, Siddiqui et al., 2007, Derry et al., 2006, Uchida et al., 2002, Mangus et al., 2003, Kahvejian et al., 2005, Jacobson, 2005, Kozlov et al., 2010b). Since the PAM2 motifs make direct contacts to the MLLE domain of PABP (Kozlov and Gehring, 2010, Kozlov et al., 2010a), proper signal integration presumably involves their competition for PABP (Funakoshi et al., 2007). A model in which the PAM2 motifs of eRF3 and poly(A) nucleases compete for PABP reflects a balance of translation termination and mRNA deadenylation activities (Kozlov and Gehring, 2010, Funakoshi et al., 2007, Ruan et al., 2010, Kozlov et al., 2010b).

In rat neurogenic cells LARP5/4b (KIAA0217) was a component of a mRNA-protein (mRNP) complex associated with PABP that could bind poly(A) in a Northwestern blotting assay although no other RNAs were tested (Angenstein et al., 2002). A recent report demonstrated that two broad regions of LARP5/4b interact with PABP to stimulate translation, although RNA binding was not examined (Schaffler et al., 2010). While human LARPs 4 and 5/4b are most homologous in their LaM-RRM, they share patchy homology in the ~500 amino acids outside this region (Bayfield et al., 2010a). Here we identify variant PAM2 motifs in LARP4 and 5/4b that contain Trp in place of the otherwise critical invariant Phe (Bayfield et al., 2010a) found in all other ~150 PAM2 sequences examined (Albrecht and Lengauer, 2004) that we refer to as PAM2w hereafter.

We show that the LaM-RRM of human LARP4 preferentially binds poly(A) and exhibits other characteristics that suggest a different recognition mode as compared to La proteins. Screening of a human cDNA library for yeast 2-hybrid interactions with LARP4 yielded RACK1 a 40S and mRNA-associated kinase (Coyle et al., 2009, Nilsson et al., 2004) which was confirmed by reciprocal immunoprecipitations from HeLa cells. LARP4 is cytoplasmic and interacts with PABP via two regions, the PAM2w and a region following the RRM that includes ~70 residues with significant homology to LARP5/4b. A peptide representing PAM2w of human LARP4 and the MLLE domain of PABP were examined by binding, NMR and crystallography which showed direct interactions similar to other PAM2-MLLE complexes. Further consistent with a translation-related function, LARP4 cosediments as two peaks on polysome profiles, with 40S ribosomes and with PABP on polysomes. After LARP4 knockdown, polysome profiles indicate deficiency in translation initiation with 35S-methionine incorporation into newly synthesized protien diminished by ~20%. LARP4 appears to promote translation in part by stabilizing mRNA as suggested by our decay analyses.

MATERIALS AND METHODS:

Cloning

HeLa polyA+ RNA (Ambion) was used to make LARP4 cDNA which was cloned into *HindIII-BamHI* sites of pFlag-CMV2 (Sigma-Aldrich). Deletion and substitutions were by PCR and QuikChange XL (Stratagene). The F-LARP4-M3 mutations were K124D, K125A, Q126D, D139K, Y141D, in the La motif, and I202D and R204D in the RRM1 β-1. All constructs were verified by sequencing.

Immunofluorescence

Immunofluorescence used anti-Flag followed by anti-mouse IgG-Cy3 or anti-LARP4 followed by anti-rabbit IgG-Cy3. Hoechst (blue) stained nuclei.

Immunoblotting

Secondary Ab used for detection was anti-rabbit IgG (GE, UK) or anti-mouse IgG (Cell Signaling), and processed for chemiluminescence using SuperSignal West Dura kit

(Thermo Scientific). In most cases, a single membrane was probed, exposed and stripped (Restore Western Blot Stripping buffer, Thermo Scientific), before probing with a different Ab.

Immunoprecipitation

Immunoprecipitation was by anti-FLAG M2 affinity gel (Sigma-Aldrich) using 20 μl of gel bead volume and 1 mg total cellular protein. 1 ml of cell lysate in PLB containing 25 mM EDTA, 2 mM DTT, and proteinase and RNA'se inhibitors, was incubated with beads pre-washed with NT2 buffer (50 mM Tris-HCl, pH 7.5, 150 mM NaCl, 1 mM MgCl, 0.05% NP-40) for 4 hrs at 4ºC followed by 5 washes with NT2. After elution with hot SDS buffer, fresh beta-mercaptoethanol was added and samples were loaded.

Antibodies

Anti-rpS6 and -PABP were from Cell Signaling, anti-Flag and anti-GAPDH from Sigma Aldrich, anti-rpL28 from Santa Cruz, anti-RACK1 from TRansduction Laboratories, and anti-Paip1 was a gift from N. Sonenberg. Rabbit anti-LARP4 was obtained using the LARP4 C-terminal sequence CGVTRRNGKEQYVPPRSPK as antigen and affinity purified using the same peptide (Open Biosystems).

Polysome profiles

Polysome profiles were prepared from fresh extract made from HEK-293 cells by standard methods (Baroni et al., 2008) using a Programmable Density Gradient Fractionation System Spectrophotometer (Foxy Jr. model, Teledyne Isco, Lincoln). Gradients was made using a Gradient Master (Biocomp). After 15 min exposure to cycloheximide (100 μg/ml) cells were lysed with polysome lysis buffer (PLB) (10 mM HEPES pH 7.0, 100 mM KCl, 5 mM MgCl, 5% NP-40). 150 μl of cell lysate (2 mg total protein) was layered on 5-45% sucrose gradients and centrifuged at 39,000 X g for 2 hrs.

RNA binding

RNA binding using EMSA was described (Huang et al., 2006) with recombinant La-NTD(1-235) and LARP4-NTD(1-286) purified from *E. coli*. Sequence of the 36'mer

RNA: 5'-GAACACUUUGGCGCUCAAUGCGCCCUUCGUUAAAAA-3'. Each 32P-labeled RNA was purified by excision a tight band from denaturing 20% polyacrylamide gel.

Yeast 2-hybrid

Yeast 2-hybrid used full length LARP4 and was performed by Hybrigenics S.A Services (Paris, France) using a human liver cDNA library.

siRNAs

siRNAs targeting LARP4 #1, #2 and PABP were from Invitrogen, and LARP4 #3 was from Dharmacon. siRNAs sequences: LARP4 #1: AACAGAGGAAUCUUCUA-UUAGAUCC, LARP4 #2: AAGAACUGAAGAUGGCUCUUUAGGG, LARP4 #3: GAAUGUUGCUGGAACGUAAUU, PABP: AGGUGGUUUGUGAUGAAAAUU. Control siRNA was "Stealth RNAi Negative Universal Control Hi GC" from Invitrogen.

35S-methionine pulse labeling

48 hrs after siRNA transfection, at ~80% confluence, the cells were incubated in methionine-free media for 15 min followed by media containing 35S-methionine at 100 μCi/ml. Extracts were prepared and total protein concentration was determined (BioRad assay). Equal amounts were loaded for SDS/PAGE. After Coomassie staining, the gel was photographed then dried and processed using a Fuji phosphorimager and quantified using Fuji software.

siRNA-luciferase

HEK-293 cells growing in 6-well plates were transfected with siRNA (10 nM final). 24 hrs later 100 ng of the luciferase reporter plasmid (pGL3/RLuc/HCVIRES/FLuc) (Shahbazian et al., 2006, Dowling et al., 2007) was transfected. The luciferase ORF and other components of this plasmid including the SV40 promoter and the SV40 late poly(A) addition signal following the Firefly luciferase ORF as part of the transcription unit were confirmed by sequencing (not shown). 40 hrs later cells were harvested,

protein extracted and quantitated for luciferase assay. Equal amounts of protein were assayed using the Luciferase Reporter Assay System (Promega).

F-LARP4 expression/luciferase

to each 6-well plate of cells, 1 μg of F-LARP4 or F-vector plasmid together with 100 ng luciferase plasmid, each quantitated by OD260 and confirmed by gel electrophoresis, were co-transfected using Fugene 6 (Roche). 40 hrs later, total protein was extracted and processed for luciferase assay.

mRNA Decay

24 hrs after plating, a mixture of F-LARP4 plasmid and luciferase plasmid was co-transfected. After 40 hrs (~80% confluence) cells were treated with actinomycin-D (Sigma, used at 10 ug/ml) and RNA isolated at intervals thereafter.

Proteins for isothermal titration calorimetry (ITC) and structural studies

La(1-194) was expressed and purified as reported (Jacks et al., 2003). LARP4(111-303) was subcloned with N-terminal hexahistidine into a pET-Duet-1 expression vector and expressed in *E. coli* Rosetta II cells. Cell pellets were lysed by sonication in 20 mM Tris, 300 mM NaCl, 10 mM imidazole, pH 8.0 and centrifuged to separate the soluble and insoluble fractions of the cell. LARP4(111-303) was purified by affinity chromatography on a 5 mL HisTrap column (GE Healthcare) with a gradient of 10–300 mM imidazole. After the cleavage of the His-tag with TEV protease, the protein was purified from the cleaved tag, the His-tagged TEV and any undigested product by a second Ni^{2+} affinity step. The samples were then applied onto a 5 mL Hi-Trap heparin column to remove nucleic acids contaminants. Protein concentrations were calculated based upon the near-UV absorption (ε_{280}) using theoretical extinction coefficients derived from ExPASy (Gasteiger, 2005).

The MLLE domain (residues 544-626) of human PABPC1 was expressed and purified as described previously (Kozlov and Gehring, 2010).

Preparation of RNA for ITC

A(15), A(10) and U(15) were purchased from IBA GmbH (Göttingen, Germany) and dissolved in 20 mM Tris, 100 mM, KCl, 0.2 mM EDTA, 1 mM DTT at pH 7.25. Concentration was determined by UV, using a molar extinction coefficient at 260 nm calculated by the nearest-neighbor model (SantaLucia et al., 1996).

Peptides

PAM2w (TGLNPNAKVWQEIA) corresponding to LARP4 (13-26) was synthesized by Fmoc solid-phase peptide synthesis. PAM2w-long (GPLGSQVASKGTG-LNPNAKVWQEIAPGNTDATPVTHGTESSWHEIAAT) corresponding to LARP (7-49) was cloned into pGEX-6p1 and expressed from *E. coli* BL-21 as a fusion protein that was cleaved by PreScission Protease to release free peptide with a five amino acid extension at the N-terminus. Both peptides were purified by reverse phase chromatography on a C18 column (Vydac, Hesperia, CA) and verified by mass spectroscopy.

ITC experiments

RNA-protein titrations were carried out in 20 mM Tris, 100 mM, KCl, 0.2 mM EDTA, 1 mM DTT, pH 7.25, at room temperature (298 K) using a high-sensitivity iTC-200 microcalorimeter from Microcal (GE Healthcare) following the protocol previously reported (Hands-Taylor et al., 2010). In each experiment, volumes of 2 μL of an RNA solution were titrated into a protein solution in the same buffer, using a computer-controlled 40-μL microsyringe, with a spacing of 180 s between each injection. Each titration was corrected for heat of dilution by subtracting the measured enthalpies of the injections following saturation. Because La-RNA interactions exhibited large enthalpy of binding, whereas for LARP4-RNA the enthalpy of binding was substantially smaller, higher concentrations were used in the latter experiments to improve the signal-to-noise ratio and to ensure that we were well above the limit of sensitivity of the iTC200 instrument. In particular, for the experiments with La, a protein concentration of 15 μM and an RNA concentration of 120 μM were used; for the experiments with LARP4, we used a protein concentration of 40 μM and an RNA concentration of 380 μM.

ITC of PAM2w-MLLE interactions were carried out in 50 mM NaH_2PO_4, 100 mM NaCl, pH 7.0 with protein concentrations of 170 μM for 4.5 mM LARP4 (13-26) peptide, and protein concentration 85 μM for 1.6 mM LARP4 (7-49).

Integrated heat data obtained for the ITCs were fitted using a nonlinear least-squares minimization algorithm to a theoretical titration curve, using the MicroCal-Origin 7.0 software package from which the binding parameters ΔH° (reaction enthalpy change in kcal·mol^{-1}), K_b (binding constant in M^{-1}), and n (molar ratio between the two proteins in the complex) were derived. The reaction entropy was calculated using the relationships $\Delta G° = -RT \cdot \ln K_b$ (R 1.987 cal·mol^{-1}·K^{-1}, T 298 K) and $\Delta G° = \Delta H° - T\Delta S°$.

Protein Crystallization

Conditions for the MLLE domain in complex with the PAM2w peptide were identified utilizing hanging drop vapor diffusion with the AmSO4 crystallization suite (QIAGEN). The best crystals were obtained at 22˚C by seeding microcrystals into a 1 ml drop of PABPC1 (544-626)/LARP4 (13-26) (10 mg/ml) in 1:2 molar ratio mixed with 1 ml of reservoir solution containing 0.25 M potassium iodide and 1.9 M ammonium sulfate. The solution for cryoprotection contained the reservoir solution with the addition of 15% (v/v) glycerol. Crystals contain one MLLE and one PAM2w molecule in the asymmetric unit corresponding to V_m = 1.76 Å^3 Da^{-1} and a solvent content of 30.2%.

Structure solution and refinement

Diffraction data from a single crystal of the MLLE/PAM2w complex were collected at the McGill Macromolecular X-ray Diffraction Facility and Cornell High Energy Synchrotron Source (CHESS). Data processing and scaling were performed with HKL2000 (Otwinowski and Minor, 1997) The structures were determined by molecular replacement with Phaser (Read, 2001), using the coordinates of MLLE/Paip2 complex (PDB 3KUS). The initial MLLE/PAM2w model was completed and adjusted with the program Coot (Emsley and Cowtan, 2004) and improved by several cycles of refinement, using the program REFMAC 5.2 (Murshudov et al., 1999) and model refitting. At the latest stage of refinement, we also applied the translation-libration-screw (TLS) option

(Winn et al., 2003) with final density for PABPC1 residues 544-626 and LARP4 residues 15-25. The PDB ID code for the LARP4 PAM2w/MLLE structure is 3PKN.

RESULTS

We compared the N-terminal regions containing the LaM-RRM of human La(1-235) and LARP4(1-286), referred to as La-NTD and LARP4-NTD, for RNA binding using the electrophoretic mobility shift assay (EMSA). Of the homopolymers tested, A(20) exhibited the best affinity for LARP4-NTD, as reflected by the ratio of free to bound RNA, whereas U(20) showed less binding and C(20) and G(20) showed no binding (Fig. 4.1A-D). In this assay, the concentration at which 50% of the probe is shifted into a stable complex reflects the *K*d (Bayfield and Maraia, 2009). Accordingly, the results of Fig. 4.1A suggest that the *K*d of LARP4-NTD for A(20) is ≤750 nM. Less than 50% of U(20) was shifted at 3.0 uM LARP4-NTD, the highest concentration tested (Fig. 4.1B). Moreover, the smear observed between the bound and free U(20) (Fig. 4.1B) suggests less stable binding. La-NTD bound more U(20) than A(20) as expected (Fig. 4.1E).

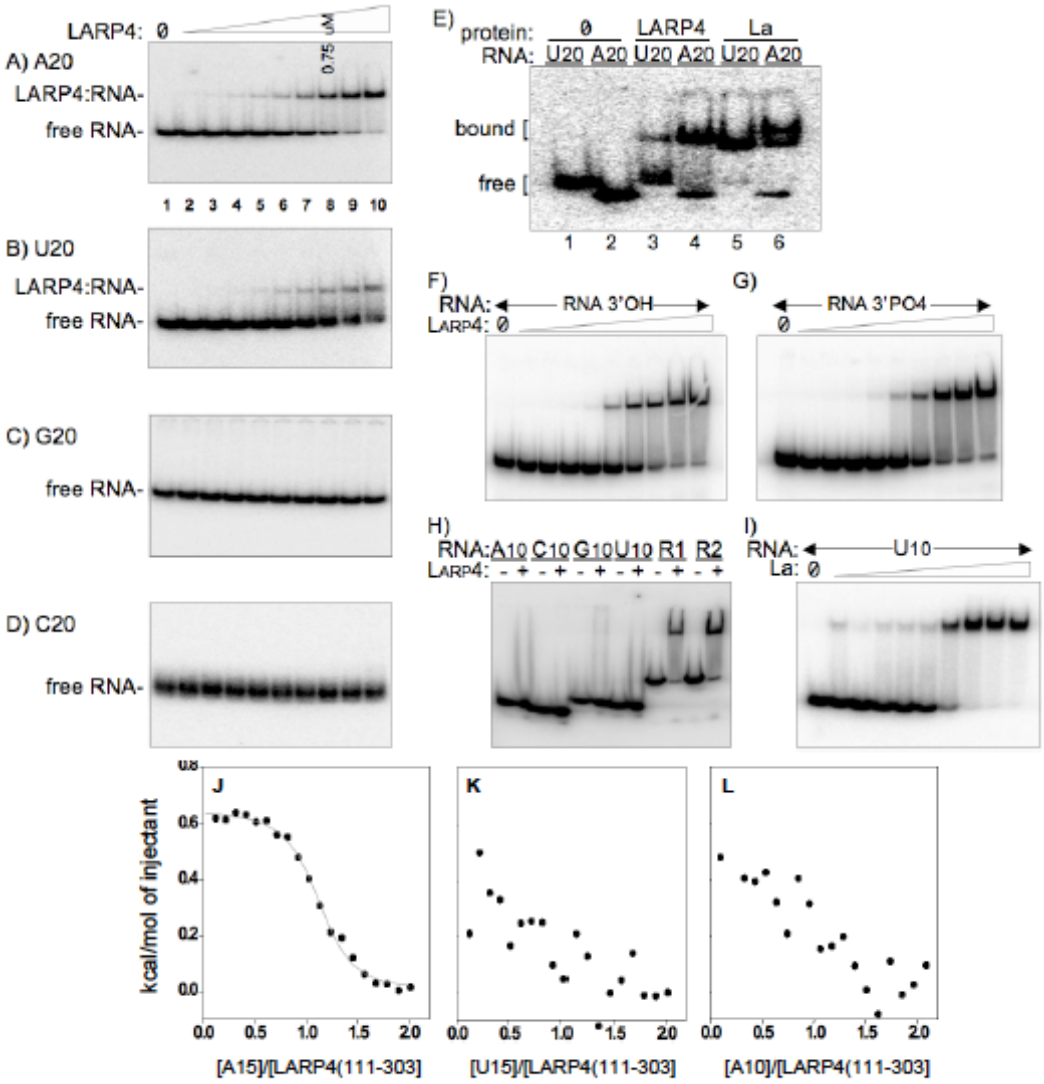

Figure 4.1 Human LARP4(1-286) preferentially binds poly(A) with a length requirement longer than 10 nucleotides. A-D) Electrophoretic mobility shift assay (EMSA) of homopolymeric 20'mer RNAs for binding to the RNA binding domain of LARP4 protein, LARP(1-286), also referred to as LARP4-NTD. Two-fold serial dilutions of LARP4(1-286) were used, with 750 nM final concentration in lane 8 as indicated. E) EMSA of A(20) and U(20) for La(1-235) and LARP4(1-286). F-G) Comparison of LARP4(1-286) binding to otherwise identical 36'mer RNAs (see sequence in Materials) that end with a 3' OH (F) or a 3' phosphate (G) (see Materials). H) LARP4(1-286) does not bind 10'mer RNAs. R1 and R2 are the same 36'nt RNAs used in panels F & G. I) La(1-235) binds to U10. J-L) Isothermal titration calorimetric analysis of LARP4(111-303) interactions

with A(15) (J), U(15) (K) and A(10) (L). The K_d and other thermodynamic parameters derived from this analyses are reported in Table 1.

Table 4. 1

Thermodynamic parameters of the interactions of La(1-194) and LARP4(111-303) with single stranded RNA sequences. The reported values represent the average and the standard deviations over three independent measurements.

	n	**K_d ($1/K_b$)** nM	**ΔH°** kcal mol^{-1}	**-TΔS°** kcal mol^{-1}	**$\Delta G°_{298K}$** kcal mol^{-1}
La(1-194)/ U(15)	0.8	752	-39.0±0.2	30.7±0.2	-8.3±0.4
La(1-194)/ A(10)	-	-	-	-	-
La(1-194)/ A(15)	-	-	-	-	-
LARP4(111-303)/ U(15)	-	-	-	-	-
LARP4(111-303)/ A(10)	-	-	-	-	-
LARP4(111-303) A(15)	1.0	714	0.7±0.1	-9.1±0.3	-8.4±0.4

We examined LARP4-NTD for sensitivity to 3' phosphate on ligand RNA, to which the genuine La proteins from multiple species are sensitive (Long et al., 2001, Stefano, 1984, Terns et al., 1992, Yoo and Wolin, 1994, Dong et al., 2004). Using otherwise identical 36 nt RNAs that end with AAAAA-3'OH or AAAAA-3'PO4 we could observe no difference in binding to the LARP4 protein over a range of concentrations (Fig. 4.1F & G), whereas the AAAAA-3'PO4 RNA exhibited ~6 fold less binding to La than the AAAAA-3'OH RNA (not shown). Although we tried repeatedly to find an expected difference in -3'OH and -3'PO4 binding, we could not.

A notable feature of RNA recognition by La is its ready ability to bind short oligo RNAs as evidenced by the ability of 4-6 nt RNAs to compete effectively with longer RNAs for in *vitro binding* (Stefano, 1984), a cocrystal of La with a 5 nt RNA (Kotik-Kogan et al., 2008), and binding to 9 or 10 nt RNAs as monitored by EMSA (Kotik-

Kogan et al., 2008, Teplova et al., 2006). LARP4 does not bind A(10) or the other 10'mers (Fig. 4.1H) even at concentrations well above that required to bind A(20), U(20) and the 36'mer RNAs used in Fig. 4.1F & G, designated R1 and R2 in Fig. 4.1H. Binding to La-NTD shows that the U(10) and A(10) are active as a ligand (Fig. 4.1I, data not shown).

To examine further the RNA binding properties of the LaM-RRM of LARP4 we employed isothermal titration calorimetry (ITC). By measuring heat generated or absorbed during binding, ITC provides the affinity, stoichiometry and enthalpy change (ΔH^o) of the interaction. Fig. 4.1J-L shows interactions of a LARP4(111-303) fragment with three RNAs. In the titration of LARP4(111-303) with A(15), binding occurs as one event centered on a molar ratio of one (Fig. 4.1J). Further analysis reveal that LARP4(111-303) interacts with A(15) with a *K*d of 714 nM, with entropically driven binding (Table 4.1, Supp Figs S1-2). By contrast LARP4(111-303) displayed very weak association with U(15) and A(10) (Fig. 4.1K & L), with *K*d beyond the threshold that could be rigorously measured by ITC, i.e. $\geq$ 0.1 mM. Therefore, LARP4 binds to A(15) at least 200 fold tighter than U(15) and A(10).

LARP4 cosediments with 40S ribosome subunits and polyribosomes. We examined LARP4 distribution in polysome profiles prepared in parallel in the presence and absence of puromycin (Fig. 4.2A & B). Control proteins rpS6 and rpL28 served as markers of 40S and 60S subunits respectively, that also cosedimented with polyribosomes (Fig. 4.2A). La was another marker, most abundant in fractions (fxns) #1 & 2, as expected (Brenet et al., 2009, Cardinali et al., 2003). Endogenous LARP4 was in two peaks, 40S (fxn #3) and polyribosomes (fxn #10), similar to rpS6 (Fig. 4.2A). By comparison, PABP was most abundant on polysomes, and Paip1 was most abundant in fxn #1, decreasing thereafter (Fig. 4.2A). Puromycin shifted a substantial amount of LARP4 to fxn #2 (Fig. 4.2B), in a pre-40S fraction that typically contains mRNPs, shifted by one fraction from the bulk of the 40S subunits as represented by the chromatograph and the rpS6 panel, although a significant amount also remained with the 40S peak in fxn #3 (Fig. 4.2B).

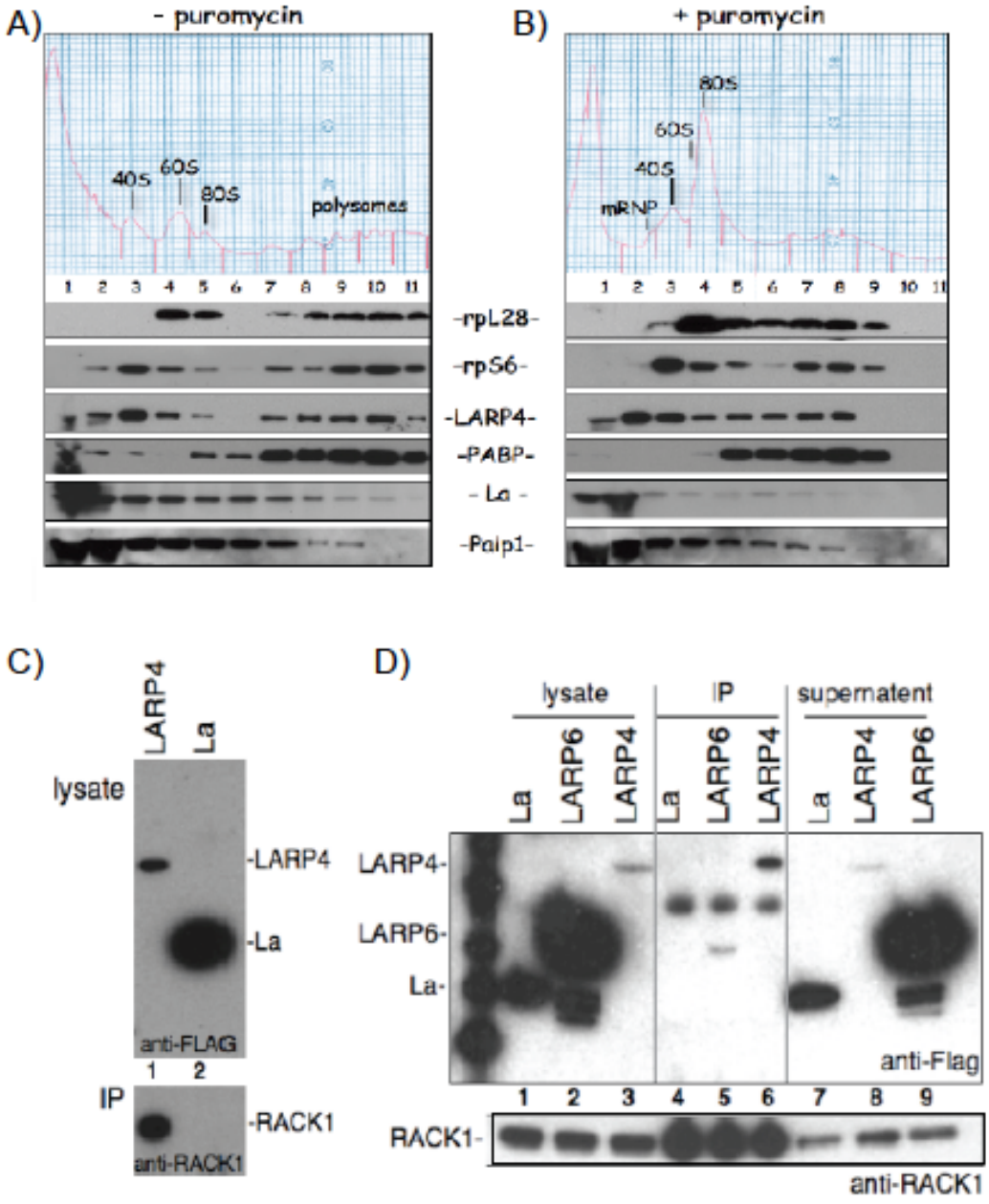

Figure 4.2 Human LARP4 cosediments with 40S subunits and polyribosomes, and associates with RACK1. A-B) Polysome profiles in the presence (A) and absence (B) of puromycin: numbered fractions were collected, fractionated by SDS/PAGE and immunoblotted onto a membrane that was probed, exposed, stripped and reprobed to detect the proteins indicated between the panels. C) Co-IP of RACK1 with FLAG-LARP4 (F-LARP4) but not the control protein, F-La, using anti-FLAG Ab. Cells were transfected with F-LARP4 or F-La and processed for IP. Upper panel shows input

extracts (lysate) prior to IP using anti-FLAG for immunoblot detection. Lower panel shows the IP material using anti-RACK1 for immunoblot detection. D) Co-IP of F-LARP4 but not the control proteins F-LARP6 or F-La with RACK1 using anti-RACK1 Ab for the IP. Cells were transfected with F-LARP4, F-LARP6 or F-La and processed for IP. Upper panel shows input extracts (lysate, lanes 1-3), the IP'ed material (lanes 4-6), and supernatant (lanes 7-9) using anti-FLAG for immunoblot detection. Lower panel shows a region of the same blot in upper panel after stripping and reprobing using anti-RACK1 for immunoblot detection.

LARP4 interacts with RACK1 in yeast 2-hybrids and in HeLa cells. Sedimentation with 40S suggested that LARP4 may associate with other translation components. This was supported by yeast 2-hybrid screening of a human liver cDNA library for LARP4 association. The library was screened for five-fold coverage for a total of 81 million interactions. Table 4.2 lists four independent clones that interacted with LARP4 that encode RACK1, two of which were isolated multiple times (not shown). Interaction quality was the highest attainable ("A" PBS column, Table 4.2). The 4 clones collectively encode only the C-terminal portion of RACK1, with the minimal interaction region comprising amino acids 200-317, indicating that this is sufficient for LARP4 interaction.

Table 4. 2 Yeast 2-hybrid results from human cDNA library using LARP4 as bait.

GNB2L1 = guanine nucleotide binding protein (G protein), beta polypeptide 2-like 1, RACK1 (Receptor for Activated C Kinase 1) (Nilsson et al., 2004)

Clone Name	Type Seq	Gene Name	Start..Stop	Frame	%Id 5p	%Id 3p	PBS
pB27_A-123	5p/3p	GNB2L1	414..988	IF	100.0	99.5	A
pB27_A-67	5p/3p	GNB2L1	468..998	IF	99.1	99.6	A
pB27_A-127	5p/3p	GNB2L1	510..1036	IF	98.4	56.8	A
pB27_A-17	5p/3p	GNB2L1	597..998	IF	99.7	99.2	A

Co-IP from HeLa cells validated the LARP4 RACK1 interaction. The upper panel of Fig. 4.2C shows the input and the lower panel shows the IP. RACK1 was co-IP'ed with F-LARP4 but not F-La even though the latter was expressed at a higher level (Fig. 4.2C). Reciprocal IP, using anti-RACK1 Ab is shown in Fig. 4.2D. F-LARP4 was enriched in the anti-RACK1 IP relative to the input lysate and supernatant whereas F-La and F-LARP6 were not even though these were expressed at much higher levels than LARP4 (Fig. 4.2D). Since RACK1 is a 40S-associated protein, its ability to interact with LARP4 may explain at least in part, the apparent association of LARP4 with 40S subunits observed above.

LARP4 knockdown decreases cellular protein synthesis. Changes in the relative areas of polysome versus 80S peaks in polysome profiles can reflect alterations in translation (Foiani et al., 1991). We examined polysome profiles after treatment of HeLa cells with control siRNA and siRNA against LARP4 (Fig. 4.3A & B). LARP4 knockdown led to a decrease in the polysome area with concomitant increase in the 80S peak (Fig. 4.3A & B). This change reflects conversion of polyribosomes to monoribosomes upon LARP4 knockdown, suggesting decreased translation initiation (Hartwell and McLaughlin, 1969, Foiani et al., 1991) with a 10-15% decrease in translation.

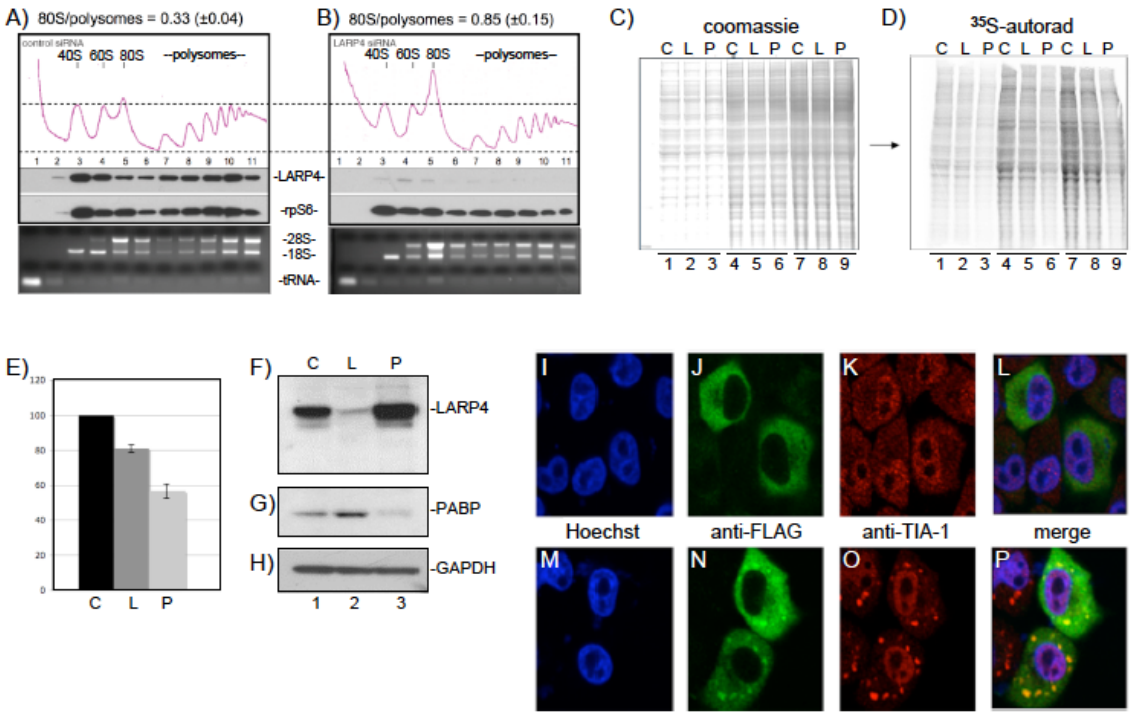

Figure 4.3 LARP4 knockdown decreases cellular protein synthesis. A-B) Polysome profiles of extracts made from cells treated with control siRNA (A) or siRNA directed to LARP4 (B). Quantitative areas under the 80S and polysome OD254 nm tracings are shown as numerical fractions above the panels. Immunoblots of the collected fractions for LARP4 and rpS6 are shown below the OD254 nm tracings. Ethidium-stained RNA gels showing 28S & 18S rRNAs and tRNA are shown below. C) Coomassie blue stained gel containing extracts from cells treated with control siRNA or siRNA directed to LARP4 or PABP (labeled C, L, P, respectively above the lanes) and pulsed for 30 minutes with ^{35}S-methionine. 50, 100 and 150 ug of each extract was loaded in lanes 1-3, 4-6, and 7-9 respectively. D) The gel in C was dried and exposed for autoradiography on a Fuji phosphorimager. E) Quantitation of the total ^{35}S was performed and expressed as ^{35}S-met incorporation per unit of protein on the Y-axis for each siRNA-treated cell extract on the X-axis, error bars reflect triplicate data. F-H) Immunoblot showing relative levels of LARP4, PABP and GAPDH from the three extracts used for C-D above; a single membrane was incubated sequentially with the three Abs for H-J. LARP4 localizes to stress granules after exposure to arsenite. I-P) After transfection with F-LARP4, cells were mock treated (I-L) or treated with arsenite (M-P) which is used widely to induce stress granules and examined with anti-FLAG (green) and anti-TIA-1

(red) antibody. LARP4 distribution was homogeneously cytoplasmic in the mock treated cells (J) whereas a significant fraction became localized in punctate foci after arsenite (N). Stress granule marker TIA-1 also organized into distinct loci after arsenite (K vs O). Image merging revealed superimposed LARP4 foci and TIA-1 foci (P). Endogenous LARP4 also localized to stress granules, (Supplementary Fig. S4.7Q-X).

We also examined incorporation of 35S-methionine into newly synthesized protein. After treatment with control siRNA or siRNA against LARP4 or PABP, cells were pulsed for 30 min with aliquots of a media containing 35S-met, extracts were prepared and fractionated by SDS/PAGE, stained with coomassie blue and photographed (Fig. 4.3C). This gel was dried and autoradiographed (Fig. 4.3D) and 35S was quantified (Fig. 4.3E, error bars reflect triplicates). Cells with LARP4 siRNA showed a 15-20% reduction in 35S-met incorporation, and PABP siRNA showed a ~50% reduction relative to control siRNA (Fig. 4.3E). Reduction of LARP4 and PABP in these cells relative to the control protein GAPDH was demonstrated by sequential probing of the same immunoblot which revealed that LARP4 levels appeared to increase upon PABP knockdown (Fig. 4.3F-H), possibly reflecting some kind of system of homeostatic regulation.

Conditions that inhibit translation lead to accumulation of mRNAs and associated initiation factors such as PABP, 40S subunits, and RACK1, as well as TIA-1 and certain other mRNA binding proteins in stress granules in which they are transiently inactive but can be reactivated for translation (Kedersha et al., 2000, Buchan and Parker, 2009). Since LARP4 was found associated with 40S subunits, RACK1 and PABP, and was shifted in polysome profiles to a pre-40S mRNP fraction with puromycin, a translation inhibitor known to induce stress granules (Kedersha et al., 2000), we examined stress granules for F-LARP4 and detected colocalization with TIA-1 a key component of stress granules (Fig. 4.3I-P). The endogenous LARP4 also colocalized to stress granules with FMRP (Schaffler et al., 2010) after treatment with arsenite (Fig. S4.7Q-X of the published manuscript), consistent with the idea that LARP4 is associated with mRNPs engaged for translation initiation that assemble into stress granules after exposure to arsenite.

LARP4 interacts with PABP in part through a variant PAM2 sequence. Studies of PAM2 sequences have led to a consensus, SxLNxNAxxF, of which interactions via L and F at positions 3 and 10 mediate much binding to PABC (Kozlov et al., 2004). Of all PAM2 sequences catalogued to date, the F at consensus position 10 is the only invariant residue (Albrecht and Lengauer, 2004, Kozlov and Gehring, 2010, Kozlov et al., 2010a). We found sequence near the N-termini of LARP4 that is homologous to PAM2 (Fig. 4.4A). LARP4 contains a conserved W (LARP4 pos. 22) in place of F10 and was not previously identified as a PAM2 candidate (Albrecht and Lengauer, 2004). Potential PAM2 motifs in LARPs 4 and 5/4b was first noted in a review (Bayfield et al., 2010a)**.** Here, we show the homologous sequences of LARPs 4 and 5/4b (Fig. 4.4A). The LARP4 PAM2 sequence is highly conserved (Fig. S4.3 of the published manuscript).

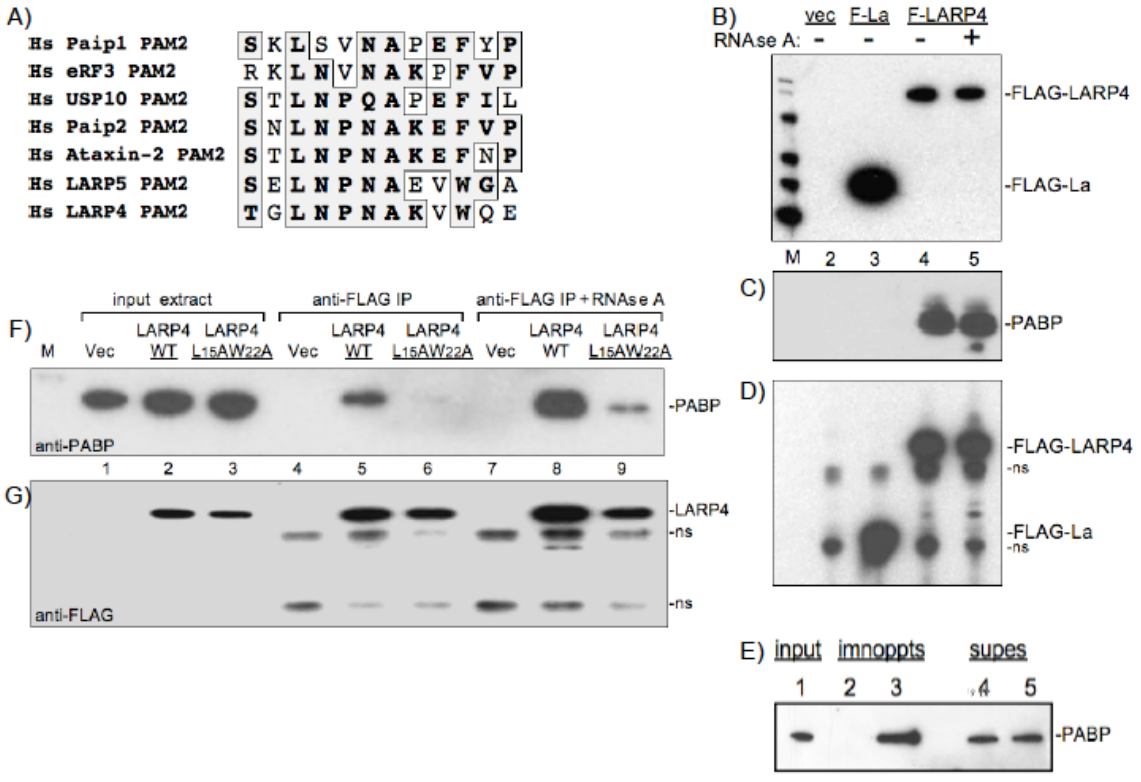

Figure 4.4 LARP4 contains a putative variant PAM2 (PAM2w) motif and interacts with poly-A binding protein (PABP). A) Sequence alignment of the PAM2 motifs of six *Homo sapiens* (Hs) proteins as listed: PAN3 (poly-A nuclease), eRF3 (elongation release factor 3), Paip1, Paip2, Ataxin-2, USP10, with the homologous sequences from LARP5, and LARP4. B) Immunoblot of input extracts from cells transfected with vector only

(vec), F-La and F-LARP4 that were mock treated (-) or treated with RNAse A (+) as indicated above the lanes, as visualized with anti-FLAG Ab. C) The extracts shown in B were subjected to immunoprecipitation (IP) and the products examined by immunoblot using anti-PABP Ab. D) The blot in C was stripped and then probed using anti-FLAG Ab. E) Immunoblot, using anti-PABP Ab, of input extract (lane 1) and after IP with control IgG (lane 2) and anti-LARP4 Ab raised against a C-terminal peptide of LARP4 (lane 3). PABP remaining in the supernatants are shown in lanes 4 & 5. F) Immunoblot of input extracts from cells after transfection with empty vector, F-LARP4 and F-LARP4-L15A,W22A (lanes 1-3), and after IP (lanes 4-6 and 7-9) visualized using anti-PABP Ab. G) The membrane was stripped and reprobed using anti-Flag Ab.

Immunoprecipitation (IP) using anti-FLAG Ab was done on extracts of cells expressing F-La or F-LARP4 (Fig. 4.4B). PABP was co-IP'ed with F-LARP4 but not with F-La, and the interaction was resistant to RNase A (Fig. 4.4C). By contrast, co-IP of the translation-associated factor, eIF4G was sensitive to RNAse A, and rpS6 was not in the IP (not shown). Affinity-purified Ab against native LARP4 also co-IP'ed PABP (Fig. 4.4E). By quantitative immunodepletion, ~10% of total PABP remained associated with LARP4 after IP (not shown). Substitution of LARP4 PAM2w residues L15 and W22 with alanines decreased the amount of PABP that co-IP'ed with F-LARP4 (Fig. 4.4F-G).

IP of F-LARP4 followed by microarray analysis identified ~2000 LARP4-associated mRNAs, many-fold more than parallel IPs of other RNA binding proteins, although with no apparent enrichment of any gene ontology (GO) group (not shown). However, despite various strategies and due to technical limitations, we have been unable to decipher which of these are bound directly to LARP4 independent of their binding to PABP. Nonetheless, many mRNAs including GAPDH mRNA, which we then decided to use as a control for some experiments, were not found associated in the anti-LARP4 IP (not shown). The poly(A) specificity of LARP4 and interaction with PABP is consistent with a general association with a large number of mRNAs.

A peptide of LARP4 PAM2w residues 13-26 bind the PABP MLLE domain. The conserved motif near the N-terminus of LARP4 most closely resembles the PAM2 motif found in Paip2 and ataxin-2 (Fig. 4.4A). We carried out ITC experiments with a

fragment of the N-terminus of LARP4 (residues 7-49) to determine if the putative PAM2 sequence would bind in solution to the MLLE domain of PABPC1 (Fig. 4.5A). The analysis clearly revealed binding with a *K*d of 26 uM. We then prepared a smaller peptide that contains only the variant PAM2 site (residues 13-26). ITC analysis showed even better binding with a *K*d of 22 uM (Fig. 4.2A). The affinity of the LARP4 PAM2w motif is intermediate between the highest and lowest PAM2 affinities measured for MLLE, which range from 0.12 to 28 uM (Lim et al., 2006, Kozlov and Gehring, 2010, Kozlov et al., 2010a, Kozlov et al., 2010b). We also carried out NMR analysis (Kozlov et al., 2004) to confirm the specificity of the interaction and to map the binding site on the MLLE Domain (Fig. S4.4 of the published manuscript). Titration of 15N-MLLE domain with LARP4 PAM2w peptide produced large chemical shift changes that mapped to the canonical PAM2 binding site on the MLLE domain (Fig. S4.4 of the published manuscript).

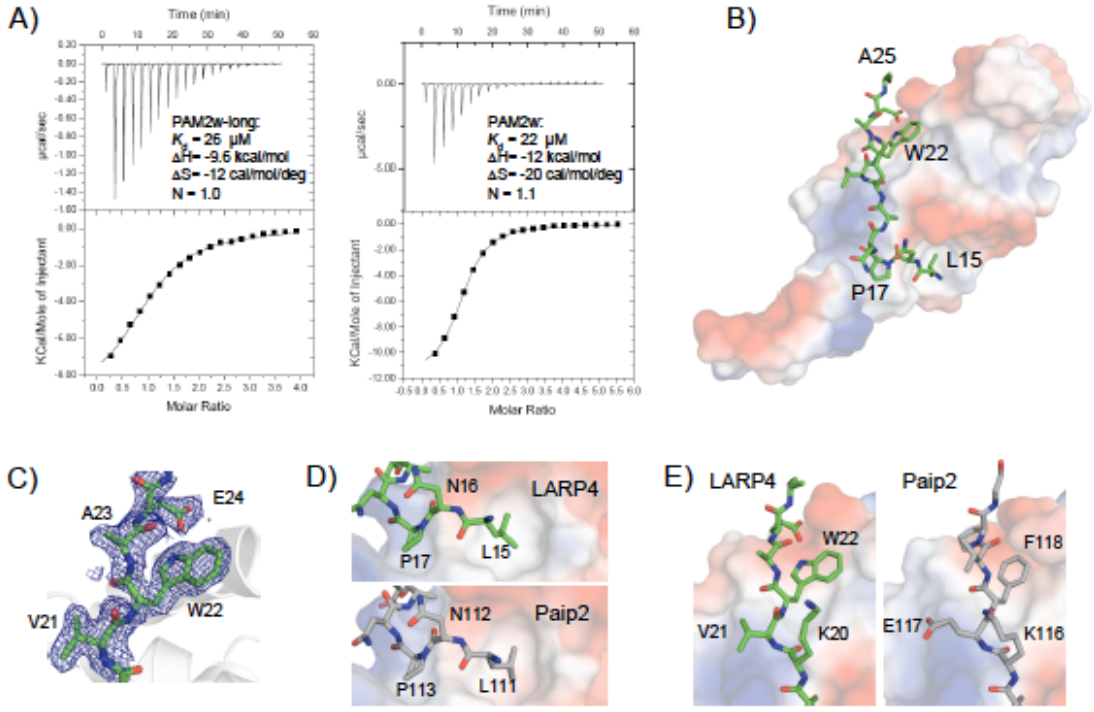

Figure 4.5 Binding of the PAM2w peptide of LARP4 to the MLLE domain of PABP. A) Isothermal titration calorimetry. Upper panels show the baseline corrected thermogram and the lower panels show the integrated areas of the heat released for binding of a PAM2w-long (*left*) and PAM2w (*right*). The dissociation constant (K_d), enthalpy (ΔH),

and entropy (ΔS) and stoichiometry (N) are indicated. B) X-ray crystal structure of LARP4 PAM2w bound to the MLLE domain of PABPC1. The PAM2w peptide (green) wraps around the surface of MLLE domain colored according to the electrostatic potential (negative in red, positive in blue). C) Electron density omit map (2Fo – Fc, 1σ contour) of the bound PAM2w peptide bound showing the tryptophan residue. D) Side-by-side comparison of PAM2w (green) from LARP4 and PAM2 peptide (grey, PDB entry 3KUS) from Paip2 bound to MLLE. The peptide N-termini show strikingly similar conformations and interactions with the MLLE domain. E) Comparison of C-termini. In LARP4, tryptophan (W22) replaces the phenylalanine found in other PAM2 peptides (Kozlov et al., 2004, Kozlov and Gehring, 2010, Kozlov et al., 2010a, Kozlov et al., 2010b). The larger indole ring is accommodated by a displacement of Gln560 of MLLE (not shown) to generate a shallow hydrophobic pocket. The PDB ID code is 3PKN.

Structure of the LARP4 PAM2w-MLLE complex. To obtain structural insight into the LARP4 PAM2w-MLLE interaction, we co-crystallized MLLE (PABP residues 544-626) with a peptide representing LARP4 PAM2w (residues 13-26, Table 4.2). The 1.8 Å MLLE/LARP4 diffraction data set was phased by molecular replacement using crystal structure of MLLE/Paip2. The LARP4 PAM2w peptide wraps around MLLE domain similar to the Paip2 and Ataxin-2 complexes (Fig. 4.5B).

Comparison of the LARP4/MLLE and Paip2/MLLE structures reveal a high degree of similarity (Fig. 4.5B-E). Starting from the N-terminus of the LARP4 peptide, Leu15 inserts into the hydrophobic pocket formed by MLLE domain side chains (Fig 5D). Additional hydrophobic contacts involve Pro17 and Ala19 of LARP4 and MLLE domain, as observed for the MLLE/Paip2 complex (Kozlov et al., 2010a). In previous mutagenesis studies, the invariant Phe in PAM2 (Phe118 in Paip2) was shown to be a major binding determinant in the MLLE-PAM2 interaction (Kozlov et al., 2004, Kozlov and Gehring, 2010, Kozlov et al., 2010b). Since Phe is invariant in all other PAMs2 in this position a major question was how substitution by Trp22 of LARP4 PAM2w would alter the interaction. The cocrystal revealed that the MLLE domain accommodates the larger side chain of Trp22 in almost the same way as Phe118 of Paip2 (Fig. 4.5D).

Two regions of LARP4 mediate association with PABP and polysomes. We wanted to know if a region of LARP4 other than PAM2w was required for efficient association with PABP, as is the case for other PAM2-containing proteins. Several F-LARP4 constructs, schematized in Fig. 4.6J, were analyzed for co-IP of PABP in the presence of RNase A (Fig. 4.6A-D), and polysome association (Fig. 4.6E-I). First, an initial set of proteins was analyzed by probing extracts for PABP, Flag epitope, endogenous LARP4 and GAPDH (Fig. 4.6A). Deletion of the C-terminal region led to higher levels of F-LARP4-NTD and F-LARP4-PAMD-NTD than the others (Fig. 4.6A, a-Flag panel). The other constructs were not grossly overexpressed as seen in lane 4, Fig. 4.6A, a-LARP4 panel, in which endogenous LARP4 and F-LARP4-PAMD are distinguished by size, detected by anti-LARP4 Ab that recognizes the LARP4 C-terminal peptide.

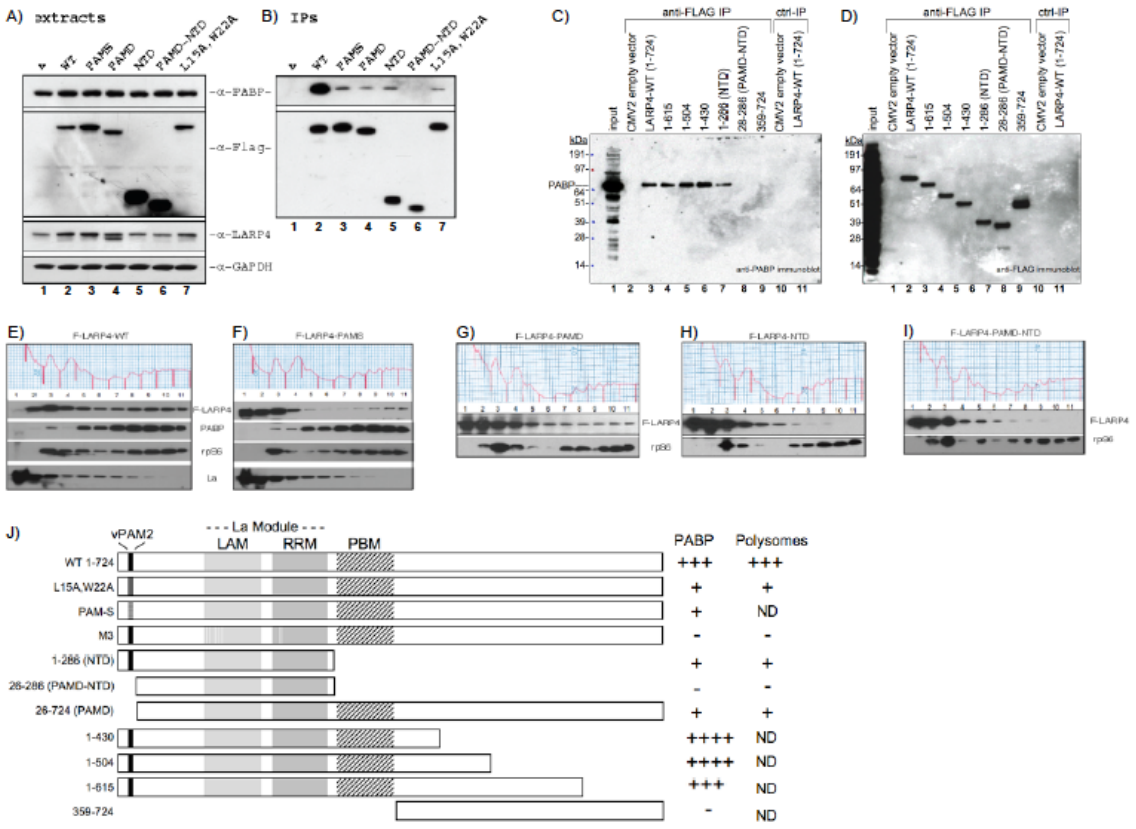

Figure 4.6 Two LARP4 regions are required for association with PABP and polyribosomes. A) Immunoblot of extracts after transient transfection with a subset of Flag-tagged constructs depicted in J. The membrane was sequentially probed with the Ab indicated to the right. B) Immunoblot of IP'ed material probed as for A. C) Further

mapping of the PABP interaction region of LARP4 C-terminal to the RRM; probed with anti-PABP. D) The blot in C was probed with anti-FLAG Ab. E-I) Five polysome profiles run in parallel, after transfection with the indicated constructs. Fractions were analyzed by immunoblot as indicated. J) Schematic showing the F-LARP4 constructs used here and in figure 4.7 (N-terminl Flag not shown) with summarized results to the right. The PAM2w, LaM and RRM motifs are shown. PBM refers to putative PABP binding motif mapped here. PAM-S contains alanines at LARP4 residues 15-22.

These mutated F-LARP4s co-IP'ed less PABP than WT F-LARP4 (Fig. 4.6B, upper panel). Only when both PAM2 and the whole C-terminal region downstream of RRM were deleted, as in PAMD-NTD, was association with PABP completely lost (Fig. 4.6B).

For more fine mapping we examined additional constructs. LARP4(1-615), LARP4(1-504) and LARP4(1-430) co-IP'ed PABP as well as Full length LARP4(1-724) (Fig. 4.6C, lanes 3-6), while LARP4(1-286) again showed less efficient association (lane 7). LARP4(26-286), a.k.a., PAMD-NTD, which lacks the PAM2w and entire C-terminal region, and LARP4(359-724) showed no association with PABP (Fig. 4.6C, lanes 8 & 9). Fig. 4.6D is a control that shows the F-LARP4 proteins pulled down in the IPs. The data indicate that the sequence downstream of the LARP4 RRM required for efficient PABP association resides within or includes LARP4 amino acids 287-358. Constructs intermediate between LARP4 1-286 and 1-430 as well as 287-724 designed to map the region further failed to accumulate in cells and could not be tested (not shown).

Figs. 6E-I show distribution of some of the F-LARP4 constructs in polysome profiles run in parallel. The F-LARP4-WT pattern (Fig. 4.6E) was similar to endogenous LARP4: a peak at 40S (fxn #3) and progressively less in fxns #2 & 1, and a second peak in fxns #8-10. F-LARP4-PAMS, in which residues 15-22 were replaced by alanines, was more abundant in fxns #1 & 2, with less remaining on polysomes relative to F-LARP4 (Fig. 4.6F). F-LARP4-PAMD was similar to PAMS with little remaining on polysome fxns 8-11 (Fig. 4.6G). F-LARP4-NTD and F-LARP4-PAMD-NTD were the most severely diminished for polysome association in fxns 8-11 (Fig. 4.6H-I). These results are similar to that found for PABP co-IP, namely that PAM2w as well as sequences C-

terminal to the RRM are required for optimum association with polysomes. The other constructs, used above for fine mapping were not examined by polysome profiling. These results along with the LARP4-M3 mutant in Fig. 4.7 are summarized in schematic form in Fig. 4.6J.

Mutations in LARP4 RNA binding motifs disrupt polysome association. We examined F-LARP4-M3 which carries point substitutions in key residues of the LaM and RRM designed to impair RNA binding. The identity of the amino acids that replace the wild type residues were selected to be compatible with the b-strand and a-helix structure of the LARP4 LaM-RRM as predicted by the Protein Structure Prediction Meta Server (Kaján and Rychlewski, 2007). F-LARP4-WT and F-LARP4-M3 were compared in parallel (Fig. 4.7A-B). In these gradients the 40S peaks were split into fxns 3 and 4. F-LARP4-WT was distributed in two peaks, one in fxn 3-4 and the other in fxn 10, similar to rpS6 (Fig. 4.7A). By contrast, F-LARP4-M3 showed significant decrease in polysome association and a shift to a peak in fxn 2 (Fig. 4.7A-B), suggesting that LARP4 uses its RNA binding motifs to maintain association with 40S components and polysomes. Consistent with this, F-LARP4-M3 was reproducibly found not to be associated with PABP by co-IP (not shown), further suggesting that the LARP4-PABP interaction is stabilized by RNA binding by LARP4.

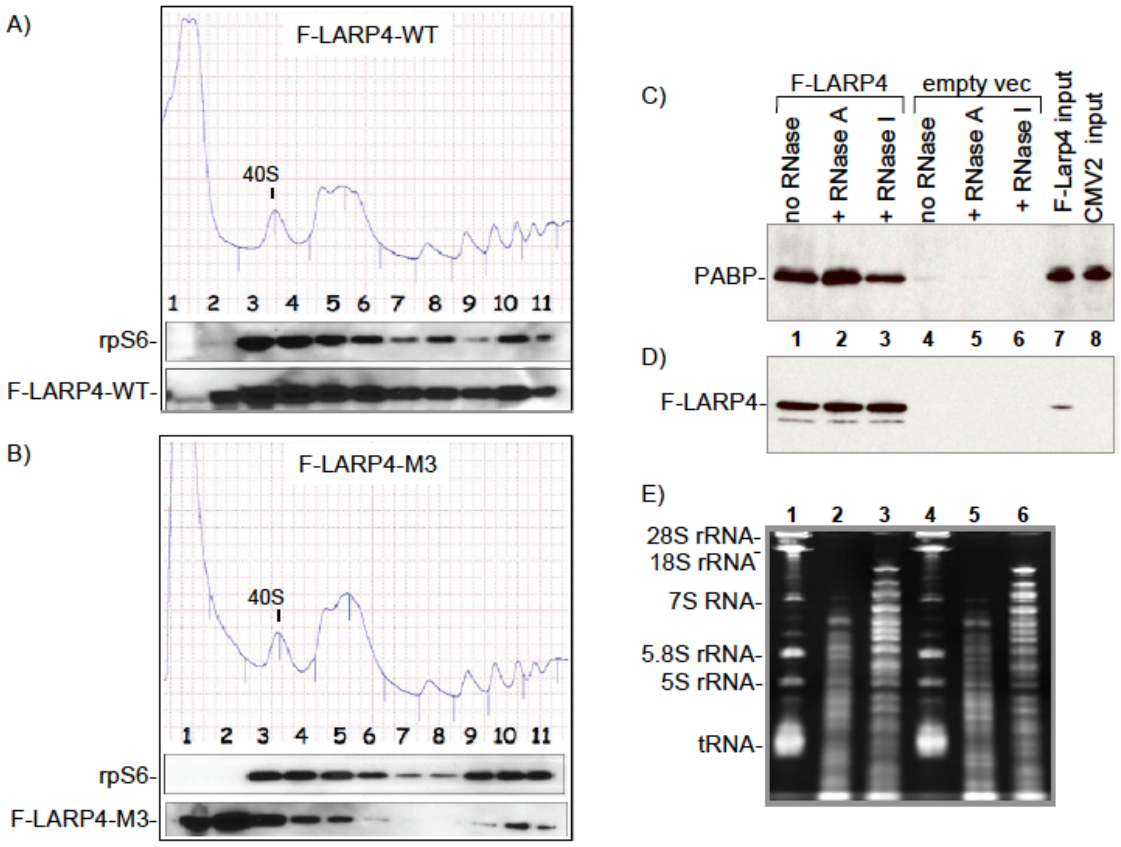

Figure 4.7 LARP4 RNA binding domain contributes to PABP and polysome association. A-B) Two polysome profiles run in parallel after transfection with the indicated constructs, F-LARP4-WT and F-LARP4-M3 which contains mutations in the RNA binding domain (see text); the 40S peaks are indicated. Fractions were analyzed by immunoblots, shown under the profiles. C-D) PABP-LARP4 interaction is resistant to RNase A which does not cleave poly(A) but partially sensitive to RNase I. Immunoblot of IP'ed material after mock treatment (no RNAse) or incubation with RNase A or RNase I as indicated, probed first for PABP (C) and then F-LARP4 (D). E) RNAs remaining in supernatants of samples 1-6 in C & D after IP.

The poly(A) binding specificity of LARP4 suggests that it may associate with PABP on the poly(A) tracts of mRNAs. Our IP experiments that used RNAse A might not reveal this since RNAse A is pyrimidine specific and has relatively little or no activity for poly(A) (Sorrentino, 1998). To examine this further we compared the

sensitivity of the LARP4-PABP association by co-IP in the presence and absence of the endonucleases RNases A and I, the latter of which exhibits no sequence preference (Biolabs, 2010). If bridged by poly(A), the PABP-LARP4 interaction should be relatively insensitive to RNase A but sensitive to RNase I. Wild type F-LARP4 or empty vector were transfected to HeLa cells and an extract was made from each. Aliquots were mock treated (no RNase) or treated with RNase A or RNase I during the incubation with anti-Flag Ab. After washing, the IP'ed PABP and F-LARP4 proteins were analyzed by immunoblotting (Fig. 4.7C-D). The amount of PABP associated with LARP4 in the mock and RNase A treated extract was more than in the RNase I treated extract (Fig. 4.7C). This difference was not due to loading or to the amount of extract used as can be seen by the F-LARP4 in the IP on the same blot (Fig. 4.7D). Effectiveness of the RNase treatments was evident from the RNA remaining in the extract after IP (Fig 4.7E). The cellular RNAs indicated to the left were intact in the mock treated but degraded in the RNase treated samples (Fig. 4.7E). This differential sensitivity to RNases A and I is consistent with the idea that LARP4 interacts with PABP in the presence of poly(A) RNA and that this contributes to the stability of their association.

LARP4 can prolong mRNA half-life. Experiments with a transfected luciferase reporter that contains the SV40 poly(A) addition signal used previously to examine translation (Shahbazian et al., 2006, Dowling et al., 2007) suggested that LARP4 stimulated luciferase expression by promoting accumulation of luciferase mRNA (Fig. 4.8A-C). The results obtained were very reproducible (not shown) but revealed that the extent of effects of LARP4 knockdown on luciferase activity (Fig. 4.8A, lanes 1-4) were more striking than on endogenous protein synthesis as monitored by polysome profiles and 35S-met incorporation (Fig. 4.3A-E). Although we do not know the basis for this discrepancy many cellular factors have been noted that affect luciferase activity (Shifera and Hardin, 2010) and it is therefore possible that LARP4 affects a factor(s) that is luciferase specific. The advantage of the luciferase system however is that it represents a method by which levels of a specific mRNA can be related to translation since changes in luciferase mRNA, protein synthesis and enzyme activity are tightly linked (Brasier and Ron, 1992). Therefore we could test if effects of LARP4 on luciferase are mediated at

least in part at the level of mRNA accumulation. Our approach was to cover a wide range of LARP4 levels by transfecting cells with either of three siRNAs against LARP4 or with F-LARP4 expression constructs and the appropriate controls.

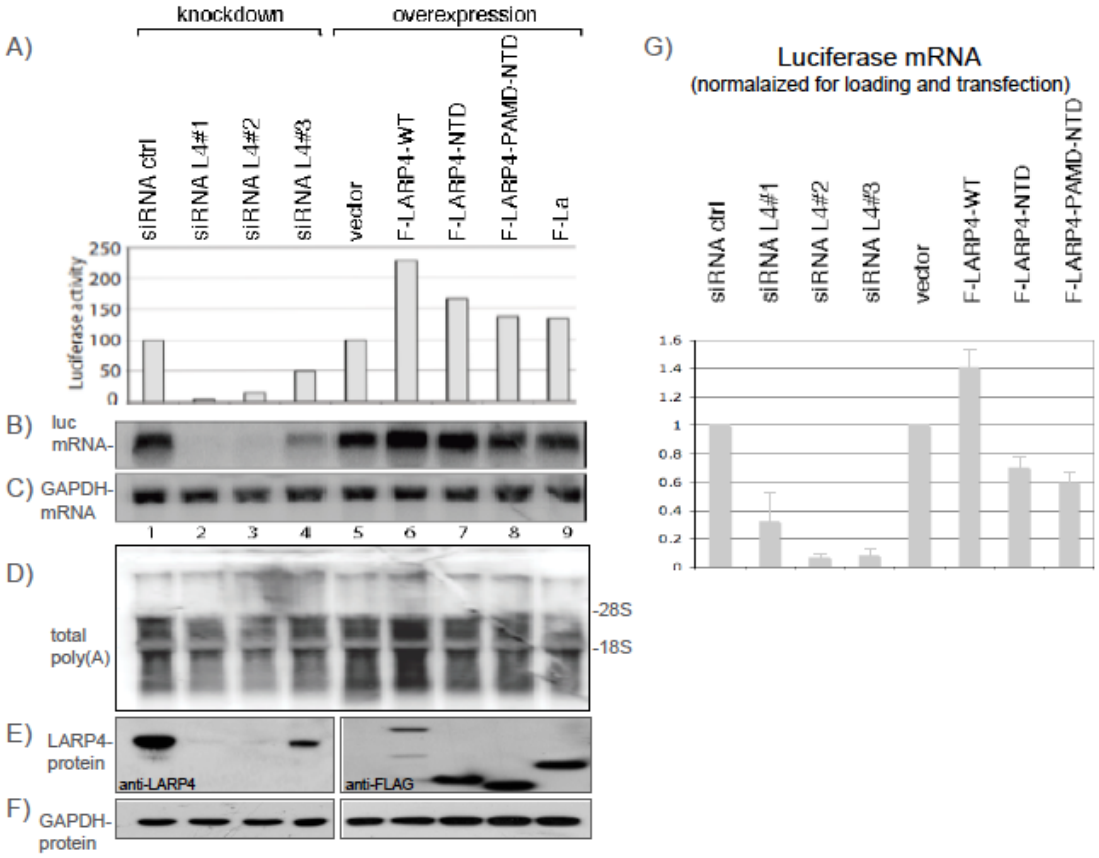

Figure 4.8 Effects of LARP4 on transfected luciferase reporter activity reflect luciferase mRNA levels. A-F) Cells transfected with siRNA (lanes 1-4) or F-LARP constructs (lanes 5-9) and corresponding controls were secondarily transfected with luciferase reporter plasmid after which extracts were prepared for luciferase activity (A), Northern (B-D), and Immunoblot (E-F). The panels in B-D reflect a single membrane sequentially probed for the RNAs indicated to the left. The immunoblots in E were processed using anti-LARP (left panel) or anti-FLAG (right panel). G) The experiment represented in A-F was repeated in triplicate using a VA1 plasmid together with the luciferase reporter plasmid to normalize for transfection efficiency. A Northern blot from each of the three experiments was generated and probed for luciferase mRNA, GADPH mRNA for normalization for loading, and VA1 RNA for normalization for transfection. The graph

shows luciferase mRNA levels after normalization for loading and transfection. Error bars reflect triplicate data.

Luciferase activity and mRNA levels, using GAPDH mRNA on the same blot for normalization (Fig. 4.8A-C) revealed an apparent good correlation. Three siRNAs each led to decreased luciferase mRNA levels relative to control siRNA (Fig. 4.8, lanes 1-4). F-LARP4 reproducibly led to the most luciferase mRNA and activity whereas the NTD and PAMD-NTD mutants and F-La exhibited less (Fig. 4.8, lanes 5-9) even though the latter accumulated to higher levels than F-LARP4 (Fig. 4.8E, lanes 5-9).

Fig. 4.8G, shows the results of the above experiment repeated in triplicate after equal aliquots of a mixture of luciferase plasmid and VA1 plasmid were used for transfection, the latter of which is transcribed by RNA polymerase III into a small stable 160 nt VA1 RNA that served as a transfection control. Luciferase mRNA was normalized for loading using endogenous GAPDH mRNA and for transfection using VA1 RNA. The data suggest that LARP4 promotes luciferase mRNA accumulation and moreover that F-LARP4 may promote luciferase mRNA stability.

Given the proposed involvement of several PAM2-containing proteins in controlling mRNA turnover via PABP, we examined LARP4 for effects on mRNA stability (Tritschler et al., 2010, Ruan et al., 2010, Kozlov et al., 2010b, Funakoshi et al., 2007, Kozlov and Gehring, 2010). As noted in the Introduction, competition between the PAM2-containing proteins eRF3, PAN2/3 and Tob-Ccr4-Caf1 is thought to impact mRNA homeostasis (Funakoshi et al., 2007, Ruan et al., 2010, Kozlov et al., 2010b). For this we chose to express LARP4 ectopically because this produces robust luciferase mRNA levels that can be followed for decay whereas LARP4 knockdown leads to low luciferase mRNA levels which are technically difficult to follow. We initially examined luciferase mRNA. Actinomycin D was used to inhibit mRNA synthesis and mRNA decay was followed over time, using the noncoding RNAs, 7SK, and 18S rRNA as controls. GAPDH was chosen as an additional control because it was not among the ~2000 mRNAs found associated with F-LARP4 (not shown) and it has a longer half-life than luciferase mRNA. High quality Northern blots from three independent experiments were generated and sequentially probed (one is shown in Fig. S4.5 of the published

manuscript). Quantitation of each RNA, corrected for loading and using GraphPad Prism to analyze the data (Ysla et al., 2008), is shown in Fig. 4.9A-F. Each graph contains the results from three Northern blots for one of the mRNAs examined; each line on the graph represents the specific mRNA corrected for by one of the three loading controls on the same blot, 7SK, 18S, and GAPDH mRNA (the individual decay curves are shown in Fig. S4.6 of the published manuscript). The error bars reflect triplicate data for the examined RNA corrected for by the loading control RNA. This showed that expression of F-LARP4 stabilized luciferase mRNA as compared to the vector control, the latter in which luciferase mRNA decayed with a half-life of ~4 hours (Fig. 4.9A, vector), in agreement with previous reports (Ayala-Breton et al., 2009, Fan et al., 2003). We conclude that enhanced expression of LARP4 prolonged luciferase mRNA.

F-LARP4 prolonged the half-life of total polyA RNA, as monitored by oligo-dT probing, relative to the vector control (Fig. 4.9B), albeit less so than for luciferase mRNA. F-LARP4 also prolonged FAIM mRNA half-life (Fig. 4.9C). C-myc mRNA, which was undetectable after 2 hrs., was also prolonged by F-LARP4 relative to the vector control (Fig. 4.9D). After two hours, c-myc mRNA exhibited distinct decay curves in the LARP4 and control cells. By contrast, the nonpolyadenylated histone H2A mRNA was not significantly different in F-LARP and vector cells at 2 hrs or at any time (Fig. 4.9E). GAPDH mRNA was not significantly different in the F-LARP4 and the control cells, highly stable in both (Fig. 4.9F). These results indicate that overexpression of LARP4 can stabilize some mRNAs.

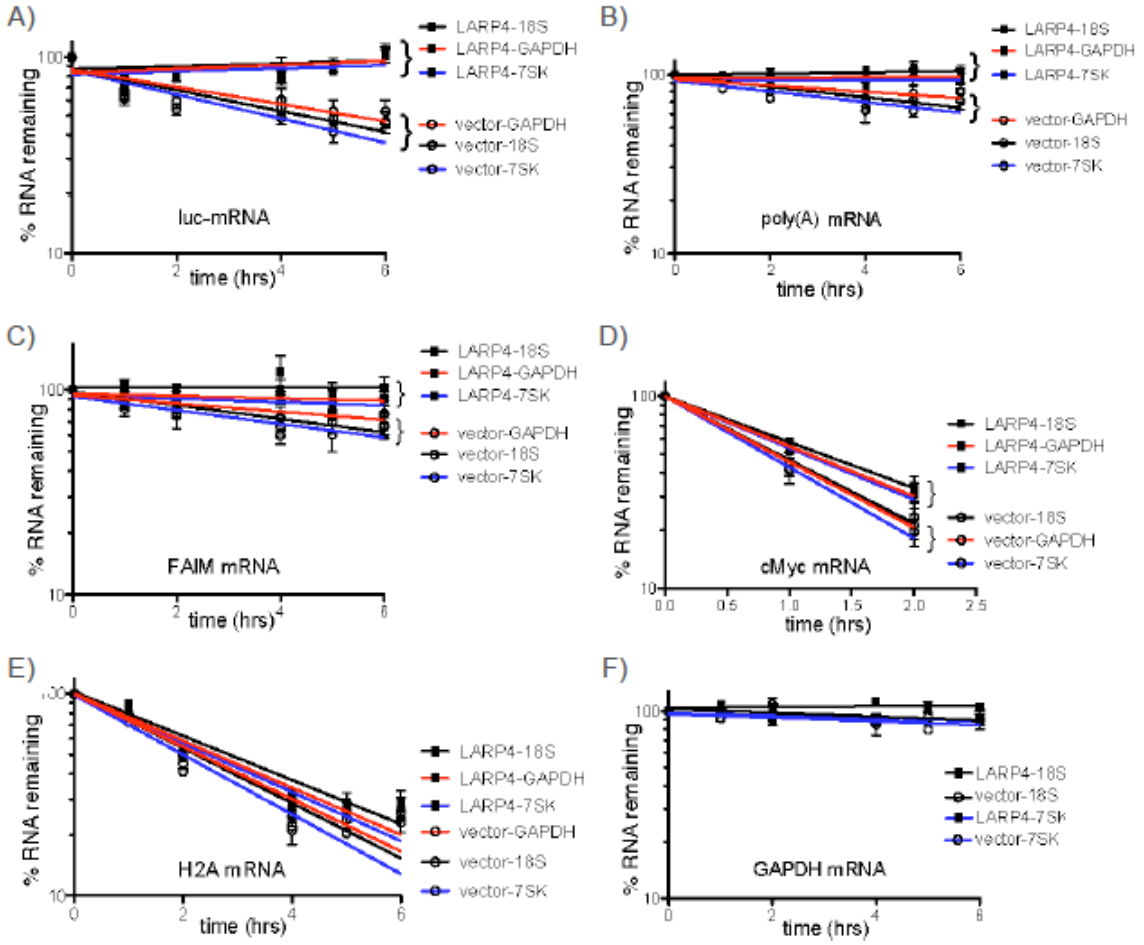

Figure 4.9 LARP4 can promote mRNA stability. Cells were transfected with a mixture of F-LARP4 and luciferase plasmid or empty vector and luciferase plasmid. 40 hrs later cells were treated with actinomycin D and RNA was isolated at time zero and intervals thereafter as indicated. Three independent experiments were carried out and a Northern blot was made from each (one of the blots sequentially probed is shown in Fig. S4.5 of the published manuscript). The blots were sequentially probed for the RNAs indicated above the x-axes. The blots were also probed for 18S rRNA, GAPDH mRNA & 7SK snRNA which were used to normalize for loading. Each graph shows the decay curves for LARP4-transfected and empty vector-transfected cells; each line reflects the time course for the RNA as corrected for by either 18S rRNA, 7SK snRNA or GAPDH mRNA as indicated; error bars reflect data from the three data sets.

DISCUSSION

We characterized a new protein, LARP4, that appears to be involved in mRNA metabolism and translation. Multiple data indicate that LARP4 is intimately associated with translating polyadenylated mRNAs. The conserved RNA binding LaM-RRM of LARP4 exhibits binding preference for poly(A) as well as other unexpected properties of a LaM-RRM-containing protein (Fig. 4.1, Table 4.1). The results expand our appreciation of the potential diversity of the LaM-RRM in RNA recognition.

The LARP4 LaM-RRM is flanked on both sides by PABP-interacting regions. The region N-terminal to the LaM-RRM contains a conserved PAM2w sequence that we showed is important for PABP interaction. PAM2 sequences mediate direct contacts to the MLLE Domain of PABP (Kozlov et al., 2004, Kozlov and Gehring, 2010, Kozlov et al., 2010a). Direct binding as monitored by ITC as well as NMR and crystallography showed that the LARP4 PAM2w makes contacts with the MLLE Domain of PABP.

The region C-terminal to the LaM-RRM that is required for efficient interaction with PABP was mapped to a sequence that resides within or includes LARP4 residues 287-358. The RNase I data suggest the possibility that the mechanism of interaction between PABP and this region of LARP4 may involve RNA bridging although this remains to be determined. We also presented evidence that is consistent with a model in which LARP4 and PABP interact in the presence of RNA and that this contributes to the stability of their interaction. Our characterization represents the first detailed mechanism by which a LARP interacts with PABP.

LARP4 cosediments with 40S ribosome subunits and was found to interact with RACK1, a 40S- and mRNA-associated protein (Coyle et al., 2009, Nilsson et al., 2004). Knockdown of LARP4 led to a decrease in translation as evidenced by conversion of polyribosomes to monosomes on sedimentation gradients and by a decrease in 35S-met incorporation into newly synthesized protein consistent with a 15-20% reduction in cellular protein synthesis. The cumulative data indicate that LARP4 is a functional component of a fraction of translating mRNPs.

LARP4 sediments as two peaks on polysome profiles, with 40S ribosome subunits and with polyribosomes. All tested LARP4 mutants that showed decreased association with PABP also showed decreased association with polyribosomes. Substitution of

residues in the RNA binding domain of LARP4 predicted to be important for RNA binding also decreased association with polyribosomes.

The results reported here are to be distinguished from the report (Schaffler et al., 2010) on a related protein, LARP5/4b. Human LARPs 4 and 5/4b are distinct proteins encoded on different chromosomes that have maintained distinct characteristics through evolution, including sequence differences in their La motifs in key residues involved in base-specific RNA recognition in human La-RNA crystals as well as conserved differences in their RRMs. LARPs 4 and 5/4b are most highly homologous in their LAM and RRM, but are less homologous in some other regions (Fig. S4.3 of the published manuscript). However, even in these most homologous regions, conserved sequence differences occur in key positions of the RRM that are sometimes involved in sequence specific RNA recognition in other RRM-containing proteins (Bayfield and Maraia, 2009), such as the loop connecting the b-2 and b-3 strands of the beta-sheet RNA binding surface of the RRM (Fig. S4.3 of the published manuscript).

LARPs 4 and 5/4b share functional relatedness, including interaction with PABP and RACK1 (Schaffler et al., 2010). That this was also demonstrated for LARP4 is significant because although it was reported that the large C-terminal domain of LARP5/4b (~400 amino acids) interacts with PABP and RACK1, this region shares limited homology with LARP4. The region 287-429 of LARP4 that we mapped as important for PABP interaction contains a stretch of about 70 amino acids with significant homology (64% identity and/or similarity) to LARP5/4b (Fig. S4.3 of the published manuscript). Fine mapping of the LARP4 region of RACK1 interaction will require further experiments. Our data advanced information regarding the RACK1 interaction as we found by yeast 2-hybrid analysis that the C-terminal half of RACK1 is sufficient for interaction with LARP4.

Conditions that inhibit translation lead to accumulation of mRNAs and associated initiation factors such as PABP, 40S subunits, and RACK1, as well as TIA-1 and certain other mRNA binding proteins in stress granules in which they are transiently inactive but can be reactivated for translation (Kedersha et al., 2000, Buchan and Parker, 2009). Since LARP4 was found associated with 40S subunits, RACK1 and PABP, and was shifted in polysome profiles to a pre-40S mRNP fraction with puromycin, a translation

inhibitor known to induce stress granules (Kedersha et al., 2000), we examined stress granules for F-LARP4 and detected colocalization with TIA-1 a key component of stress granules (Fig. S4.7 of the published manuscript). Our Ab that detects endogenous LARP4 also demonstrated stress granule localization using anti-FMRP (Schaffler et al., 2010), consistent with the idea that LARP4 is associated with mRNPs engaged for translation initiation that assemble into stress granules after exposure to arsenite.

While LARP5/4b was shown to bind PABP, its PAM2 motif was not noted or characterized in the previous report (Schaffler et al., 2010). Our analysis identified the PAM2w and showed that it indeed interacts directly with the PABP MLLE domain and with a *K*d within the range found for other PAM2 motifs. This is significant because it suggests that LARP4 (and probably 5/4b) function as parts of a network of proteins that compete for the PABP MLLE domain. Finally, while Schäffler et al. (Schaffler et al., 2010) reported that LARP5/4b stimulated protein synthesis, including as monitored by luciferase activity, they showed that it did not affect luciferase mRNA levels, whereas our analysis which included mRNA decay indicate a role for LARP4 in mRNA stability.

The variant PAM2 found in LARP4 and 5/4b most significantly differs from all other known PAM2 sequences in that they contain a Trp in place of Phe, the latter of which is a most important contributor to MLLE binding (Kozlov and Gehring, 2010). While LARP4 PAM2w contains leucine at consensus position 3, which is also a very important in MLLE binding (Kozlov et al., 2004, Kozlov and Gehring, 2010), we do not yet know if the presence of Trp in place of Phe would increase or decrease binding to MLLE. Occupation of this key position by Trp has been conserved by all LARP4 and 5/4b sequences in the database (not shown), especially intriguing in light of hierarchal competition by PAM2 proteins for the PABP MLLE (Kozlov and Gehring, 2010). We note that overexpression of LARP4 may not reflect a physiologic role in mRNA stability and that actinomycin-D can have untoward effects after 2 hr. We therefore examined this after LARP4 knockdown which appeared to have destabilizing effects on FAIM mRNA (Fig. S4.8 of the published manuscript). However, this experiment did not include the luciferase reporter, and other probings were complicated by technical irregularities. Thus, we wish to emphasize that our conclusions regarding mRNA stability are mostly limited to conditions of increased LARP4 expression, and that more detailed and

mechanistic experiments focusing on this aspect will have to await future endeavors. Nonetheless, given our data which shows that modest over expression of LARP4 can stabilize mRNAs (Fig. 4.9) it is tempting to speculate that LARP4 may do so by competing with the PAN2/3 and/or the Ccr4-Not-Caf1-Tob2 deadenylation complexes (Kozlov and Gehring, 2010). These complexes comprise a biphasic poly(A) shortening activity of mRNAs in context that appears to be relevant to their antiproliferative properties (reviewed in Mauxion et al., 2009).

ACKNOWLEDGEMENTS We thank M. Fabian, Y. Svitkin and N. Sonenberg for discussion and for providing the luciferase reporter construct and anti-Paip1, and to U. Fischer and K. Schaffler for anti-FMRP. We thank A. Hinnebusch, T. Dever, J. Wilusz, V. Pain, M. Gorospe, T. Dever, & T. Sundaresan for discussion, J. Iben for bioinformatic analysis, G. M. Wilson for discussion and help with GraphPad Prism and to S. Curry for comments. LM and MRC thank R. Tata and P. Brown for help with LARP4(111-303) cloning. This work was supported by the Intramural Research Program of the NICHD, NIH, grants to CHESS, and Canadian Institutes of Health grant MOP-14219. LM is a fellow of the European Molecular Biology Organization (EMBO). MRC acknowledges the Wellcome Trust for the Centre of Biomolecular Spectroscopy.

Supplemental materials

Supplemental materials for this paper are not shown, due to the large number of pages. The materials can be found here (http://www.ncbi.nlm.nih.gov/pmc/articles/PMC3028612/).

Connecting text 3

PABPC1 is the dominant and most abundant isoform of cytoplasmic poly(A) binding protein in human. Most studies, as well as the previous three chapters, are based on PABPC1. However, other isoforms of cytoplasmic PABP exist in human. Critical isoform specific functions have been reported in vertebrate development and cell differentiation etc. In the following chapter, we used genome editing technology to change composition of cytoplasmic PABP in a human cell-line. This creates an opportunity, not available before, to examine isoform specific function of PABP.

Chapter 5: Loss of PABPC1 is compensated by elevated PABPC4 in HEK293, correlating with transcriptome changes

Jingwei Xie[1], Kalle Gehring[1, 2]

[1] Department of Biochemistry and Groupe de Recherche Axé sur la Structure des Protéines, McGill University, Montreal, Quebec H3G 0B1, Canada

[2] To whom correspondence should be addressed: Dept. of Biochemistry, McGill University, 3649 Promenade Sir William Osler, Rm. 473, Montreal, QC H3G 0B1, Canada. Tel.: 514-398-7287; Fax: 514-398-2983; E-mail: kalle.gehring@mcgill.ca.

Abstract

Cytoplasmic poly(A) binding protein (PABP) is an important translation factor. Multiple PABP isoforms exist in mammals, with PABPC1 as the most abundant one. Here we used CRISPR/Cas genome editing to disrupt PABPC1. PABPC4, a minor isoform, compensates for the loss of PABPC1 and leads to gene profile changes revealed by transcriptome analysis. Pathway analysis shows that elevation of PABPC4 correlates with c-Myc level. This study provides insights into understanding critical PABP isoform specific functions in development and differentiation etc.

5.1. Introduction

Cytoplasmic poly(A) binding protein (PABP) is a key component of the translational machinery; it is critical for the closed loop formation of mRNA and stimulates mRNA translation into protein (Sonenberg and Hinnebusch, 2009). PABP plays a direct role in 60S subunit joining and is integral to the formation of the translation initiation complex on the mRNA (Kahvejian et al., 2005). PABP also protects mRNA transcripts from decay (Coller et al., 1998).

Most structural and functional studies of cytoplasmic PABPs are based on PABPC1.

PABPC1 is the most abundant of several cytoplasmic poly(A) binding proteins (PABPs) found in vertebrates and has been known for four decades (Blobel, 1973). PABPC1 consists of four RNA-binding domains (RRM1-4) followed by a linker region and a conserved C-terminal MLLE domain. The RRM domains mediate the circularization of mRNA through the binding of the 3' poly(A) tail and eIF4F complex on the mRNA 5' cap (Safaee et al., 2012, Kahvejian et al., 2005, Deo et al., 1999, Imataka et al., 1998). The linker region may promote the self-association of PABPC1 on mRNA although the molecular details of the interaction are unknown (Melo et al., 2003, Simon and Seraphin, 2007). The C-terminus of PABPC1 contains a MLLE domain that mediates binding of a peptide motif, PAM2, found in many PABP-binding proteins (Xie et al., 2014).

Five other less abundant cytoplasmic PABP exist in higher vertebrate. PABP isoforms are suggested to be functionally different in vertebrate development (Gorgoni et al., 2011). PABPC3 (tPABP or PABPC2 in mouse) is testis-specific (Kleene et al., 1998). PABPC4 (iPABP) is inducible in activated T cells (Yang et al., 1995) and serves a critical role in erythroid differentiation (Kini et al., 2014). PABPC1L (ePABP) functions in oocytes and early embryos (Seli et al., 2005, Guzeloglu-Kayisli et al., 2008, Voeltz et al., 2001). PABPC1L is substituted by PABPC1 later in development, but remains expressed in ovaries and testes of adult (Vasudevan et al., 2006). PABPC4L and PABPC5 (Blanco et al., 2001) lack the linker and MLLE region.

There are additional binding sites for PABPC1 on mRNA transcripts. RRM domains of PABPC1 bind various RNA sequences other than pure poly-adenosines. Although RRM1-2 and RRM3-4 of PABPC1 can both interact with poly(A) RNA, the RRM3-4 has higher affinity to AU sequences than RRM1-2 (Sladic et al., 2004). It is also shown by CLIP-seq that only a low percentage (2.6%) of sequencing reads are pure poly(A) (Kini et al., 2016). PABPC1 binds to an auto-regulatory sequence in the 5'- UTR of its own mRNA, and controls its own translation (de Melo Neto et al., 1995, Wu and Bag, 1998, Hornstein et al., 1999). CLIP-seq study in mouse reveals that PABPC1 binds to a subset of A-rich sequences in 5'-UTR, besides predominant binding to 3'-UTR of mRNAs (Kini et al., 2016). These PABPC1 interactions at 5'-UTR can impact and coordinate post-transcriptional controls on mRNAs (Kini et al., 2016).

The functional specificity or redundancy of cytoplasmic PABPs is not quite understood

yet. There have been increasing interests in PABPC4 in recent years. PABPC4, a minor isoform of PABP, was first identified as an inducible protein in activated T-cells (Yang et al., 1995). Depletion of PABPC4 interferes with embryonic development of *Xenopus laevis,* and cannot be rescued by isoforms PABPC1 or PABPC1L (Gorgoni et al., 2011). PABPC4 plays an essential role in erythroid differentiation, and its depletion inhibits terminal erythroid maturation (Kini et al., 2014). Motif analyses of PABPC4 affected mRNAs reveal a high-value AU-rich motif in the 3' untranslated regions (UTR) (Kini et al., 2014).

A major difficulty in studying roles of PABP isoforms is the abundance of PABPC1 compared with other minor isoforms. To investigate specific or redundant roles of PABP isoforms, we disrupted PABPC1 in human cells with CRISPR/Cas9 gene editing system. An elevated level of PABPC4 compensated the loss of PABPC1, which suggested certain redundancy between the two isoforms. However, transcriptome profile changed in PABPC4 elevated cells. Gene set enrichment analysis indicated that c-Myc was the most common gene in enriched pathways. Further, we showed correlated changes between PABP isoforms and c-Myc levels. These studies expand our understanding of cytoplasmic PABPs and suggest importance of a fine-tuned PABP isoform usage network.

5.2. Materials and methods

5.2.1 Cell culture and plasmids

Cells were cultured in DMEM supplemented with antibiotics and 10% fetal bovine serum. 10^5 cells per well were plated in 24-well plate the day before transfection. 0.8 μg DNA plasmid was mixed with 2 μl Lipofectamine 2000 in Opti-MEM and then added to cells. After 24 hours, cells were trypsin digested and split onto cover slides. pFRT/TO/FLAG/HA-DEST PABPC4 was a gift from Thomas Tuschl (Addgene plasmid # 19882) (Landthaler et al., 2008). DNA fragment expressing PABPC1 (NM_002568) or PABPC1 (1-542) were cloned into pCDNA3-EGFP between BamH I and Not I.

5.2.2 CRISPR/Cas9 genome editing

Target sequences were identified in Pabpc1 using CasFinder (http://arep.med.harvard.edu/CasFinder/) (Mali et al., 2013). hCas9 was a gift from George Church (Addgene plasmid #41815). gBlocks expressing gRNA and the target sites were synthesized at Integrated DNA Technologies. The synthesized gBlocks were PCR amplified with primers gRNAforward/reverse for transfection into cells. 0.1×10^6 HEK293T cells were transfected with 1 μg Cas9 plasmid, 1 μg gRNA, and 0.5 μg linealized NeoR gene fragment, using Lipofectamine 2000 as per the manufacturer's protocols. Cells were split after 24 hrs, and selected in 400 μg/mL G418. Single cell colonies were examined by western blotting for cells with PABPC1 null mutations.

5.2.3 Primer and siRNA sequences

Primer/siRNA	Sequence/catalog #
siPABPC1	AAGGUGGUUUGUGAUGAAAAU
siPABPC4-1	GCUUUGGCUUUGUGAGUUA
siPABPC4-2	GGUAAGACCCUAAGUGUCA
siControl	Qiagen (SI03650318)
gRNAForward	TGTACAAAAAAGCAGGCTTTAAAGGAACCA
gRNAReverse	TAATGCCAACTTTGTACAAGAAAGCTGGGT
Pabpc1_C_termR	AACACCGGTGGCACTGTTAACTGC
Pabpc1_midF:	ACTCCTGCTGTCCGCACCGTTCCA
Pabpc1_3UTRR	ATCAATTCTGTTACTTAAAACAGAA
Pabpc1_MLLER	GTTAACTGCTTTCTGGGCAGCCTCT
Pabpc1_L10	TCACCCAAGAAATGTGATTTTTATTAAGAAATCATTAAA
(genome)	TCCATACCTGTTGCATTGTAA
Pabpc1_U9	GCAAACCTCAGATCGAAGAAGACAGCATAAACACTTTT
(genome)	CACTCAGTAAGTTTTCCCAGTT

5.2.4 Genomic DNA extraction

Cells were pelleted and resuspend in 3 mL of TE buffer and 100μL of 20% SDS. 20 μL of Proteinase K 20 mg/mL stock solution was added to mix gently by inversion and incubate overnight at 55°C. 1 mL of saturated NaCl solution was added to the mixture.

The solution was then precipitated overnight in 10 mL 100% EtOH (Room temperature). DNA was transferred to 5 mL of 70% EtOH, and incubated overnight on rocker. DNA was then moved to a new Eppendorf tube and left air-dry. Water was used to resuspend the DNA to required concentration, and DNA was stored at -20 °C.

5.2.5 RNA extraction and cDNA library preparation

Total RNA was extracted from confluent 10-cm dishes using Trizol (Thermo-Fisher 15596-026) as per manufacturer's instructions. RNA was air-dried and dissolved in distilled water. Dissolved RNA was further purified using Qiagen miRNeasy micro kit (Cat #217084). RNA from replicates of HEK293 or clone-c1c4 cells were aliquoted and stored at -80 °C for later quantitative RT-PCR analysis or sent for mRNAseq stranded library preparation at Genome Quebec Innovation Center.

5.2.6 RNA-seq and Differential gene expression analysis

Pair-ended RNA sequencing with read length of 100 bases was performed at the Genome Quebec Innovation Center using the illumina Hiseq 2000 sequencer. Reads were trimmed from the 3' end to have a phred score of at least 30. Illumina sequencing adapters were removed from the reads, and all reads were required to have a length of at least 32. Trimming and clipping were done with Trimmomatic (http://www.usadellab.org/cms/index.php?page=trimmomatic). The filtered reads were aligned to reference genome b37. The alignment was done with the combination of tophat/bowtie software to generate a Binary Alignment Map file (Trapnell et al., 2009). Read counts were obtained using HTSeq as input. The differencial gene expression analysis was done using DESeq (Anders and Huber, 2010) and edgeR (Robinson et al., 2010) Bioconductor package. The results of the differential transcript expression analysis were generated using cuffdiff. FPKM values calculated by cufflinks were used as input (Trapnell et al., 2012).

5.2.7 Preranked gene set enrichment analysis

Differential genes from Deseq were ranked by their fold of changes (FC) and p-values (Ranking score = $\log_2$FC $\times(-\log_{10}$(p-value)) (Supplemental Table 5.3) (Plaisier et al.,

2010). The ranked gene list was used as input for GSEA and leading edge analysis (Mootha et al., 2003, Subramanian et al., 2005). The detailed GSEA parameters were as follows: the number of permutations is 1000, and the permutation type was configured to the gene set.

5.2.8 Immunofluorescence and confocal microscopy

Cells were fixed with 4% PFA in 1x PBS, and penetrated by cold methanol (-20°C) or 0.1% Triton X-100 in 1x PBS for 10 minutes. Cells were blocked with 5% normal goat serum (Millipore S26) in PBS for 1 hour. Then cells were incubated in 1x PBS, supplemented with anti-PABPC1 (Santa Cruz sc32318, 1:200) and anti-PABPC4 (PTGlab AP-14960, 1:200). Cells were washed in PBS 3 times, before being incubated with corresponding second antibodies conjugated with Alexa488 or Alexa647 (Sigma-Aldrich A31620, A31628, A31571) at 1:200 – 1:500 dilutions. DAPI (Roche) was added to washing buffer at 0.5 μg/ml to treat cells for 10 minutes. Cover slides were finally mounted in ProLong Gold anti-fade reagent (Life Technology P36930). Images were collected on Zeiss LSM 310 confocal microscope in the McGill University Life Sciences Complex Advanced BioImaging Facility (ABIF).

5.2.9 Quantitative RT-PCR

Total RNA was extracted from cells with Trizol (Life Technology). cDNA libraries were prepared using SuperScript First-Strand Synthesis System for RT-PCR (Life Technology). Validated Taqman assays were purchased for quantification of GAPDH (Applied Biosystems Hs 02758991), c-Myc (Applied Biosystems Hs00153408), and 18sRNA (Applied Biosystems Hs 99999901). qRT-PCR were run and analyzed in Stepone Plus PCR system (Applied Biosystems).

5.2.10 Western blotting

Protein samples were heated at 95°C and separated by SDS-PAGE. Proteins were then transferred to PVDF membrane (Millipore) in Tris/Glycine buffer with 20% methanol in cold room. PVDF membrane was blocked in 1x TBST (pH 7.5), containing 0.05% Tween-20 and 5% skim milk powder or bovine serum albumin. The membrane was then

incubated with primary antibodies, including anti-PABPC1 (Abcam ab21060, Cell signaling 4992 or Santa Cruz sc32318 1:1000), anti-PABPC4 (Abcam ab76763), anti-c-Myc (Santa Cruz sc 40), anti-tubulin (Sigma-Aldrich T9028 1:5000) and anti-GFP (Clontech 632381 1:2000). Membrane was then washed three times in 1x TBST and incubated with goat-anti-rabbit (Jackson ImmunoResearch 111-035-046 1:5000) or goat-anti-mouse (Jackson ImmunoResearch 115-035-071 1:5000) for 0.5 hour. After wash, membrane was developed with Amersham ECL prime kit (GE healthcare RPN2236) and imaged with Alpha Innotech imaging system.

5.3. Results

5.3.1 PABPC4 compensates loss of PABPC1 in HEK293

PABPC1 is the predominant isoform of cytoplasmic PABP in cells. We selected two target sites in exon 10 of Pabpc1 locus, and incorporated the sequences into gBlocks expressing guide RNA scaffolds (Fig. S5.1). The two scaffold RNAs were separately transfected into HEK293, together with Cas9 plasmid and a linearized NeoR gene for antibiotic selection. Random deletion, insertion or mutation was introduced around the targeted sites. Single cell colonies were screened with an antibody recognizing the C-terminal of PABPC1, for mutant cell-lines expressing PABPC1 mutants altered after the target sites. About 20% of the colonies had insertion or deletions leading to a shortened or disrupted PABPC1 (Fig. 5.1A). Cell-lines clone-c1 expressing an exon-skipped PABPC1 (Fig. 5.2 and Fig. S5.2), and clone-c1c4 (from target sequence 2) expressing a truncated PABPC1 (Fig. 5.1A & D) were selected for genomic DNA sequencing (Fig. 5.1C). Deletion of 3 bps in clone-c1 resulted in skipping of the whole exon 10 (Fig. S5.2). The 2bp insertion in clone-c1c4, led to truncated Pabpc1 mRNA (Fig. 5.1D) and a corresponding truncated PABPC1 (Fig. 5.1B and Fig. 5.2). An about 2-fold elevation of PABPC4 in protein and mRNA levels was observed in clone-c1c4, where the PABPC1 is truncated and decreased (Fig. 5.1A & E). The major PABP isoform in clone-c1c4 is PABPC4, instead of PABPC1 as in HEK293.

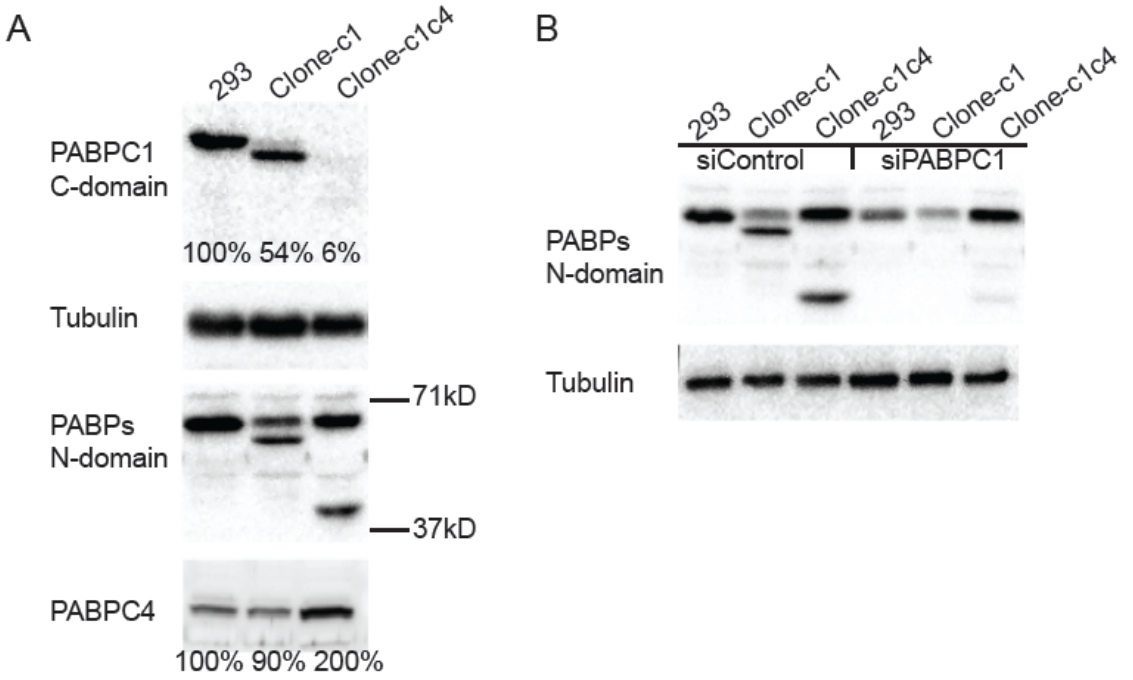

C

```
PABPC1 DNA      TTTAAAATGCAGCATTCCAAAATATG--CCCGGTGCTATCCGCCCAGCTGCT
PABPC1 mRNA     ------------CATTCCAAAATATG--CCCGGTGCTATCCGCCCAGCTGCT
Clone-c1 DNA    TTTAAAATGCAGCATTCCAAAA--TATGCCCGG---TATCCGCCCAGCTGCT
Clone-c1c4 DNA  TTTAAAATGCAGCATTCCAAAAAATATGCCCGGTGCTATCCGCCCAGCTGCT
```

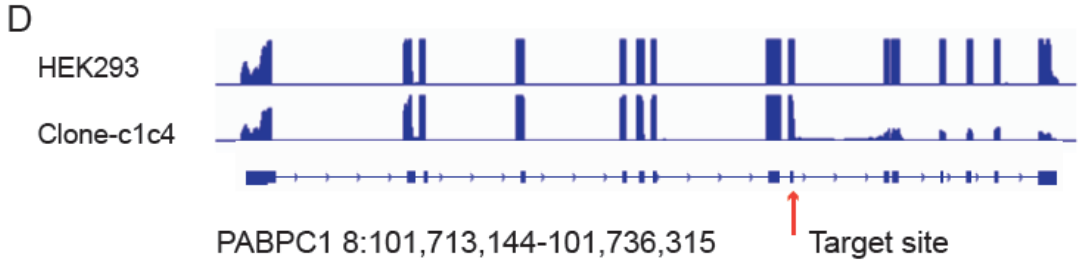

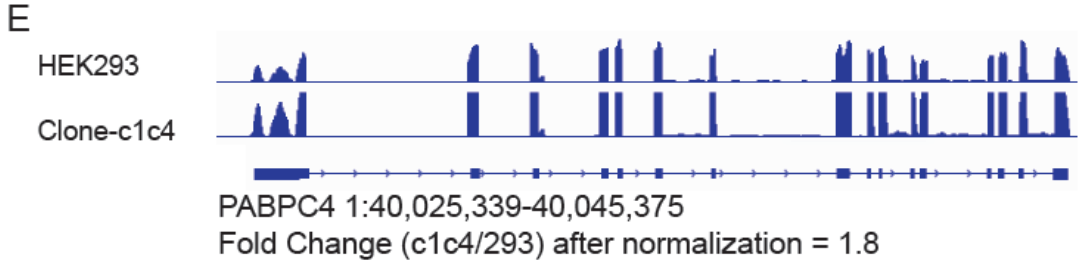

Figure 5.1 PABPC1 disruption by CRISPR/Cas9 based genome editing is compensated by elevated PABPC4 in HEK293 cells. (A) CRISPR/Cas9 genome editing of PABPC1 generated multiple mutations. Antibody recognizing C-terminal MLLE domain of PABPC1 (PABPC1 C-domain, Santa Cruz 32318) labels null mutations of PABPC1. PABPs N-domain antibody (New England Biolabs 4992), which recognizes multiple cytoplasmic PABP, reveals PABP isoform distribution. Tubulin is stained as loading control. Anti-PABPC4 shows elevated level of PABPC4 protein in clone-c1c4, when PABPC1 is truncated to about 40Kd and lowered at protein level. Percentages are relative protein levels after normalized to tubulin. (B) PABPC1 was knocked down by siRNA, in 293, clone-c1, or clone-c1c4 cells. The decreased lower bands in clone-c1 and clone-c1c4 were PABPC1 mutations. Sequences of siRNAs used are listed in materials section. (C) Genomic DNA sequences at Pabpc1 gene loci of 293, clone-c1, and clone-c1c4. Deletion of 3-bp in clone-c1 leads to skipping of exon 10 in mRNA (Fig. S5.2), and a shorter PABPC1 protein (Fig. 5.2). Clone-c1c4 has 2-bp insertion, which results in significant reduction of mRNA reads after the targeted region (D). Genomic DNA was extracted and amplified with gene specific primers. PCR products were gel purified and cloned into PCR2.1 vector for sequencing. Only one version of sequence was identified in multiple clones, indicating the homogeneity of cell-lines. (D&E) Wiggle tracks showing representative read alignment of Pabpc1 or Pabpc4 genes in HEK293 or clone-c1c4 cells. Track files are generated from the aligned reads using BedGraphToBigWig.

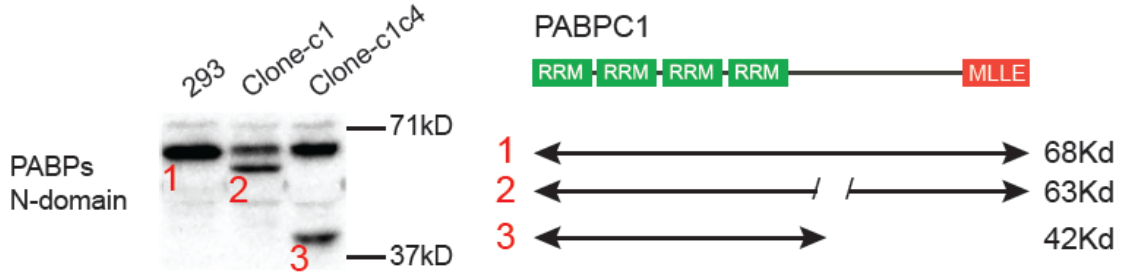

Figure 5.2 Description of PABPC1 protein in HEK293, clone-c1, and clone-c1c4. Wild-type PABPC1 is about 68Kd in molecular weight. Shortened PABPC1 is generated in clones like clone-c1, with residues 447-483 deleted. mRNA sequence of clone-c1 is

shown in Figure S5.2. In clone-c1c4, the major PABPC1 is about 42 Kd, matching the size of the major mRNA population (Fig. 5.1E).

5.3.2 Overexpression of PABPC1 represses elevated PABPC4 in clone-c1c4 cells

The shift of dominant PABP isoform from PABPC1 to PABPC4 did not change cell proliferation or morphology (data not shown). This suggests that the two isoforms are redundant in maintaining basic cellular activities. We then asked whether the elevated PABPC4 in clone-c1c4 was reversible by expression of PABPC1. Clone-c1c4 cells were overexpressed with PABPC1 or PABPC1ΔMLLE (Fig. 5.3A). PABPC1ΔMLLE overexpression repressed PABPC4 more in clone-c1c4 cells. It is not clear why deletion of the MLLE domain enhances the repression activity of PABPC1. However, it indicates that the repression comes from the RNA binding ability of the RRM domains.

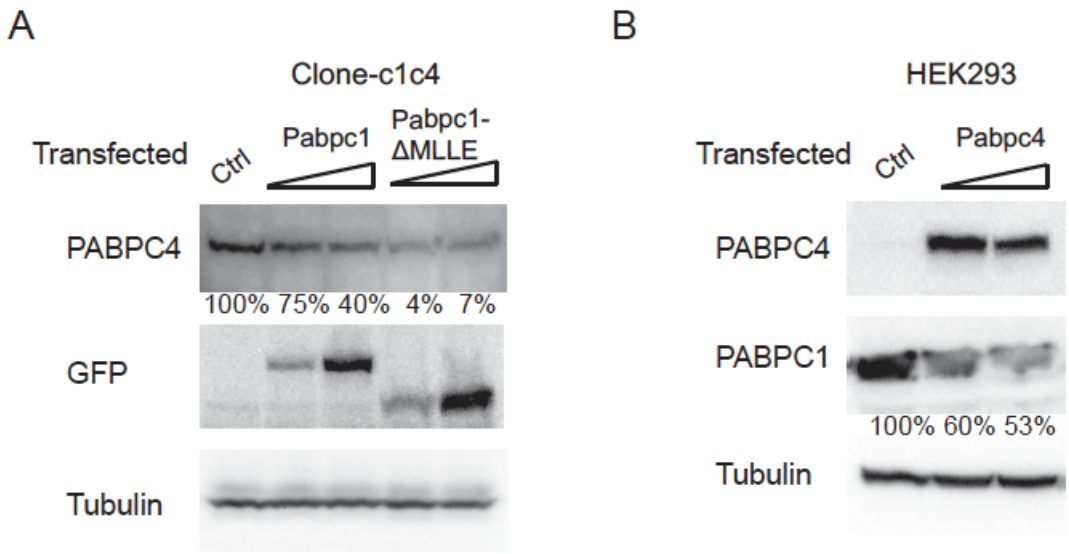

Figure 5.3 Mutual repression of PABPC1 and PABPC4. (A) Over expression of pCDNA3-EGFP (Ctrl), pCDNA3-PABPC1-EGFP, or pCDNA3-PABPC1ΔMLLE-EGFP in clone-c1c4 cells. Western blotting shows decrease of PABPC4 protein level in clone-c1c4 cells, due to over expression of PABPC1-EGFP or PABPC1ΔMLLE-EGFP. (B) Over expression of PABPC4 (construct in materials) in HEK293 reduces endogenous PABPC1 protein.

5.3.3 Overexpression of PABPC4 represses endogenous PABPC1 in HEK 293

We next overexpressed PABPC4 in HEK293, and found a reduction of endogenous PABPC1 (Fig. 5.3B). This further confirms the redundancy of isoforms PABPC1 and PABPC4. The total amount of PABP isoforms may be well regulated for cellular operations. Thus the elevation of PABPC4 in clone-c1c4 cells is due to loss of PABPC1.

5.3.4 Differential gene expression analysis in clone-c1c4 cells

The clone-c1c4 cell-line offered us a platform to study PABP isoform specific functions. To investigate the effects of PABP isoform usage shift on the transcriptome, we sent clone-c1c4 and HEK293 cells for RNA-seq. Reads were trimmed, filtered and aligned as described in methods. Read counts were obtained using HTSeq. Differential gene expression analysis was done with edgeR (Robinson et al., 2010) and DESeq (Anders and Huber, 2010) R bioconductor packages. Differentially expressed (DE) genes were ranked according to the p-values. The heat map of the gene expressions (Fig. S5.3) indicated gene expression profile changes in clone-c1c4 cells. The top 300 DE genes were labeled red on MA plot (Fig. 5.4A). Most of the top 300 DE genes were relatively highly expressed according to the counts. The top 10 DE genes were shown in table (Fig. 5.4B). Representative wiggle track views of the 10 genes displayed mRNA profiles, confirming the DE gene calling (Fig. 5.4C).

A

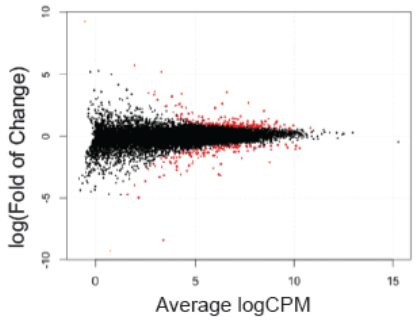

B

	gene_symbol	log_FC	log_CPM
ENSG00000079215	SLC1A3	2.268	5.975
ENSG00000102195	GPR50	-8.407	3.371
ENSG00000102316	MAGED2	-1.774	7.347
ENSG00000104419	NDRG1	2.711	7.685
ENSG00000115414	FN1	-2.113	8.757
ENSG00000130508	PXDN	-3.052	6.177
ENSG00000136997	MYC	3.559	6.587
ENSG00000165194	PCDH19	-3.157	6.248
ENSG00000176887	SOX11	1.631	7.282
ENSG00000184613	NELL2	2.652	6.333

C

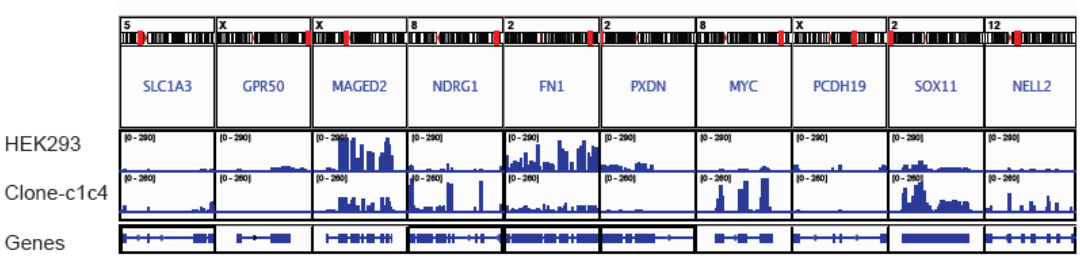

Figure 5.4 Differential gene expression in HEK293 and the modified clone-c1c4 cells. (A) MA plot of differential expression magnitude (log2 of fold change (clone-c1c4/HEK293) versus expression levels (log2 of counts per million). The red dots are the top 300 differential genes ranked by p-values. (B) The top 10 differential genes. Ensembl gene id, gene symbol, log2(fold of changes), and log2(counts per million) are shown in the table. (C) Representative view of the mRNA profile of the top 10 differential genes. The figure is generated with Integrative Genomics Viewer.

5.3.5 c-Myc is central to differential gene expression in clone-c1c4

To infer biologically important genes underlying the transcriptome changes, we used Gene Set Enrichment Analysis to examine the enrichment of 50 hallmark signature gene sets (Liberzon et al., 2015). Enriched gene sets were plotted against their normalized enrichment scores. Gene sets with p-values lower than 0.10 are marked red (Fig. 5.5A). The leading edge subset analysis of the most enriched gene sets revealed c-Myc as the most overlapped gene (Fig. 5.5B and Fig. S5.4). The increase of c-Myc in clone-c1c4 was confirmed by western blotting and qRT-PCR (Fig. 5.5C & D).

A

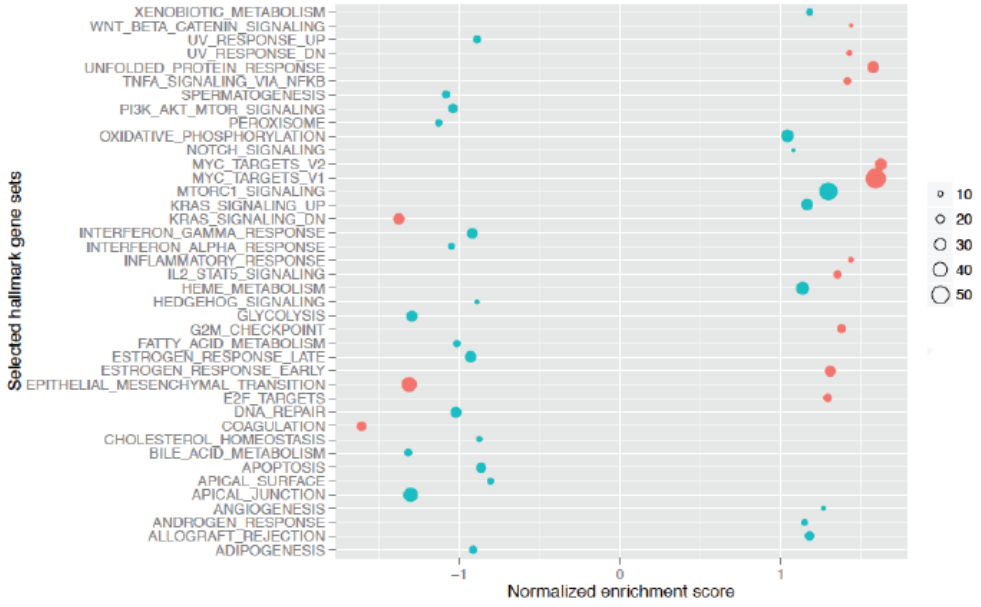
XENOBIOTIC_METABOLISM
WNT_BETA_CATENIN_SIGNALING
UV_RESPONSE_UP
UV_RESPONSE_DN
UNFOLDED_PROTEIN_RESPONSE
TNFA_SIGNALING_VIA_NFKB
SPERMATOGENESIS
PI3K_AKT_MTOR_SIGNALING
PEROXISOME
OXIDATIVE_PHOSPHORYLATION
NOTCH_SIGNALING
MYC_TARGETS_V2
MYC_TARGETS_V1
MTORC1_SIGNALING
KRAS_SIGNALING_UP
KRAS_SIGNALING_DN
INTERFERON_GAMMA_RESPONSE
INTERFERON_ALPHA_RESPONSE
INFLAMMATORY_RESPONSE
IL2_STAT5_SIGNALING
HEME_METABOLISM
HEDGEHOG_SIGNALING
GLYCOLYSIS
G2M_CHECKPOINT
FATTY_ACID_METABOLISM
ESTROGEN_RESPONSE_LATE
ESTROGEN_RESPONSE_EARLY
EPITHELIAL_MESENCHYMAL_TRANSITION
E2F_TARGETS
DNA_REPAIR
COAGULATION
CHOLESTEROL_HOMEOSTASIS
BILE_ACID_METABOLISM
APOPTOSIS
APICAL_SURFACE
APICAL_JUNCTION
ANGIOGENESIS
ANDROGEN_RESPONSE
ALLOGRAFT_REJECTION
ADIPOGENESIS
Selected hallmark gene sets
−1
0
1
Normalized enrichment score
10
20
30
40
50

B

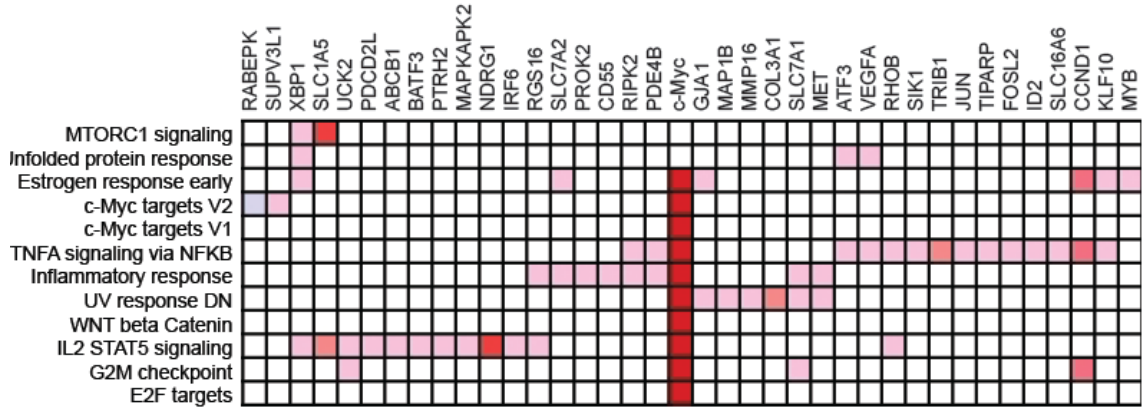
RABEPK
SUPV3L1
XBP1
SLC1A5
UCK2
PDCD2L
ABCB1
BATF3
PTRH2
MAPKAPK2
NDRG1
IRF6
RGS16
SLC7A2
PROK2
CD55
RIPK2
PDE4B
c-Myc
GJA1
MAP1B
MMP16
COL3A1
SLC7A1
MET
ATF3
VEGFA
RHOB
SIK1
TRIB1
JUN
TIPARP
FOSL2
ID2
SLC16A6
CCND1
KLF10
MYB
MTORC1 signaling
Unfolded protein response
Estrogen response early
c-Myc targets V2
c-Myc targets V1
TNFA signaling via NFKB
Inflammatory response
UV response DN
WNT beta Catenin
IL2 STAT5 signaling
G2M checkpoint
E2F targets

C

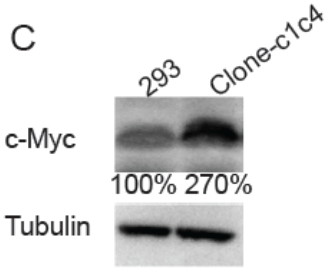
293
Clone-c1c4
c-Myc
100% 270%
Tubulin

D

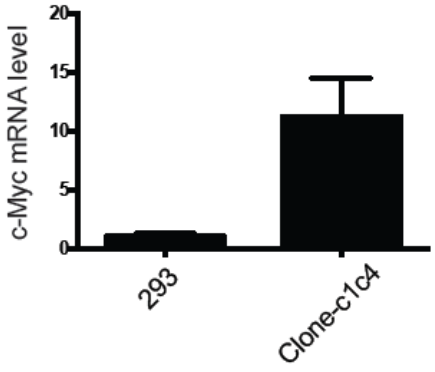
c-Myc mRNA level
20
15
10
5
0
293
Clone-c1c4

Figure 5.5 Changes of expression in clone-c1c4 cells. (A) Gene set enrichment analysis of selected hallmark gene sets (Subramanian et al., 2005). The size of circles indicates the number of significant genes. Gene sets with p-values lower than 0.1 are labeled red. (B) Leading edge overlap for the modified clone-c1c4 cells. The significantly enriched gene sets from (A) are aligned to indicate common genes. c-Myc is the most significant overlapped gene. Other overlapped genes are shown in Fig. S5.4. The intensity of color indicates fold of changes in expression. Only a subset of the genes are displayed for visibility. (C) Increased c-Myc protein in clone-c1c4 cells. The percentage indicates relative quantifications of c-Myc protein after normalization. Cells were lysed in SDS-loading buffer and boiled. c-Myc protein level is probed by antibody (Sant Cruz sc-40). Tubulin is used as loading control. (D) Increased c-Myc mRNA level. Taqman assay (Applied Biosystems Hs 00153408) reveals an increase of about 10-fold in c-Myc mRNA in clone-c1c4. GAPDH (Applied Biosystems Hs 02758991) is used as loading control.

5.3.6 c-Myc mRNA half-life is not changed in clone-c1c4

To check whether the increased c-Myc mRNA level in clone-c1c4 was transcriptional or post transcriptional, we treated HEK293 or clone-c1c4 cells with 10 μg/mL actinomycin-D to inhibit new transcription. Samples were collected at different time points to determine c-Myc mRNA half-life by quantitative RT-PCR. C-Myc mRNA levels measured by taqman assay were normalized to 18s RNA. This suggests that the increase of c-Myc mRNA level is transcriptional.

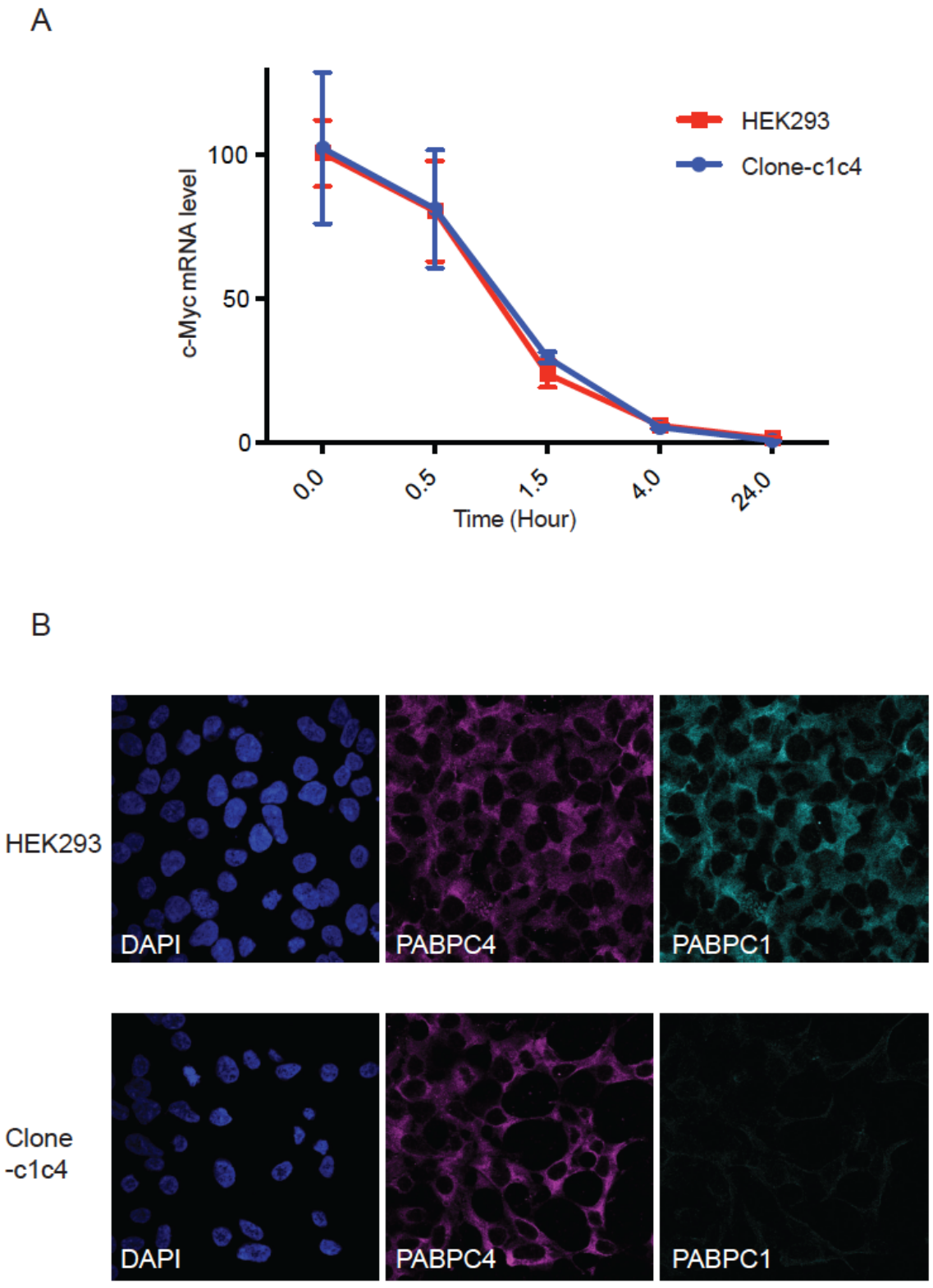

Figure 5.6 (A) c-Myc mRNA half-life is similar in HEK293 and clone-c1c4. Cells were treated by (10 μg/ml) antinomycin-D for indicated time before Trizol extraction of total

RNA. Taqman assays were used to measure c-Myc levels normalized to 18s RNA (Applied Biosystems Hs 99999901). The c-Myc mRNA levels of cells without treatment are normalized to 100 for comparison. (B) PABPC4 in clone-c1c4 is predominantly cytoplasmic. HEK293 or clone-c1c4 cells were stained with DPAI, anti-PABPC4 (Abcam ab76763), and anti-PABPC1 (Abcam ab21060). The anti-PABPC1 (Abcam ab21060) recognizes the C-terminal tail of PABPC1.

5.3.7 PABPC4 is predominantly cytoplasmic in clone-c1c4

Although the role of PABPC4 in transcriptional control is not known, there is increased nuclear distribution of PABPC4 in response to stresses (Burgess et al., 2011) or PABPN1 depletion (Bhattacharjee and Bag, 2012). We stained PABPC4 in HEK293 and clone-c1c4 cells, and found PABPC4 is predominantly cytoplasmic in both cell-lines (Fig. 5.6B). Thus the increased PABPC4 in clone-c1c4 doesn't lead to significant nuclear relocation.

5.3.8 Correlation of PABPC4 and c-Myc changes

We then knocked down Pabpc4 in clone-c1c4 cells with siRNAs. c-Myc mRNA and protein levels decreased correlated to PABPC4 depletion (Fig. 5.7A & B). This suggests that the level of PABPC4 isoforms correlates with the c-Myc level and can potentially affect the transcriptome.

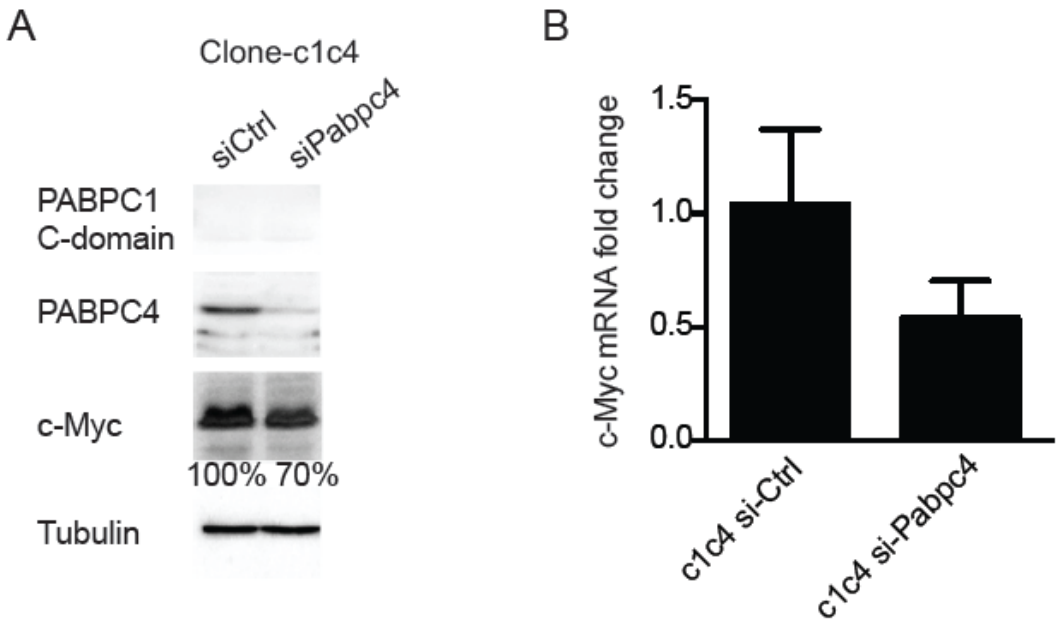

Figure 5.7 Correlation between decrease of PABPC4 and c-Myc. (A) Decrease of c-Myc protein level correlates with depletion of PABPC4. Representative blots of Pabpc4 knocked down clone-c1c4 cells. Corresponding antibodies were used to probe PABPC1, PABPC4, c-Myc, and tubulin levels. (B) Correlated c-Myc mRNA decrease after siRNA mediated knockdown of PABPC4.

5.3.9 Isoform usage of PABP and c-Myc levels

To test the effects of PABP isoform usage on c-Myc levels, we depleted PABPC1 or PABPC4 with siRNAs in HEK293 cells (Fig. 5.8A). Depletions of the two isoforms affect c-Myc mRNA levels in opposite directions. Decrease of PABPC4 lowered c-Myc mRNA, while decrease of PABPC1 raised c-Myc mRNA level. This confirms that the usage of the PABPC1 or PABPC4 isoform can exert influence on the transcriptome through c-Myc.

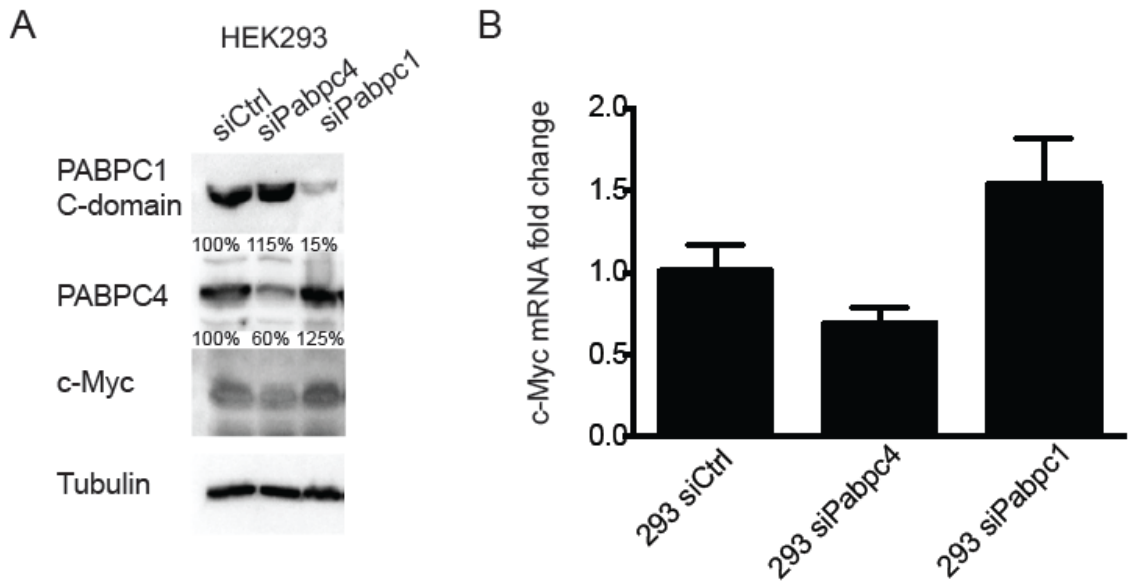

Figure 5.8 Differential effects of PABPC1 or PABPC4 depletion on c-Myc mRNA level in HEK293 cells. (A) HEK293 cells were transfected with control siRNA, siPabpc1, or siPabpc4 for 48 hrs. PABPC1 and PABPC4 were probed to examine knockdown effects. (B) Changes of c-Myc mRNA levels in siRNA treated HEK293 cells. Depletion of PABPC4 reduces c-Myc mRNA level, while depletion of PABPC1 increases c-Myc mRNA. Differences of c-Myc mRNA levels were significant at p-value of 0.05 with two-tail t-test for samples with the same variances.

5.4. Discussion

Here we reported compensation of PABPC4 induced by the loss of PABPC1 in HEK293 cells. The cells are viable suggesting functional overlap of the two isoforms. Analysis of transcriptome profile revealed differential gene expression correlated with usage of PABPC4 and PABPC1. The study helps us understand isoform specific functions of PABP in development or different tissues.

Recent genomic studies support PABPC1 recognition of RNA sequences other than pure poly(A) in mouse (Kini et al., 2016) and yeast (Baejen et al., 2014). The overall structures of RRM domains in PABP isoforms are likely to be similar, due to high sequence similarities between domains and across species. However, considerable

conserved differences are found in PABP isoforms. Some of the differences locate at interfaces critical to RNA recognition, especially in RRM3-4 domain (Fig. S5.5). These different residues may not alter the overall structures of RRM domains, but contribute to specificity in RNA recognition. It's being realized that PABP isoforms are functionally different in vertebrate development (Gorgoni et al., 2011) and other contexts. PABPC4 depletion impacts steady-state expression of a subset of mRNAs and affects erythroid differentiation (Kini et al., 2014). PABPC1L (ePABP) regulates translation and stability of maternal mRNAs (Vasudevan et al., 2006), and substituted by increasing PABPC1 after onset of zygotic transcription (Cosson et al., 2002).

The recently developed Crosslinking immunoprecipitation coupled high-throughput sequencing technique (CLIP-seq) provides a powerful tool to map association of RNA-binding proteins with RNA. Mapping the interactions of PABP isoforms with mRNA would greatly facilitate understanding of the functions of those isoforms. It is likely that PABP isoforms function through recognition of separate subsets of mRNAs, besides binding to a common mRNA pool. So far, such mapping data is only available for PABPC1 in higher eukaryotes (Kini et al., 2016). Lack of CLIP data from other PABP isoforms makes it difficult for biological inferences of differential gene expression profiles.

In this study, c-Myc is identified as a central player in remodeling the transcriptome of clone-c1c4 cells. C-Myc is a transcription factor that can shape the cellular transcriptome (Kress et al., 2015). PABP isoforms may act through a subset of mRNAs to indirectly upregulate c-Myc transcription. In the Gene Set Enrichment Analysis, WNT pathway is enriched (Fig. 5.5) and can induce c-Myc transcription (Kress et al., 2015). Mechanisms underlying correlation of PABPC4 and c-Myc remain to be revealed by further studies.

The significant increase (~10 folds) of c-Myc mRNA is tolerated in clone-c1c4. Cell cycle analysis by propidium iodide DNA staining and flow cytometry showed similar distribution in HEK293 and clone-c1c4 cells in different phases (data not shown). This may partially because c-Myc protein increases at a smaller degree (~3 folds). Elevation of

genes like Axin1 (Supplemental Table 5.1) may enhance c-Myc protein turnover (Arnold et al., 2009), which balances the sharp increase of c-Myc mRNA. Nonetheless, c-Myc targets are upregulated in clone-c1c4 extensively (Fig. 5.5B, Supplemental Table 5.3&4 GSEA sets). Variant calling on the RNA-seq data reveals no insertion, deletion or mutation in c-Myc, or genes we know to affect c-Myc transcription (Data not shown). Blast search returns no other genomic sequence for the first 13 bps of the target sequence 2 (Fig. S5.1), which was used for generation of clone-c1c4. Modulation of PABPC4 or PABPC1 levels support a correlation of PABPC4 and c-Myc levels (Fig. 5.7 & 5.8). One interesting observation is that PABPC4 overexpression in HEK293 decreases endogenous PABPC1 by ~50% (Fig. 5.3B), but does not affect c-Myc mRNA level (data not shown). It may reflect the dominant role PABPC1 compared to other PABP isoforms. Other isoforms can only function significantly when PABPC1 is at very low levels, as in clone-c1c4 (Fig. 5.7A) or PABPC1 depleted HEK293 (Fig. 5.8A).

Overall, we created in a human cell-line where the predominant PABPC1 is stably substituted by PABPC4. It opens a window to observe functional differences between the two isoforms. Validations and further investigations in different approaches will help us understand the mechanistic details underneath.

Acknowledgements

We appreciate Dr. Guennadi Kozlov for critically reading our manuscript. We are grateful for suggestions and help from colleagues during the project.

Competing interests

No competing interests declared.

Author contributions

J. X. designed and carried out the experiments. J. X. did the bioinformatics analysis. J. X. wrote the manuscript. K. G. revised the manuscript.

Funding

This study was supported by Canadian Institutes of Health Research grant MOP-14219. J. X. was supported by the CIHR Strategic Training Initiative in Chemical Biology, the CIHR Strategic Training Initiative in Systems Biology, Graduate Student Scholarship of the Quebec Network for Research on Protein Function, Engineering, and Applications (PROTEO), and the Recruitment Award of the Groupe de Recherche Axé sur la Structure des Protéines (GRASP).

Supplemental materials

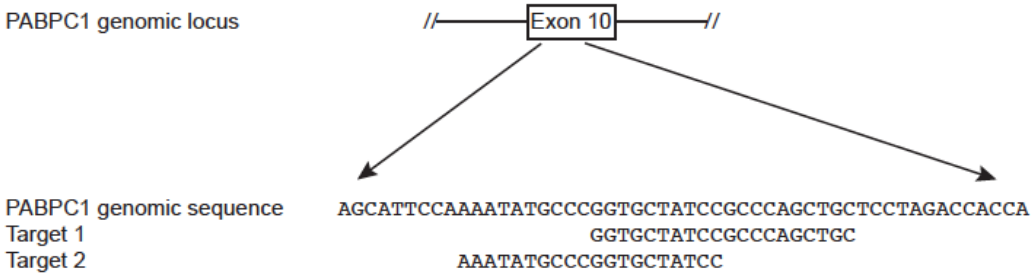

Figure S5.1 Design of gRNA sequences for targeting exon 10 of Pabpc1 gene. Two specific target sequences were identified in Pabpc1 using CasFinder (http://arep.med.harvard.edu/CasFinder/) (Mali et al., 2013). Both sequences locate at exon 10 of Pabpc1. The first 13 bps of target sequence 2, which generates the clone-c1c4, complements no other genomic sequences by BLAST search.

A

gBlocks sequence for target site 1:

TGTACAAAAAAGCAGGCTTTAAAGGAACCAATTCAGTCGACTGGATCCGGTACC
AAGGTCGGGCAGGAAGAGGGCCTATTTCCCATGATTCCTTCATATTTGCATATA
CGATACAAGGCTGTTAGAGAGATAATTAGAATTAATTTGACTGTAAACACAAAG
ATATTAGTACAAAATACGTGACGTAGAAAGTAATAATTTCTTGGGTAGTTTGCA
GTTTTAAAATTATGTTTTAAAATGGACTATCATATGCTTACCGTAACTTGAAAG
TATTTCGATTTCTTGGCTTTATATATCTTGTGGAAAGGACGAAACACCGCAGCT
GGGCGGATAGCACCGTTTTAGAGCTAGAAATAGCAAGTTAAAATAAGGCTAGTC
CGTTATCAACTTGAAAAAGTGGCACCGAGTCGGTGCTTTTTTTCTAGACCCAGC
TTTCTTGTACAAAGTTGGCATTA

gBlocks sequence for target site 2:

TGTACAAAAAAGCAGGCTTTAAAGGAACCAATTCAGTCGACTGGATCCGGTACC
AAGGTCGGGCAGGAAGAGGGCCTATTTCCCATGATTCCTTCATATTTGCATATA
CGATACAAGGCTGTTAGAGAGATAATTAGAATTAATTTGACTGTAAACACAAAG
ATATTAGTACAAAATACGTGACGTAGAAAGTAATAATTTCTTGGGTAGTTTGCA
GTTTTAAAATTATGTTTTAAAATGGACTATCATATGCTTACCGTAACTTGAAAG
TATTTCGATTTCTTGGCTTTATATATCTTGTGGAAAGGACGAAACACCGGATAG
CACCGGGCATATTTGTTTTAGAGCTAGAAATAGCAAGTTAAAATAAGGCTAGTC
CGTTATCAACTTGAAAAAGTGGCACCGAGTCGGTGCTTTTTTTCTAGACCCAGC
TTTCTTGTACAAAGTTGGCATTA

B

AAGAATTTTGGAGAAGACATGGATGATGAGCGCCTTAAGGATCTCTTTGGCAAGTTT
GGGCCTGCCTTAAGTGTGAAAGTAATGACTGATGAAAGTGGAAAATCCAAAGGATTT
GGATTTGTAAGCTTTGAAAGGCATGAAGATGCACAGAAAGCTGTGGATGAGATGAAC
GGAAAGGAGCTCAATGGAAAACAAATTTATGTTGGTCGAGCTCAGAAAAAGGTGGAA
CGGCAGACGGAACTTAAGCGCAAATTTGAACAGATGAAACAAGATAGGATCACCAGA
TACCAGGGTGTTAATCTTTATGTGAAAAATCTTGATGATGGTATTGATGATGAACGT
CTCCGGAAAGAGTTTTCTCCATTTGGTACAATCACTAGTGCAAAGGTTATGATGGAG
GGTGGTCGCAGCAAAGGGTTTGGTTTTGTATGTTTCTCCTCCCCAGAAGAAGCCACT
AAAGCAGTTACAGAAATGAACGGTAGAATTGTGGCCACAAAGCCATTGTATGTAGCT
TTAGCTCAGCGCAAAGAAGAGCGCCAGGCTCACCTCACTAACCAGTATATGCAGAGA
ATGGCAAGTGTACGAGCTGTTCCCAACCCTGTAATCAACCCCTACCAGCCAGCACCT
CCTTCAGGTTACTTCATGGCAGCTATCCCACAGACTCAGAACCGTGCTGCATACTAT
CCTCCTAGCCAAATTGCTCAACTAANACCAAGTCCTCGCTGGACTGCTCAGGGTGCC
AGACCTCATCC--------TAACACATCAACACAGACAATGGGTCCACGTCCTGCAG
CTGCAGCCGCTGCAGCTACTCCTGCTGTCCGCACCGTTCCACAGTATAAATATGCTG
CAGGAGTTCGCAATCCTCAGCNACATCTTAATGCACAGCCNCAAGTTACNATGCAAC
AGCCTGCTGTTCATGTACAAGGTCAGGAACCTTTGACTGCTTNCATGNTGNCNTCTG
CCCCTCCTCANAGCAAAAGCAAATGNNGNNGAACGGCT

Figure S5.2 Pabpc1 mRNA sequence of clone-c1. Total RNA was extracted by Trizol from clone-c1 cells, and reverse-transcribed to cDNA using oligo(T) and random hexamers. Pabpc1 specific primers were then used to amplify fragments of Pabpc1. A single band from the amplified products was ligated into PCR2.1 by T/A cloning. Only one version of mRNA sequence was returned, suggesting that the exon-skipping in Pabpc1 is homogenous in clone-c1.

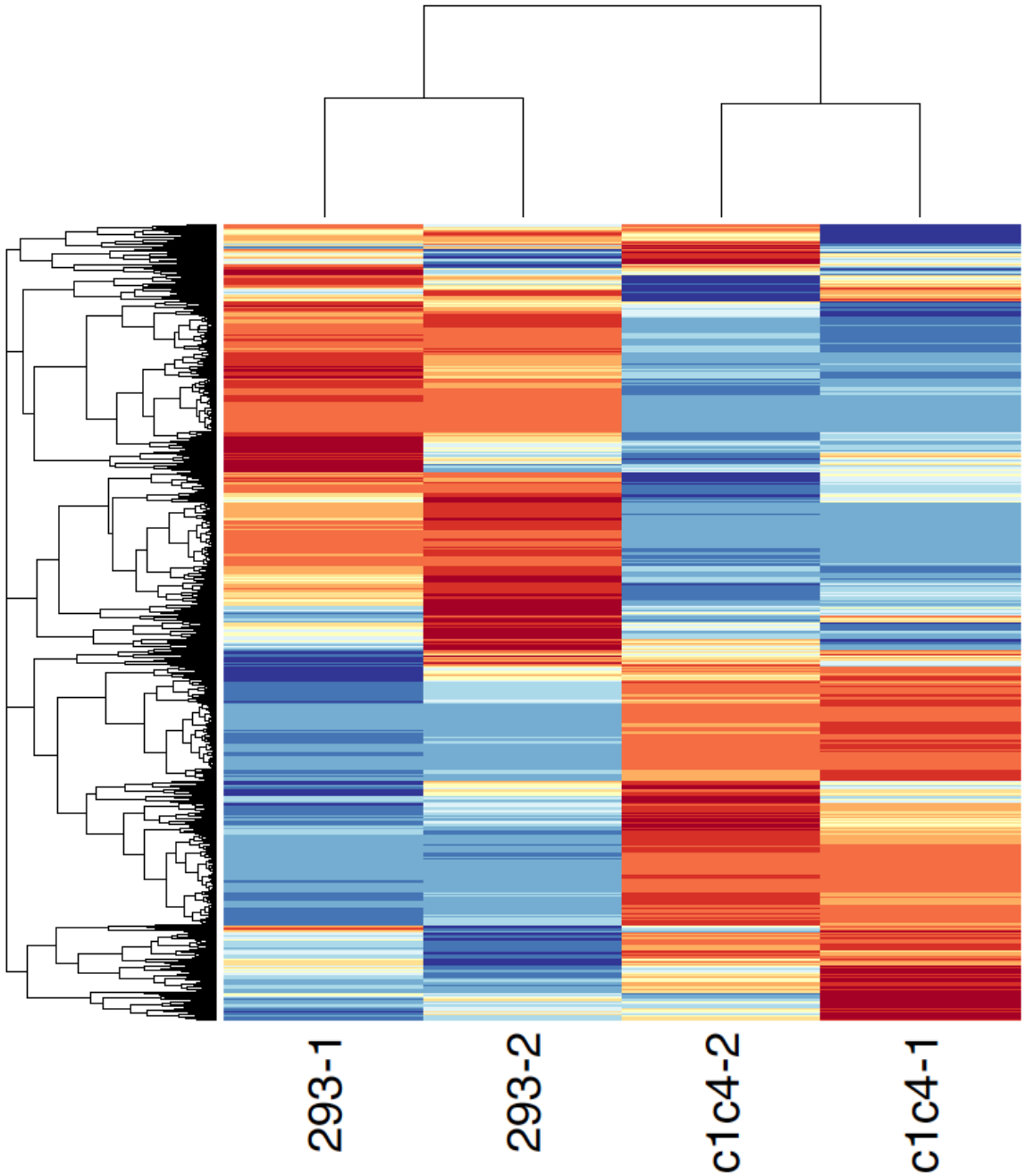

Figure S5.3 Heat map of the gene expressions. The heat map is generated with scaled FPKM values of the samples. Red indicates higher expressions. Blue indicates lower expressions.

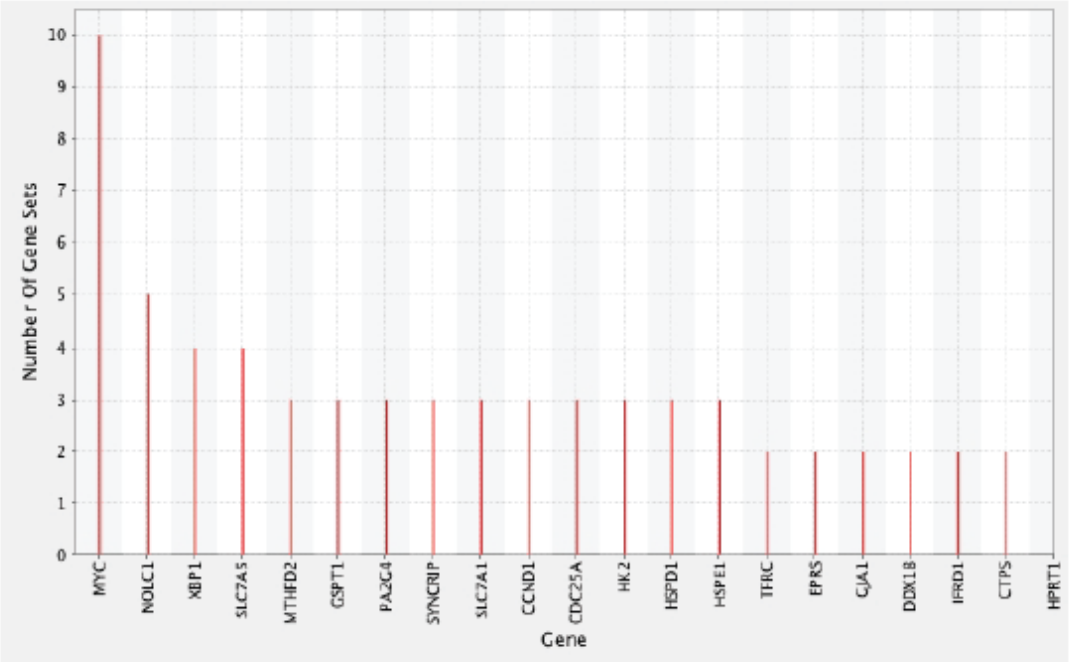

Figure S5.4 Counts of overlapped genes from the leading edge analysis of GSEA. The frequency of a gene found in enriched gene sets is plotted against gene names.

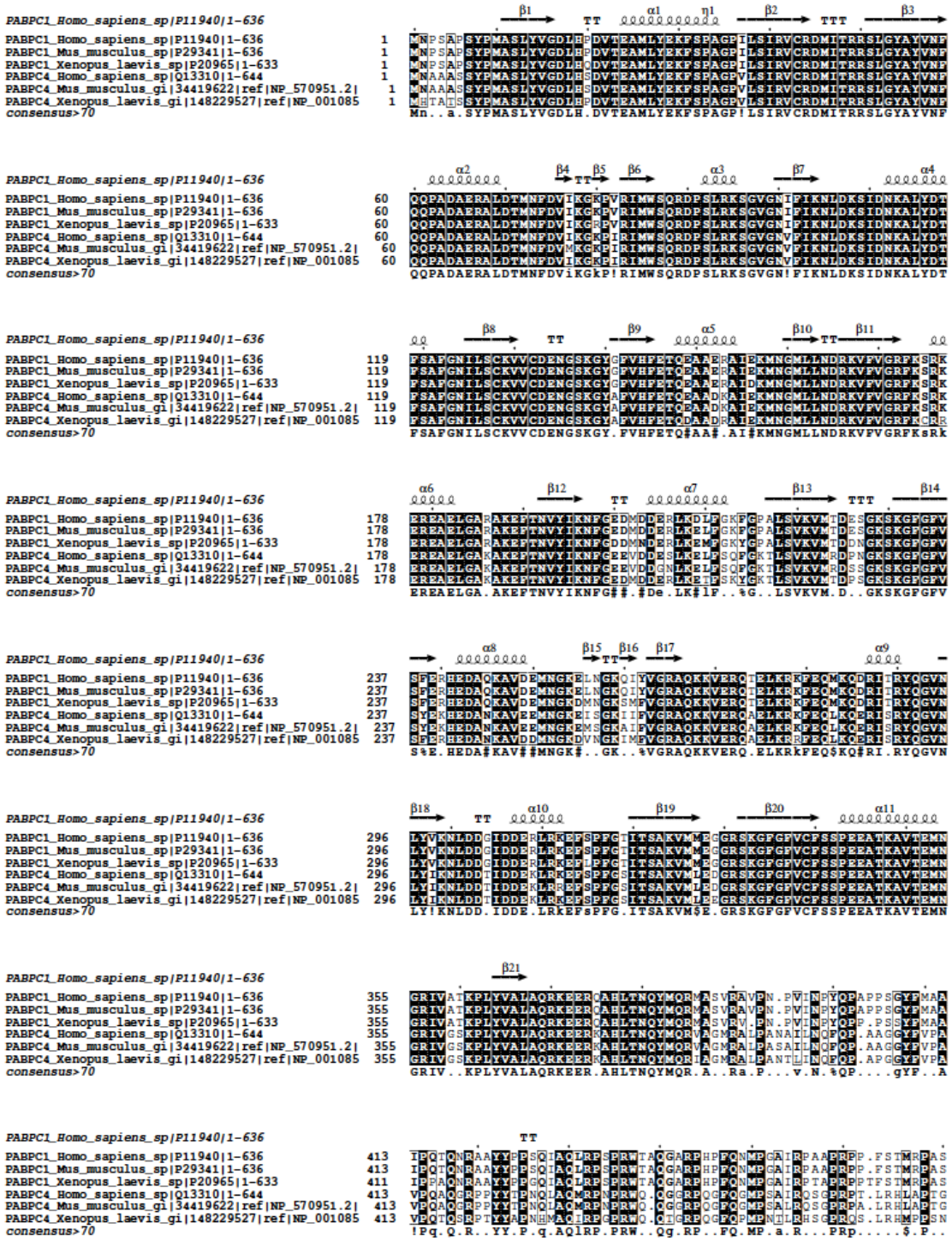
PABPC1_Homo_sapiens_sp|P11940|1-636
PABPC1_Homo_sapiens_sp|P11940|1-636
PABPC1_Mus_musculus_sp|P29341|1-636
PABPC1_Xenopus_laevis_sp|P20965|1-633
PABPC4_Homo_sapiens_sp|Q13310|1-644
PABPC4_Mus_musculus_gi|34419622|ref|NP_570951.2|
PABPC4_Xenopus_laevis_gi|148229527|ref|NP_001085
consensus>70

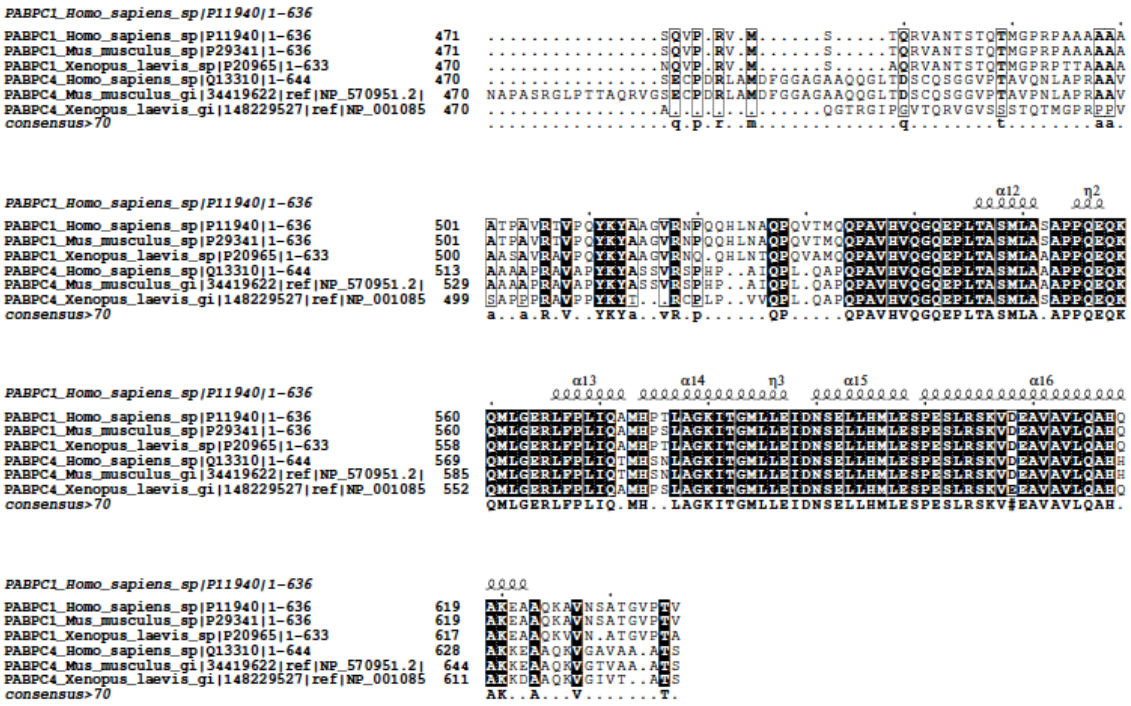

Figure S5.5 Alignment of PABPC1 and PABPC4 sequences. Sequences from *Homo sapiens*, *Mus musculus* and *Xenopus laevis* are included to highlight conserved residues. M-Coffee is used for alignment (http://tcoffee.crg.cat/apps/tcoffee/do:mcoffee)(Di Tommaso et al., 2011).

Chapter 6. Summary and perspectives

PABP is an old and new protein. Here, I have presented my work on the regulation, interactions and functions of PABP. This helps us to further understand the intricate network around PABP. Some topics regarding PABP are of particular interest for future endeavors.

6.1 What are the conformational changes of PABP on and off RNA?

Cytoplasmic PABP plays a double role regarding poly(A) tail of mRNA. mRNA is stabilized and protected by PABPC1 from deadenylation by Ccr4/Not deadenylases (Tucker et al., 2002). Meanwhile, PABPC1 is required for microRNA-mediated gene silencing via GW182 (Braun et al., 2011, Chekulaeva et al., 2011, Fabian et al., 2011, Zekri et al., 2013) or deadenylation by Pan2/Pan3 deadenylases (Lowell et al., 1992, Zheng et al., 2008). The dissociation of PABP is a key event in mRNA decay. PABP adopts different conformations when in complex with poly(A) or Paip2 (Lee et al., 2014). The conformational changes may be critical in PABP's functions regarding translation or decay of mRNA. We have made remarkable progress in crystallizing PABP/poly(A) and PABP/Paip2 (not shown in the thesis). It would be exciting to compare the two structures side by side, showing how PABP shifts from one status to another. Knowledge of the molecular details can clarify critical sites on PABP for modification or interaction etc.

6.2 How does PABP bind Paip1 and RNA at the same time?

The PAM1 motif of Paip1 is similarly acidic and should also compete with RNA binding to PABP, yet, curiously, Paip1 stimulates translation. Paip1, which binds to PABP in vitro and in vivo, triggers a 7-fold stimulation of translation of a luciferase reporter mRNA in COS-7 cells, and deletion of its PABP-interaction sites abrogated the effect (Martineau et al., 2008b). This supports the existence of multiple PABP conformations. Structural studies of PABP/Paip1, or PABP/Paip1/RNA will further our understanding of PABP as a versatile molecular machine.

6.3 Do PABP isoforms bind to distinct nRNA subsets?

The recently developed crosslinking immunoprecipitation coupled high-throughput sequencing technique (CLIP-seq) provides a powerful tool to map association of RNA-binding proteins with RNA. Mapping the interactions of PABP isoforms with mRNA would greatly facilitate understanding of the functions of those isoforms. It is likely that PABP isoforms function through recognition of separate subsets of mRNAs, besides binding to a common mRNA pool. So far, such mapping data is only available for PABPC1 in higher eukaryotes (Kini et al., 2016). Lack of CLIP data from other PABP isoforms makes it difficult for biological inferences of differential gene expression profiles.

One technical challenge of CLIP is to specifically precipitate target protein from cell lysate. The high protein sequence similarity between PABPC1 and PABPC4 makes the challenge to precipitate tougher. In Chapter 5, I have shown that a cell-line clone-c1c4 expressed elevated PABPC4 and truncated PABPC1. I have found antibodies to immunoprecipitate PABPC4 protein from clone-c1c4 cells. This could be used to generate a PABPC4 associated mRNA pool. Comparison of PABPC1 and PABPC4 mRNA pools can help understand mechanisms behind isoform specific functions.

6.4 How do PABP isoforms coordinate in cells?

PABPC1 is the most abundant cytoplasmic PABP in most cases. It is logical that most cellular processes requiring PABP is carried out by PABPC1 isoform. The high sequence similarity of the PABP isoforms indicates conservation of 3-D structures. PABP isoforms may function in the way in facilitating closed loop formation of mRNA, which involves interactions with poly(A) and eIF4G. When and how do minor PABP isoforms function? It may be closely related to developmental stages and tissue contexts. Revealing the isoform specific mRNA pools may throw a light on the mechanisms underneath.

6.5 How does PABP recognize non-pure poly(A) RNA?

Only a low percentage (2.6%) of sequencing reads bound by PABPC1 are pure poly(A) (Kini et al., 2016). However, all structural studies of PABP/RNA to our knowledge are based on pure poly(A). How PABP isoforms bind various sequences of RNA is an important question to address in understanding PABP functions outside of 3' UTR and PABP isoform specific functions. A combination of NMR and X-ray crystallography can elucidate the interplay of RNAs and PABPs. The Gehring laboratory has rich experience in NMR studies of PABP RRM domains, and has assigned a number of them. It will be interesting to see how RRM domains recognize different RNA partner in solution.

6.6 What are the mediators between PABPC1 and P-body formation?

In Chapter 2, I have shown that PABPC1 protein level is critical to PB assembly. Depletion of PABPC1 decreases the number of constitutive PBs. When the PABPC1-depleted cells are stressed, PBs reform in a merged manner with SGs. We have demonstrated that GW182 could be one candidate linking PABPC1 level and PB formation. GW182 provides one explanation for the relation between PABPC1 and P-bodies. The detailed mechanism, nonetheless, is far from clear. The compensation of PABP isoform at disruption of PABPC1 by genome editing (chapter 5) prevents study of P-bodies in a simple background of PABPC1.

6.7 Use of PAM2 to target protein to mRNA

Most PABPs are tightly associated with mRNA. We know PAM2 motifs interacting with MLLE domain of PABP at a range of affinities. The development of super-PAM2 makes targeting of MLLE domain more specific at higher affinity. Tendency of PB proteins to aggregate when overexpressed adds to the difficulty of PB assembly studies. Using incorporated superPAM2 to target protein to SGs is a good way to evaluate roles of proteins in PB assembly and dissect specific interactions.

PAM2 can also be used to tether protein to mRNA, when PABP is present. No extra RNA motifs or protein tags are required. It could be useful when high local concentration of a cargo protein is needed. The PAM2 can be inserted in to any unstructured part of a protein, to bind MLLE domain. This can be a useful tool, especially for in vivo studies where targeting a protein to mRNA can be challenging.

6.8 Summary

The PABP network is only a tiny part of the cellular activities in cells. The more I learn about nature, the more formidable it becomes to me. The development of novel technologies empowers us to perceive nature better. Our knowledge grows together with our ignorance in amount. And behind every bit of knowledge we know about nature, there are the dedication of generations of researchers. During my doctoral research, I furthered our understanding of PABP a little bit. Nonetheless, I saw far more things we don’t understand. Hopefully, future researchers will find here a solid base to reach higher.

References

ALBRECHT, M. & LENGAUER, T. 2004. Survey on the PABC recognition motif PAM2. *Biochem Biophys Res Commun,* 316**,** 129-38.

AMRANI, N., GHOSH, S., MANGUS, D. A. & JACOBSON, A. 2008. Translation factors promote the formation of two states of the closed-loop mRNP. *Nature,* 453**,** 1276-80.

ANDERS, S. & HUBER, W. 2010. Differential expression analysis for sequence count data. *Genome Biol,* 11**,** R106.

ANDERSON, P. & KEDERSHA, N. 2006. RNA granules. *J Cell Biol,* 172**,** 803-8.

ANDREI, M. A., INGELFINGER, D., HEINTZMANN, R., ACHSEL, T., RIVERA-POMAR, R. & LUHRMANN, R. 2005. A role for eIF4E and eIF4E-transporter in targeting mRNPs to mammalian processing bodies. *RNA,* 11**,** 717-27.

ANGENSTEIN, F., EVANS, A. M., SETTLAGE, R. E., MORAN, S. T., LING, S. C., KLINTSOVA, A. Y., SHABANOWITZ, J., HUNT, D. F. & GREENOUGH, W. T. 2002. A receptor for activated C kinase is part of messenger ribonucleoprotein complexes associated with polyA-mRNAs in neurons. *J Neurosci,* 22**,** 8827-37.

ARNOLD, H. K., ZHANG, X., DANIEL, C. J., TIBBITTS, D., ESCAMILLA-POWERS, J., FARRELL, A., TOKARZ, S., MORGAN, C. & SEARS, R. C. 2009. The Axin1 scaffold protein promotes formation of a degradation complex for c-Myc. *EMBO J,* 28**,** 500-12.

AYACHE, J., BENARD, M., ERNOULT-LANGE, M., MINSHALL, N., STANDART, N., KRESS, M. & WEIL, D. 2015. P-body assembly requires DDX6 repression complexes rather than decay or Ataxin2/2L complexes. *Mol Biol Cell,* 26**,** 2579-95.

AYALA-BRETON, C., ARIAS, M., ESPINOSA, R., ROMERO, P., ARIAS, C. F. & LOPEZ, S. 2009. Analysis of the kinetics of transcription and replication of the rotavirus genome by RNA interference. *J Virol,* 83**,** 8819-31.

BAEJEN, C., TORKLER, P., GRESSEL, S., ESSIG, K., SODING, J. & CRAMER, P. 2014. Transcriptome maps of mRNP biogenesis factors define pre-mRNA recognition. *Mol Cell,* 55**,** 745-57.

BAER, B. W. & KORNBERG, R. D. 1980. Repeating structure of cytoplasmic poly(A)-ribonucleoprotein. *Proc Natl Acad Sci U S A,* 77**,** 1890-2.

BAER, B. W. & KORNBERG, R. D. 1983. The protein responsible for the repeating structure of cytoplasmic poly(A)-ribonucleoprotein. *J Cell Biol,* 96**,** 717-21.

BARONI, T. E., CHITTUR, S. V., GEORGE, A. D. & TENENBAUM, S. A. 2008. Advances in RIP-chip analysis : RNA-binding protein immunoprecipitation-microarray profiling. *Methods Mol Biol,* 419**,** 93-108.

BARTELS, C., XIA, T. H., BILLETER, M., GUNTERT, P. & WUTHRICH, K. 1995. The program XEASY for computer-supported NMR spectral analysis of biological macromolecules. *J Biomol NMR,* 6**,** 1-10.

BAYFIELD, M. A. & MARAIA, R. J. 2009. Precursor-product discrimination by La protein during tRNA metabolism. *Nat Struct & Mol Biol,* 16**,** 430-7.

BAYFIELD, M. A., YANG, R. & MARAIA, R. J. 2010a. Conserved and divergent features of the structure and function of La and La-related proteins (LARPs). *Biochim Biophys Acta*.

BAYFIELD, M. A., YANG, R. & MARAIA, R. J. 2010b. Conserved and divergent features of the structure and function of La and La-related proteins (LARPs). *Biochim Biophys Acta,* 1799**,** 365-78.

BERLANGA, J. J., BAASS, A. & SONENBERG, N. 2006. Regulation of poly(A) binding protein function in translation: Characterization of the Paip2 homolog, Paip2B. *RNA,* 12**,** 1556-68.

BHATTACHARJEE, R. B. & BAG, J. 2012. Depletion of nuclear poly(A) binding protein PABPN1 produces a compensatory response by cytoplasmic PABP4 and PABP5 in cultured human cells. *PLoS One,* 7**,** e53036.

BIOLABS, N. E. 2010. RNase I. http://www.neb.com/nebecomm/products/productM0243.asp.

BLAGDEN, S. P., GATT, M. K., ARCHAMBAULT, V., LADA, K., ICHIHARA, K., LILLEY, K. S., INOUE, Y. H. & GLOVER, D. M. 2009. Drosophila Larp associates with poly(A)-binding protein and is required for male fertility and syncytial embryo development. *Dev Biol*.

BLANCO, P., SARGENT, C. A., BOUCHER, C. A., HOWELL, G., ROSS, M. & AFFARA, N. A. 2001. A novel poly(A)-binding protein gene (PABPC5) maps to an X-specific subinterval in the Xq21.3/Yp11.2 homology block of the human sex chromosomes. *Genomics,* 74**,** 1-11.

BLOBEL, G. 1973. A protein of molecular weight 78,000 bound to the polyadenylate region of eukaryotic messenger RNAs. *Proc Natl Acad Sci U S A,* 70**,** 924-8.

BOUSQUET-ANTONELLI, C. & DERAGON, J. M. 2009. A comprehensive analysis of the La-motif protein superfamily. *RNA,* 15**,** 750-64.

BRASIER, A. R. & RON, D. 1992. Luciferase reporter gene assay in mammalian cells. *Methods Enzymol,* 216**,** 386-97.

BRAUN, J. E., HUNTZINGER, E., FAUSER, M. & IZAURRALDE, E. 2011. GW182 proteins directly recruit cytoplasmic deadenylase complexes to miRNA targets. *Mol Cell,* 44**,** 120-33.

BRAUN, J. E., HUNTZINGER, E. & IZAURRALDE, E. 2012. A molecular link between miRISCs and deadenylases provides new insight into the mechanism of gene silencing by microRNAs. *Cold Spring Harb Perspect Biol,* 4.

BRENET, F., SOCCI, N., SONENBERG, N. & HOLLAND, E. 2009. Akt phosphorylation of La regulates specific mRNA translation in glial progenitors. *Oncogene,* 28. **,** 128-39.

BRENGUES, M. & PARKER, R. 2007. Accumulation of polyadenylated mRNA, Pab1p, eIF4E, and eIF4G with P-bodies in Saccharomyces cerevisiae. *Mol Biol Cell,* 18**,** 2592-602.

BROOK, M., MCCRACKEN, L., REDDINGTON, J. P., LU, Z. L., MORRICE, N. A. & GRAY, N. K. 2012. The multifunctional poly(A)-binding protein (PABP) 1 is subject to extensive dynamic post-translational modification, which molecular modelling suggests plays an important role in co-ordinating its activities. *Biochem J,* 441**,** 803-12.

BUCHAN, J. R. & PARKER, R. 2009. Eukaryotic stress granules: the ins and outs of translation. *Mol Cell,* 36**,** 932-41.

BURGESS, H. M., RICHARDSON, W. A., ANDERSON, R. C., SALAUN, C., GRAHAM, S. V. & GRAY, N. K. 2011. Nuclear relocalisation of cytoplasmic poly(A)-binding proteins PABP1 and PABP4 in response to UV irradiation reveals mRNA-dependent export of metazoan PABPs. *J Cell Sci,* 124**,** 3344-55.

BURROWS, C., LATIP, N. A., LAM, S. J., CARPENTER, L., SAWICKA, K., TZOLOVSKY, G., GABRA, H., BUSHELL, M., GLOVER, D. M., WILLIS, A. E. & BLAGDEN, S. P. 2010. The RNA binding protein Larp1 regulates cell division, apoptosis and cell migration. *Nucleic Acids Res*.

CAI, L., FRITZ, D., STEFANOVIC, L. & STEFANOVIC, B. 2009. Binding of LARP6 to the conserved 5' stem-loop regulates translation of mRNAs encoding type I collagen. *J Mol Biol,* 395**,** 309-26.

CARDINALI, B., CARISSIMI, C., GRAVINA, P. & PIERANDREI-AMALDI, P. 2003. La protein is associated with terminal oligopyrimidine mRNAs in actively translating polysomes. *J Biol Chem,* 278**,** 35145-51.

CHANG, H., LIM, J., HA, M. & KIM, V. N. 2014. TAIL-seq: genome-wide determination of poly(A) tail length and 3' end modifications. *Mol Cell,* 53**,** 1044-52.

CHEKULAEVA, M., MATHYS, H., ZIPPRICH, J. T., ATTIG, J., COLIC, M., PARKER, R. & FILIPOWICZ, W. 2011. miRNA repression involves GW182-mediated recruitment of CCR4-NOT through conserved W-containing motifs. *Nat Struct Mol Biol,* 18**,** 1218-26.

CHEN, C. Y. & SHYU, A. B. 2013. Deadenylation and P-bodies. *Adv Exp Med Biol,* 768**,** 183-95.

COLLER, J. M., GRAY, N. K. & WICKENS, M. P. 1998. mRNA stabilization by poly(A) binding protein is independent of poly(A) and requires translation. *Genes Dev,* 12**,** 3226-35.

COSSON, B., COUTURIER, A., LE GUELLEC, R., MOREAU, J., CHABELSKAYA, S., ZHOURAVLEVA, G. & PHILIPPE, M. 2002. Characterization of the poly(A) binding proteins expressed during oogenesis and early development of Xenopus laevis. *Biol Cell,* 94**,** 217-31.

COUGOT, N., BABAJKO, S. & SERAPHIN, B. 2004. Cytoplasmic foci are sites of mRNA decay in human cells. *J Cell Biol,* 165**,** 31-40.

COYLE, S. M., GILBERT, W. V. & DOUDNA, J. A. 2009. Direct link between RACK1 function and localization at the ribosome in vivo. *Mol Cell Biol,* 29**,** 1626-34.

CRAIG, A. W., HAGHIGHAT, A., YU, A. T. & SONENBERG, N. 1998. Interaction of polyadenylate-binding protein with the eIF4G homologue PAIP enhances translation. *Nature,* 392**,** 520-3.

DE MELO NETO, O. P., STANDART, N. & MARTINS DE SA, C. 1995. Autoregulation of poly(A)-binding protein synthesis in vitro. *Nucleic Acids Res,* 23**,** 2198-205.

DECKER, C. J. & PARKER, R. 2012. P-bodies and stress granules: possible roles in the control of translation and mRNA degradation. *Cold Spring Harb Perspect Biol,* 4**,** a012286.

DECKER, C. J., TEIXEIRA, D. & PARKER, R. 2007. Edc3p and a glutamine/asparagine-rich domain of Lsm4p function in processing body assembly in Saccharomyces cerevisiae. *J Cell Biol,* 179**,** 437-49.

DELAGLIO, F., GRZESIEK, S., VUISTER, G. W., ZHU, G., PFEIFER, J. & BAX, A. 1995. NMRPipe: a multidimensional spectral processing system based on UNIX pipes. *J Biomol NMR,* 6**,** 277-93.

DEO, R. C., BONANNO, J. B., SONENBERG, N. & BURLEY, S. K. 1999. Recognition of polyadenylate RNA by the poly(A)-binding protein. *Cell,* 98**,** 835-45.

DERRY, M. C., YANAGIYA, A., MARTINEAU, Y. & SONENBERG, N. 2006. Regulation of poly(A)-binding protein through PABP-interacting proteins. *Cold Spring Harb Symp Quant Biol,* 71**,** 537-43.

DI TOMMASO, P., MORETTI, S., XENARIOS, I., OROBITG, M., MONTANYOLA, A., CHANG, J. M., TALY, J. F. & NOTREDAME, C. 2011. T-Coffee: a web server for the multiple sequence alignment of protein and RNA sequences using structural information and homology extension. *Nucleic Acids Res,* 39**,** W13-7.

DONG, G., CHAKSHUSMATHI, G., WOLIN, S. L. & REINISCH, K. M. 2004. Structure of the La motif: a winged helix domain mediates RNA binding via a conserved aromatic patch. *EMBO J,* 23**,** 1000-7.

DOWLING, R. J., ZAKIKHANI, M., FANTUS, I. G., POLLAK, M. & SONENBERG, N. 2007. Metformin inhibits mammalian target of rapamycin-dependent translation initiation in breast cancer cells. *Cancer Res,* 67**,** 10804-12.

ELDEN, A. C., KIM, H. J., HART, M. P., CHEN-PLOTKIN, A. S., JOHNSON, B. S., FANG, X., ARMAKOLA, M., GESER, F., GREENE, R., LU, M. M., PADMANABHAN, A., CLAY-FALCONE, D., MCCLUSKEY, L., ELMAN, L., JUHR, D., GRUBER, P. J., RUB, U., AUBURGER, G., TROJANOWSKI, J. Q., LEE, V. M., VAN DEERLIN, V. M., BONINI, N. M. & GITLER, A. D. 2010. Ataxin-2 intermediate-length polyglutamine expansions are associated with increased risk for ALS. *Nature,* 466**,** 1069-75.

EMSLEY, P. & COWTAN, K. 2004. Coot: model-building tools for molecular graphics. *Acta Crystallogr D Biol Crystallogr,* 60**,** 2126-32.

EULALIO, A., BEHM-ANSMANT, I. & IZAURRALDE, E. 2007a. P bodies: at the crossroads of post-transcriptional pathways. *Nat Rev Mol Cell Biol,* 8**,** 9-22.

EULALIO, A., BEHM-ANSMANT, I., SCHWEIZER, D. & IZAURRALDE, E. 2007b. P-body formation is a consequence, not the cause, of RNA-mediated gene silencing. *Mol Cell Biol,* 27**,** 3970-81.

EULALIO, A., HUNTZINGER, E. & IZAURRALDE, E. 2008. GW182 interaction with Argonaute is essential for miRNA-mediated translational repression and mRNA decay. *Nat Struct Mol Biol,* 15**,** 346-53.

EZZEDDINE, N., CHANG, T. C., ZHU, W., YAMASHITA, A., CHEN, C. Y., ZHONG, Z., YAMASHITA, Y., ZHENG, D. & SHYU, A. B. 2007. Human TOB, an antiproliferative transcription factor, is a poly(A)-binding protein-dependent positive regulator of cytoplasmic mRNA deadenylation. *Mol Cell Biol,* 27**,** 7791-801.

EZZEDDINE, N., CHEN, C. Y. & SHYU, A. B. 2012. Evidence providing new insights into TOB-promoted deadenylation and supporting a link between TOB's

deadenylation-enhancing and antiproliferative activities. *Mol Cell Biol,* 32**,** 1089-98.

FABIAN, M. R., CIEPLAK, M. K., FRANK, F., MORITA, M., GREEN, J., SRIKUMAR, T., NAGAR, B., YAMAMOTO, T., RAUGHT, B., DUCHAINE, T. F. & SONENBERG, N. 2011. miRNA-mediated deadenylation is orchestrated by GW182 through two conserved motifs that interact with CCR4-NOT. *Nat Struct Mol Biol,* 18**,** 1211-7.

FABIAN, M. R., MATHONNET, G., SUNDERMEIER, T., MATHYS, H., ZIPPRICH, J. T., SVITKIN, Y. V., RIVAS, F., JINEK, M., WOHLSCHLEGEL, J., DOUDNA, J. A., CHEN, C. Y., SHYU, A. B., YATES, J. R., 3RD, HANNON, G. J., FILIPOWICZ, W., DUCHAINE, T. F. & SONENBERG, N. 2009. Mammalian miRNA RISC recruits CAF1 and PABP to affect PABP-dependent deadenylation. *Mol Cell,* 35**,** 868-80.

FAN, X., ROY, E., ZHU, L., MURPHY, T. C., KOZLOWSKI, M., NANES, M. S. & RUBIN, J. 2003. Nitric oxide donors inhibit luciferase expression in a promoter-independent fashion. *J Biol Chem,* 278**,** 10232-8.

FELDMAN, M. E., APSEL, B., UOTILA, A., LOEWITH, R., KNIGHT, Z. A., RUGGERO, D. & SHOKAT, K. M. 2009. Active-site inhibitors of mTOR target rapamycin-resistant outputs of mTORC1 and mTORC2. *PLoS Biol,* 7**,** e38.

FOIANI, M., CIGAN, A. M., PADDON, C. J., HARASHIMA, S. & HINNEBUSCH, A. G. 1991. GCD2, a translational repressor of the GCN4 gene, has a general function in the initiation of protein synthesis in Saccharomyces cerevisiae. *Mol Cell Biol,* 11**,** 3203-16.

FOURNIER, M. J., COUDERT, L., MELLAOUI, S., ADJIBADE, P., GAREAU, C., COTE, M. F., SONENBERG, N., GAUDREAULT, R. C. & MAZROUI, R. 2013. Inactivation of the mTORC1-eukaryotic translation initiation factor 4E pathway alters stress granule formation. *Mol Cell Biol,* 33**,** 2285-301.

FUNAKOSHI, Y., DOI, Y., HOSODA, N., UCHIDA, N., OSAWA, M., SHIMADA, I., TSUJIMOTO, M., SUZUKI, T., KATADA, T. & HOSHINO, S. 2007. Mechanism of mRNA deadenylation: evidence for a molecular interplay between translation termination factor eRF3 and mRNA deadenylases. *Genes Dev,* 21**,** 3135-48.

GALLOUZI, I. E., PARKER, F., CHEBLI, K., MAURIER, F., LABOURIER, E., BARLAT, I., CAPONY, J. P., TOCQUE, B. & TAZI, J. 1998. A novel phosphorylation-dependent RNase activity of GAP-SH3 binding protein: a potential link between signal transduction and RNA stability. *Mol Cell Biol,* 18**,** 3956-65.

GASTEIGER, E., GATTIKER, A., HOOGLAND, C., IVANYI, I., APPEL, R.D. AND BAIROCH, A. 2005. *In:* WALKER, J. M. (ed.) *The Proteomics Protocols Handbook.* Humana Press.

GIBBINGS, D. J., CIAUDO, C., ERHARDT, M. & VOINNET, O. 2009. Multivesicular bodies associate with components of miRNA effector complexes and modulate miRNA activity. *Nat Cell Biol,* 11**,** 1143-9.

GORGONI, B., RICHARDSON, W. A., BURGESS, H. M., ANDERSON, R. C., WILKIE, G. S., GAUTIER, P., MARTINS, J. P., BROOK, M., SHEETS, M. D. & GRAY, N. K. 2011. Poly(A)-binding proteins are functionally distinct and have essential roles during vertebrate development. *Proc Natl Acad Sci U S A,* 108**,** 7844-9.

GUZELOGLU-KAYISLI, O., PAULI, S., DEMIR, H., LALIOTI, M. D., SAKKAS, D. & SELI, E. 2008. Identification and characterization of human embryonic poly(A) binding protein (EPAB). *Mol Hum Reprod,* 14**,** 581-8.

HANDS-TAYLOR, K. L., MARTINO, L., TATA, R., BABON, J. J., BUI, T. T., DRAKE, A. F., BEAVIL, R. L., PRUIJN, G. J., BROWN, P. R. & CONTE, M. R. 2010. Heterodimerization of the human RNase P/MRP subunits Rpp20 and Rpp25 is a prerequisite for interaction with the P3 arm of RNase MRP RNA. *Nucleic Acids Res,* 38**,** 4052-66.

HARTWELL, L. H. & MCLAUGHLIN, C. S. 1969. A mutant of yeast apparently defective in the initiation of protein synthesis. *Proc Natl Acad Sci U S A,* 62**,** 468-74.

HE, N., JAHCHAN, N. S., HONG, E., QIANG LI, BAYFIELD, M. A., MARAIA, R. J., LUO, K. & ZHOU, Q. 2008. A La-related protein modulates 7SK snRNP integrity to suppress P-TEFb-dependent transcriptional elongation and tumorigenesis. *Mol Cell,* 29**,** 588-599.

HOLCIK, M. & SONENBERG, N. 2005. Translational control in stress and apoptosis. *Nat Rev Mol Cell Biol,* 6**,** 318-27.

HORNSTEIN, E., HAREL, H., LEVY, G. & MEYUHAS, O. 1999. Overexpression of poly(A)-binding protein down-regulates the translation or the abundance of its own mRNA. *FEBS Lett,* 457**,** 209-13.

HOSODA, N., KOBAYASHI, T., UCHIDA, N., FUNAKOSHI, Y., KIKUCHI, Y., HOSHINO, S. & KATADA, T. 2003. Translation termination factor eRF3 mediates mRNA decay through the regulation of deadenylation. *J Biol Chem,* 278**,** 38287-91.

HUANG, K. L., CHADEE, A. B., CHEN, C. Y., ZHANG, Y. & SHYU, A. B. 2013. Phosphorylation at intrinsically disordered regions of PAM2 motif-containing

proteins modulates their interactions with PABPC1 and influences mRNA fate. *RNA,* 19**,** 295-305.

HUANG, Y., BAYFIELD, M. A., INTINE, R. V. & MARAIA, R. J. 2006. Separate RNA-binding surfaces on the multifunctional La protein mediate distinguishable activities in tRNA maturation. *Nat Struct Mol Biol,* 13**,** 611-8.

HUNTZINGER, E., BRAUN, J. E., HEIMSTADT, S., ZEKRI, L. & IZAURRALDE, E. 2010. Two PABPC1-binding sites in GW182 proteins promote miRNA-mediated gene silencing. *EMBO J,* 29**,** 4146-60.

HUNTZINGER, E., KUZUOGLU-OZTURK, D., BRAUN, J. E., EULALIO, A., WOHLBOLD, L. & IZAURRALDE, E. 2013. The interactions of GW182 proteins with PABP and deadenylases are required for both translational repression and degradation of miRNA targets. *Nucleic Acids Res,* 41**,** 978-94.

IMATAKA, H., GRADI, A. & SONENBERG, N. 1998. A newly identified N-terminal amino acid sequence of human eIF4G binds poly(A)-binding protein and functions in poly(A)-dependent translation. *EMBO J,* 17**,** 7480-9.

JACKS, A., BABON, J., KELLY, G., MANOLARIDIS, I., CARY, P. D., CURRY, S. & CONTE, M. R. 2003. Structure of the C-terminal domain of human La protein reveals a novel RNA recognition motif coupled to a helical nuclear retention element. *Structure (Camb),* 11**,** 833-43.

JACOBSON, A. 2005. The end justifies the means. *Nat Struct Mol Biol,* 12**,** 474-5.

JINEK, M., FABIAN, M. R., COYLE, S. M., SONENBERG, N. & DOUDNA, J. A. 2010. Structural insights into the human GW182-PABC interaction in microRNA-mediated deadenylation. *Nat Struct Mol Biol,* 17**,** 238-40.

KAHVEJIAN, A., SVITKIN, Y. V., SUKARIEH, R., M'BOUTCHOU, M. N. & SONENBERG, N. 2005. Mammalian poly(A)-binding protein is a eukaryotic translation initiation factor, which acts via multiple mechanisms. *Genes Dev,* 19**,** 104-13.

KAJÁN, L. & RYCHLEWSKI, L. 2007. Evaluation of 3D-Jury on CASP7 models. Protein Structure Prediction Meta Server, BioInfoBank Institute. http://meta.bioinfo.pl/3djury.pl?meta=v2&id=20292. *BMC Bioinformatics.,* 8**,** 304.

KARIM, M. M., SVITKIN, Y. V., KAHVEJIAN, A., DE CRESCENZO, G., COSTA-MATTIOLI, M. & SONENBERG, N. 2006. A mechanism of translational repression by competition of Paip2 with eIF4G for poly(A) binding protein (PABP) binding. *Proc Natl Acad Sci U S A,* 103**,** 9494-9.

KATO, M., HAN, T. W., XIE, S., SHI, K., DU, X., WU, L. C., MIRZAEI, H., GOLDSMITH, E. J., LONGGOOD, J., PEI, J., GRISHIN, N. V., FRANTZ, D.

E., SCHNEIDER, J. W., CHEN, S., LI, L., SAWAYA, M. R., EISENBERG, D., TYCKO, R. & MCKNIGHT, S. L. 2012. Cell-free formation of RNA granules: low complexity sequence domains form dynamic fibers within hydrogels. *Cell,* 149**,** 753-67.

KATZENELLENBOGEN, R. A., EGELKROUT, E. M., VLIET-GREGG, P., GEWIN, L. C., GAFKEN, P. R. & GALLOWAY, D. A. 2007. NFX1-123 and poly(A) binding proteins synergistically augment activation of telomerase in human papillomavirus type 16 E6-expressing cells. *J Virol,* 81**,** 3786-96.

KATZENELLENBOGEN, R. A., VLIET-GREGG, P., XU, M. & GALLOWAY, D. A. 2010. Cytoplasmic poly(A) binding proteins regulate telomerase activity and cell growth in human papillomavirus type 16 E6-expressing keratinocytes. *J Virol,* 84**,** 12934-44.

KEDERSHA, N., CHO, M. R., LI, W., YACONO, P. W., CHEN, S., GILKS, N., GOLAN, D. E. & ANDERSON, P. 2000. Dynamic shuttling of TIA-1 accompanies the recruitment of mRNA to mammalian stress granules. *J Cell Biol,* 151**,** 1257-68.

KEDERSHA, N., PANAS, M. D., ACHORN, C. A., LYONS, S., TISDALE, S., HICKMAN, T., THOMAS, M., LIEBERMAN, J., MCINERNEY, G. M., IVANOV, P. & ANDERSON, P. 2016. G3BP-Caprin1-USP10 complexes mediate stress granule condensation and associate with 40S subunits. *J Cell Biol,* 212**,** 845-60.

KEDERSHA, N., STOECKLIN, G., AYODELE, M., YACONO, P., LYKKE-ANDERSEN, J., FRITZLER, M. J., SCHEUNER, D., KAUFMAN, R. J., GOLAN, D. E. & ANDERSON, P. 2005. Stress granules and processing bodies are dynamically linked sites of mRNP remodeling. *J Cell Biol,* 169**,** 871-84.

KHALEGHPOUR, K., KAHVEJIAN, A., DE CRESCENZO, G., ROY, G., SVITKIN, Y. V., IMATAKA, H., O'CONNOR-MCCOURT, M. & SONENBERG, N. 2001a. Dual interactions of the translational repressor Paip2 with poly(A) binding protein. *Mol Cell Biol,* 21**,** 5200-13.

KHALEGHPOUR, K., SVITKIN, Y. V., CRAIG, A. W., DEMARIA, C. T., DEO, R. C., BURLEY, S. K. & SONENBERG, N. 2001b. Translational repression by a novel partner of human poly(A) binding protein, Paip2. *Mol Cell,* 7**,** 205-16.

KHOUTORSKY, A., YANAGIYA, A., GKOGKAS, C. G., FABIAN, M. R., PRAGER-KHOUTORSKY, M., CAO, R., GAMACHE, K., BOUTHIETTE, F., PARSYAN, A., SORGE, R. E., MOGIL, J. S., NADER, K., LACAILLE, J. C. & SONENBERG, N. 2013. Control of synaptic plasticity and memory via suppression of poly(A)-binding protein. *Neuron,* 78**,** 298-311.

KIM, H. J., RAPHAEL, A. R., LADOW, E. S., MCGURK, L., WEBER, R. A., TROJANOWSKI, J. Q., LEE, V. M., FINKBEINER, S., GITLER, A. D. &

BONINI, N. M. 2014. Therapeutic modulation of eIF2alpha phosphorylation rescues TDP-43 toxicity in amyotrophic lateral sclerosis disease models. *Nat Genet,* 46**,** 152-60.

KINI, H. K., KONG, J. & LIEBHABER, S. A. 2014. Cytoplasmic poly(A) binding protein C4 serves a critical role in erythroid differentiation. *Mol Cell Biol,* 34**,** 1300-9.

KINI, H. K., SILVERMAN, I. M., JI, X., GREGORY, B. D. & LIEBHABER, S. A. 2016. Cytoplasmic poly(A) binding protein-1 binds to genomically encoded sequences within mammalian mRNAs. *RNA,* 22**,** 61-74.

KLEENE, K. C., MULLIGAN, E., STEIGER, D., DONOHUE, K. & MASTRANGELO, M. A. 1998. The mouse gene encoding the testis-specific isoform of Poly(A) binding protein (Pabp2) is an expressed retroposon: intimations that gene expression in spermatogenic cells facilitates the creation of new genes. *J Mol Evol,* 47**,** 275-81.

KOTIK-KOGAN, O., VALENTINE, E. R., SANFELICE, D., CONTE, M. R. & CURRY, S. 2008. Structural analysis reveals conformational plasticity in the recognition of RNA 3' ends by the human La protein. *Structure,* 16**,** 852-62.

KOZLOV, G., DE CRESCENZO, G., LIM, N. S., SIDDIQUI, N., FANTUS, D., KAHVEJIAN, A., TREMPE, J. F., ELIAS, D., EKIEL, I., SONENBERG, N., O'CONNOR-MCCOURT, M. & GEHRING, K. 2004. Structural basis of ligand recognition by PABC, a highly specific peptide-binding domain found in poly(A)-binding protein and a HECT ubiquitin ligase. *EMBO J,* 23**,** 272-81.

KOZLOV, G. & GEHRING, K. 2010. Molecular basis of eRF3 recognition by the MLLE domain of poly(A)-binding protein. *PLoS One,* 5**,** e10169.

KOZLOV, G., MENADE, M., ROSENAUER, A., NGUYEN, L. & GEHRING, K. 2010a. Molecular determinants of PAM2 recognition by the MLLE domain of poly(A)-binding protein. *J Mol Biol,* 397**,** 397-407.

KOZLOV, G., SAFAEE, N., ROSENAUER, A. & GEHRING, K. 2010b. Structural basis of binding of P-body-associated proteins GW182 and ataxin-2 by the Mlle domain of poly(A)-binding protein. *J Biol Chem,* 285**,** 13599-606.

KOZLOV, G., SIDDIQUI, N., COILLET-MATILLON, S., TREMPE, J. F., EKIEL, I., SPRULES, T. & GEHRING, K. 2002. Solution structure of the orphan PABC domain from Saccharomyces cerevisiae poly(A)-binding protein. *J Biol Chem,* 277**,** 22822-8.

KOZLOV, G., TREMPE, J. F., KHALEGHPOUR, K., KAHVEJIAN, A., EKIEL, I. & GEHRING, K. 2001. Structure and function of the C-terminal PABC domain of human poly(A)-binding protein. *Proc Natl Acad Sci U S A,* 98**,** 4409-13.

KRESS, T. R., SABO, A. & AMATI, B. 2015. MYC: connecting selective transcriptional control to global RNA production. *Nat Rev Cancer,* 15**,** 593-607.

KUHN, U. & WAHLE, E. 2004. Structure and function of poly(A) binding proteins. *Biochim Biophys Acta,* 1678**,** 67-84.

LANDTHALER, M., GAIDATZIS, D., ROTHBALLER, A., CHEN, P. Y., SOLL, S. J., DINIC, L., OJO, T., HAFNER, M., ZAVOLAN, M. & TUSCHL, T. 2008. Molecular characterization of human Argonaute-containing ribonucleoprotein complexes and their bound target mRNAs. *RNA,* 14**,** 2580-96.

LEE, S. H., OH, J., PARK, J., PAEK, K. Y., RHO, S., JANG, S. K. & LEE, J. B. 2014. Poly(A) RNA and Paip2 act as allosteric regulators of poly(A)-binding protein. *Nucleic Acids Res,* 42**,** 2697-707.

LEE, T., LI, Y. R., CHESI, A., HART, M. P., RAMOS, D., JETHAVA, N., HOSANGADI, D., EPSTEIN, J., HODGES, B., BONINI, N. M. & GITLER, A. D. 2011. Evaluating the prevalence of polyglutamine repeat expansions in amyotrophic lateral sclerosis. *Neurology,* 76**,** 2062-5.

LEE, Y. S., PRESSMAN, S., ANDRESS, A. P., KIM, K., WHITE, J. L., CASSIDY, J. J., LI, X., LUBELL, K., LIM DO, H., CHO, I. S., NAKAHARA, K., PREALL, J. B., BELLARE, P., SONTHEIMER, E. J. & CARTHEW, R. W. 2009. Silencing by small RNAs is linked to endosomal trafficking. *Nat Cell Biol,* 11**,** 1150-6.

LESSING, D. & BONINI, N. M. 2008. Polyglutamine genes interact to modulate the severity and progression of neurodegeneration in Drosophila. *PLoS Biol,* 6**,** e29.

LIBERZON, A., BIRGER, C., THORVALDSDOTTIR, H., GHANDI, M., MESIROV, J. P. & TAMAYO, P. 2015. The Molecular Signatures Database (MSigDB) hallmark gene set collection. *Cell Syst,* 1**,** 417-425.

LIM, C. & ALLADA, R. 2013. ATAXIN-2 activates PERIOD translation to sustain circadian rhythms in Drosophila. *Science,* 340**,** 875-9.

LIM, N. S., KOZLOV, G., CHANG, T. C., GROOVER, O., SIDDIQUI, N., VOLPON, L., DE CRESCENZO, G., SHYU, A. B. & GEHRING, K. 2006. Comparative peptide binding studies of the PABC domains from the ubiquitin-protein isopeptide ligase HYD and poly(A)-binding protein. Implications for HYD function. *J Biol Chem,* 281**,** 14376-82.

LIU, J., RIVAS, F. V., WOHLSCHLEGEL, J., YATES, J. R., 3RD, PARKER, R. & HANNON, G. J. 2005a. A role for the P-body component GW182 in microRNA function. *Nat Cell Biol,* 7**,** 1261-6.

LIU, J., VALENCIA-SANCHEZ, M. A., HANNON, G. J. & PARKER, R. 2005b. MicroRNA-dependent localization of targeted mRNAs to mammalian P-bodies. *Nat Cell Biol,* 7**,** 719-23.

LONG, K. S., CEDERVALL, T., WALCH-SOLIMENA, C., NOE, D. A., HUDDLESTON, M. J., ANNAN, R. S. & WOLIN, S. L. 2001. Phosphorylation of the Saccharomyces cerevisiae La protein does not appear to be required for its functions in tRNA maturation and nascent RNA stabilization. *RNA,* 7**,** 1589-602.

LOWELL, J. E., RUDNER, D. Z. & SACHS, A. B. 1992. 3'-UTR-dependent deadenylation by the yeast poly(A) nuclease. *Genes Dev,* 6**,** 2088-99.

MALI, P., YANG, L., ESVELT, K. M., AACH, J., GUELL, M., DICARLO, J. E., NORVILLE, J. E. & CHURCH, G. M. 2013. RNA-guided human genome engineering via Cas9. *Science,* 339**,** 823-6.

MANGUS, D. A., AMRANI, N. & JACOBSON, A. 1998. Pbp1p, a factor interacting with Saccharomyces cerevisiae poly(A)-binding protein, regulates polyadenylation. *Mol Cell Biol,* 18**,** 7383-96.

MANGUS, D. A., EVANS, M. C. & JACOBSON, A. 2003. Poly(A)-binding proteins: multifunctional scaffolds for the post-transcriptional control of gene expression. *Genome Biol,* 4**,** 223.

MARAIA, R. J. & BAYFIELD, M. A. 2006. The La protein-RNA complex surfaces [review]. *Mol Cell,* 21**,** 149-152.

MARKERT, A., GRIMM, M., MARTINEZ, J., WIESNER, J., MEYERHANS, A., MEYUHAS, O., SICKMANN, A. & FISCHER, U. 2008. The La-related protein LARP7 is a component of the 7SK ribonucleoprotein and affects transcription of cellular and viral polymerase II genes. *EMBO Rep,* 9**,** 569-75.

MARTINEAU, Y., DERRY, M. C., WANG, X., YANAGIYA, A., BERLANGA, J. J., SHYU, A. B., IMATAKA, H., GEHRING, K. & SONENBERG, N. 2008a. The poly(A)-binding protein-interacting protein 1 binds to eIF3 to stimulate translation. *Mol Cell Biol,* 28**,** 6658-67.

MARTINEAU, Y., DERRY, M. C., WANG, X., YANAGIYA, A., BERLANGA, J. J., SHYU, A. B., IMATAKA, H., GEHRING, K. & SONENBERG, N. 2008b. Poly(A)-binding protein-interacting protein 1 binds to eukaryotic translation initiation factor 3 to stimulate translation. *Mol Cell Biol,* 28**,** 6658-67.

MARTINEAU, Y., WANG, X., ALAIN, T., PETROULAKIS, E., SHAHBAZIAN, D., FABRE, B., BOUSQUET-DUBOUCH, M. P., MONSARRAT, B., PYRONNET, S. & SONENBERG, N. 2014. Control of Paip1-eukayrotic translation initiation factor 3 interaction by amino acids through S6 kinase. *Mol Cell Biol,* 34**,** 1046-53.

MAUXION, F., CHEN, C. Y., SERAPHIN, B. & SHYU, A. B. 2009. BTG/TOB factors impact deadenylases. *Trends Biochem Sci,* 34**,** 640-7.

MCCANN, C., HOLOHAN, E. E., DAS, S., DERVAN, A., LARKIN, A., LEE, J. A., RODRIGUES, V., PARKER, R. & RAMASWAMI, M. 2011. The Ataxin-2

protein is required for microRNA function and synapse-specific long-term olfactory habituation. *Proc Natl Acad Sci U S A,* 108**,** E655-62.

MCKINNEY, C., YU, D. & MOHR, I. 2013. A new role for the cellular PABP repressor Paip2 as an innate restriction factor capable of limiting productive cytomegalovirus replication. *Genes Dev,* 27**,** 1809-20.

MELO, E. O., DHALIA, R., MARTINS DE SA, C., STANDART, N. & DE MELO NETO, O. P. 2003. Identification of a C-terminal poly(A)-binding protein (PABP)-PABP interaction domain: role in cooperative binding to poly (A) and efficient cap distal translational repression. *J Biol Chem,* 278**,** 46357-68.

MERRET, R., MARTINO, L., BOUSQUET-ANTONELLI, C., FNEICH, S., DESCOMBIN, J., BILLEY, E., CONTE, M. R. & DERAGON, J. M. 2013. The association of a La module with the PABP-interacting motif PAM2 is a recurrent evolutionary process that led to the neofunctionalization of La-related proteins. *RNA,* 19**,** 36-50.

MOLLET, S., COUGOT, N., WILCZYNSKA, A., DAUTRY, F., KRESS, M., BERTRAND, E. & WEIL, D. 2008. Translationally repressed mRNA transiently cycles through stress granules during stress. *Mol Biol Cell,* 19**,** 4469-79.

MOOTHA, V. K., LINDGREN, C. M., ERIKSSON, K. F., SUBRAMANIAN, A., SIHAG, S., LEHAR, J., PUIGSERVER, P., CARLSSON, E., RIDDERSTRALE, M., LAURILA, E., HOUSTIS, N., DALY, M. J., PATTERSON, N., MESIROV, J. P., GOLUB, T. R., TAMAYO, P., SPIEGELMAN, B., LANDER, E. S., HIRSCHHORN, J. N., ALTSHULER, D. & GROOP, L. C. 2003. PGC-1alpha-responsive genes involved in oxidative phosphorylation are coordinately downregulated in human diabetes. *Nat Genet,* 34**,** 267-73.

MORETTI, F., KAISER, C., ZDANOWICZ-SPECHT, A. & HENTZE, M. W. 2012. PABP and the poly(A) tail augment microRNA repression by facilitated miRISC binding. *Nat Struct Mol Biol,* 19**,** 603-8.

MURSHUDOV, G. N., VAGIN, A. A., LEBEDEV, A., WILSON, K. S. & DODSON, E. J. 1999. Efficient anisotropic refinement of macromolecular structures using FFT. *Acta Crystallographica Section D-Biological Crystallography,* 55**,** 247-255.

NILSSON, J., SENGUPTA, J., FRANK, J. & NISSEN, P. 2004. Regulation of eukaryotic translation by the RACK1 protein: a platform for signalling molecules on the ribosome. *EMBO Rep,* 5**,** 1137-41.

NYKAMP, K., LEE, M. H. & KIMBLE, J. 2008. C. elegans La-related protein, LARP-1, localizes to germline P bodies and attenuates Ras-MAPK signaling during oogenesis. *RNA,* 14**,** 1378-89.

OSAWA, M., HOSODA, N., NAKANISHI, T., UCHIDA, N., KIMURA, T., IMAI, S., MACHIYAMA, A., KATADA, T., HOSHINO, S. & SHIMADA, I. 2012.

Biological role of the two overlapping poly(A)-binding protein interacting motifs 2 (PAM2) of eukaryotic releasing factor eRF3 in mRNA decay. *RNA,* 18**,** 1957-67.

OTWINOWSKI, Z. & MINOR, W. 1997. "Processing of X-ray diffraction data collected in oscillation mode.". *Methods Enzymol.*

PAGE, R. D. 1996. TreeView: an application to display phylogenetic trees on personal computers. *Comput Appl Biosci,* 12**,** 357-8.

PILLAI, R. S., BHATTACHARYYA, S. N., ARTUS, C. G., ZOLLER, T., COUGOT, N., BASYUK, E., BERTRAND, E. & FILIPOWICZ, W. 2005. Inhibition of translational initiation by Let-7 MicroRNA in human cells. *Science,* 309**,** 1573-6.

PLAISIER, S. B., TASCHEREAU, R., WONG, J. A. & GRAEBER, T. G. 2010. Rank-rank hypergeometric overlap: identification of statistically significant overlap between gene-expression signatures. *Nucleic Acids Res,* 38**,** e169.

RAMASWAMI, M., TAYLOR, J. P. & PARKER, R. 2013. Altered ribostasis: RNA-protein granules in degenerative disorders. *Cell,* 154**,** 727-36.

READ, R. J. 2001. Pushing the boundaries of molecular replacement with maximum likelihood. *Acta Crystallogr D Biol Crystallogr,* 57**,** 1373-82.

REIJNS, M. A., ALEXANDER, R. D., SPILLER, M. P. & BEGGS, J. D. 2008. A role for Q/N-rich aggregation-prone regions in P-body localization. *J Cell Sci,* 121**,** 2463-72.

RICHARDSON, R., DENIS, C. L., ZHANG, C., NIELSEN, M. E., CHIANG, Y. C., KIERKEGAARD, M., WANG, X., LEE, D. J., ANDERSEN, J. S. & YAO, G. 2012. Mass spectrometric identification of proteins that interact through specific domains of the poly(A) binding protein. *Mol Genet Genomics,* 287**,** 711-30.

RIVERA, C. I. & LLOYD, R. E. 2008. Modulation of enteroviral proteinase cleavage of poly(A)-binding protein (PABP) by conformation and PABP-associated factors. *Virology,* 375**,** 59-72.

ROBINSON, M. D., MCCARTHY, D. J. & SMYTH, G. K. 2010. edgeR: a Bioconductor package for differential expression analysis of digital gene expression data. *Bioinformatics,* 26**,** 139-40.

ROY, G., DE CRESCENZO, G., KHALEGHPOUR, K., KAHVEJIAN, A., O'CONNOR-MCCOURT, M. & SONENBERG, N. 2002. Paip1 interacts with poly(A) binding protein through two independent binding motifs. *Mol Cell Biol,* 22**,** 3769-82.

RUAN, L., OSAWA, M., HOSODA, N., IMAI, S., MACHIYAMA, A., KATADA, T., HOSHINO, S. & SHIMADA, I. 2010. Quantitative characterization of Tob

interactions provides the thermodynamic basis for translation termination-coupled deadenylase regulation. *J Biol Chem,* 285**,** 27624-31.

RYBAK, A., FUCHS, H., HADIAN, K., SMIRNOVA, L., WULCZYN, E. A., MICHEL, G., NITSCH, R., KRAPPMANN, D. & WULCZYN, F. G. 2009. The let-7 target gene mouse lin-41 is a stem cell specific E3 ubiquitin ligase for the miRNA pathway protein Ago2. *Nat Cell Biol,* 11**,** 1411-20.

S. E. HARDING, D. B. S., V. A. BLOOMFIELD 1992. *Light Scattering in Biochemistry*, The Royal Society of London.

SAFAEE, N., KOZLOV, G., NORONHA, A. M., XIE, J., WILDS, C. J. & GEHRING, K. 2012. Interdomain allostery promotes assembly of the poly(A) mRNA complex with PABP and eIF4G. *Mol Cell,* 48**,** 375-86.

SANTALUCIA, J., JR., ALLAWI, H. T. & SENEVIRATNE, P. A. 1996. Improved nearest-neighbor parameters for predicting DNA duplex stability. *Biochemistry,* 35**,** 3555-62.

SCHAFFLER, K., SCHULZ, K., HIRMER, A., WIESNER, J., GRIMM, M., SICKMANN, A. & FISCHER, U. 2010. A stimulatory role for the La-related protein 4B in translation. *RNA,* 16**,** 1488-99.

SELI, E., LALIOTI, M. D., FLAHERTY, S. M., SAKKAS, D., TERZI, N. & STEITZ, J. A. 2005. An embryonic poly(A)-binding protein (ePAB) is expressed in mouse oocytes and early preimplantation embryos. *Proc Natl Acad Sci U S A,* 102**,** 367-72.

SERMAN, A., LE ROY, F., AIGUEPERSE, C., KRESS, M., DAUTRY, F. & WEIL, D. 2007. GW body disassembly triggered by siRNAs independently of their silencing activity. *Nucleic Acids Res,* 35**,** 4715-27.

SHAHBAZIAN, D., ROUX, P. P., MIEULET, V., COHEN, M. S., RAUGHT, B., TAUNTON, J., HERSHEY, J. W., BLENIS, J., PENDE, M. & SONENBERG, N. 2006. The mTOR/PI3K and MAPK pathways converge on eIF4B to control its phosphorylation and activity. *Embo J,* 25**,** 2781-91.

SHIFERA, A. S. & HARDIN, J. A. 2010. Factors modulating expression of Renilla luciferase from control plasmids used in luciferase reporter gene assays. *Anal Biochem,* 396**,** 167-72.

SIDDIQUI, N., MANGUS, D. A., CHANG, T. C., PALERMINO, J. M., SHYU, A. B. & GEHRING, K. 2007. Poly(A) nuclease interacts with the C-terminal domain of polyadenylate-binding protein domain from poly(A)-binding protein. *J Biol Chem,* 282**,** 25067-75.

SIMON, E. & SERAPHIN, B. 2007. A specific role for the C-terminal region of the Poly(A)-binding protein in mRNA decay. *Nucleic Acids Res,* 35**,** 6017-28.

SLADIC, R. T., LAGNADO, C. A., BAGLEY, C. J. & GOODALL, G. J. 2004. Human PABP binds AU-rich RNA via RNA-binding domains 3 and 4. *Eur J Biochem,* 271**,** 450-7.

SMITH, R. W. & GRAY, N. K. 2010. Poly(A)-binding protein (PABP): a common viral target. *Biochem J,* 426**,** 1-12.

SONCINI, C., BERDO, I. & DRAETTA, G. 2001. Ras-GAP SH3 domain binding protein (G3BP) is a modulator of USP10, a novel human ubiquitin specific protease. *Oncogene,* 20**,** 3869-79.

SONENBERG, N. & HINNEBUSCH, A. G. 2009. Regulation of translation initiation in eukaryotes: mechanisms and biological targets. *Cell,* 136**,** 731-45.

SORRENTINO, S. 1998. Human extracellular ribonucleases: multiplicity, molecular diversity and catalytic properties of the major RNase types. *Cell Mol Life Sci,* 54**,** 785-94.

SOUQUERE, S., MOLLET, S., KRESS, M., DAUTRY, F., PIERRON, G. & WEIL, D. 2009. Unravelling the ultrastructure of stress granules and associated P-bodies in human cells. *J Cell Sci,* 122**,** 3619-26.

STEFANO, J. E. 1984. Purified lupus antigen La recognizes an oligouridylate stretch common to the 3' termini of RNA polymerase III transcripts. *Cell,* 36**,** 145-154.

STOECKLIN, G. & KEDERSHA, N. 2013. Relationship of GW/P-bodies with stress granules. *Adv Exp Med Biol,* 768**,** 197-211.

SUBRAMANIAN, A., TAMAYO, P., MOOTHA, V. K., MUKHERJEE, S., EBERT, B. L., GILLETTE, M. A., PAULOVICH, A., POMEROY, S. L., GOLUB, T. R., LANDER, E. S. & MESIROV, J. P. 2005. Gene set enrichment analysis: a knowledge-based approach for interpreting genome-wide expression profiles. *Proc Natl Acad Sci U S A,* 102**,** 15545-50.

SUBTELNY, A. O., EICHHORN, S. W., CHEN, G. R., SIVE, H. & BARTEL, D. P. 2014. Poly(A)-tail profiling reveals an embryonic switch in translational control. *Nature,* 508**,** 66-71.

SVITKIN, Y. V., EVDOKIMOVA, V. M., BRASEY, A., PESTOVA, T. V., FANTUS, D., YANAGIYA, A., IMATAKA, H., SKABKIN, M. A., OVCHINNIKOV, L. P., MERRICK, W. C. & SONENBERG, N. 2009. General RNA-binding proteins have a function in poly(A)-binding protein-dependent translation. *EMBO J,* 28**,** 58-68.

SVITKIN, Y. V., OVCHINNIKOV, L. P., DREYFUSS, G. & SONENBERG, N. 1996. General RNA binding proteins render translation cap dependent. *EMBO J,* 15**,** 7147-7155.

SVITKIN, Y. V., PAUSE, A. & SONENBERG, N. 1994. La autoantigen alleviates translational repression by the 5' leader sequence of the human immunodeficiency virus type 1 mRNA. *J. Virol.,* 68**,** 7001-7007.

TAYLOR, D., UNBEHAUN, A., LI, W., DAS, S., LEI, J., LIAO, H. Y., GRASSUCCI, R. A., PESTOVA, T. V. & FRANK, J. 2012. Cryo-EM structure of the mammalian eukaryotic release factor eRF1-eRF3-associated termination complex. *Proc Natl Acad Sci U S A,* 109**,** 18413-8.

TEIXEIRA, D., SHETH, U., VALENCIA-SANCHEZ, M. A., BRENGUES, M. & PARKER, R. 2005. Processing bodies require RNA for assembly and contain nontranslating mRNAs. *RNA,* 11**,** 371-82.

TEPLOVA, M., YUAN, Y.-R., ILIN, S., MALININA, L., PHAN, A. T., TEPLOV, A. & PATEL, D. J. 2006. Structural basis for recognition and sequestration of UUU-OH 3'-termini of nascent RNA pol III transcripts by La, a rheumatic disease autoantigen. *Mol Cell,* 21**,** 75-85.

TERNS, M. P., LUND, E. & DAHLBERG, J. E. 1992. 3'-end-dependent formation of U6 small nuclear ribonucleoprotein particles in *Xenopus laevis* oocyte nuclei. *Mol. Cell. Biol.,* 12**,** 3032-3040.

THOMPSON, J. D., HIGGINS, D. G. & GIBSON, T. J. 1994. CLUSTAL W: improving the sensitivity of progressive multiple sequence alignment through sequence weighting, position-specific gap penalties and weight matrix choice. *Nucleic Acids Res,* 22**,** 4673-80.

TOURRIERE, H., CHEBLI, K., ZEKRI, L., COURSELAUD, B., BLANCHARD, J. M., BERTRAND, E. & TAZI, J. 2003. The RasGAP-associated endoribonuclease G3BP assembles stress granules. *J Cell Biol,* 160**,** 823-31.

TRAPNELL, C., PACHTER, L. & SALZBERG, S. L. 2009. TopHat: discovering splice junctions with RNA-Seq. *Bioinformatics,* 25**,** 1105-11.

TRAPNELL, C., ROBERTS, A., GOFF, L., PERTEA, G., KIM, D., KELLEY, D. R., PIMENTEL, H., SALZBERG, S. L., RINN, J. L. & PACHTER, L. 2012. Differential gene and transcript expression analysis of RNA-seq experiments with TopHat and Cufflinks. *Nat Protoc,* 7**,** 562-78.

TRITSCHLER, F., BRAUN, J. E., MOTZ, C., IGREJA, C., HAAS, G., TRUFFAULT, V., IZAURRALDE, E. & WEICHENRIEDER, O. 2009. DCP1 forms asymmetric trimers to assemble into active mRNA decapping complexes in metazoa. *Proc Natl Acad Sci U S A,* 106**,** 21591-6.

TRITSCHLER, F., HUNTZINGER, E. & IZAURRALDE, E. 2010. Role of GW182 proteins and PABPC1 in the miRNA pathway: a sense of deja vu. *Nat Rev Mol Cell Biol,* 11**,** 379-84.

TSUKAHARA, F., URAKAWA, I., HATTORI, M., HIRAI, M., OHBA, K., YOSHIOKA, T., SAKAKI, Y. & MURAKI, T. 1998. Molecular characterization of the mouse mtprd gene, a homologue of human TPRD: unique gene expression suggesting its critical role in the pathophysiology of Down syndrome. *J Biochem,* 123**,** 1055-63.

TUCKER, M., STAPLES, R. R., VALENCIA-SANCHEZ, M. A., MUHLRAD, D. & PARKER, R. 2002. Ccr4p is the catalytic subunit of a Ccr4p/Pop2p/Notp mRNA deadenylase complex in Saccharomyces cerevisiae. *EMBO J,* 21**,** 1427-36.

UCHIDA, N., HOSHINO, S., IMATAKA, H., SONENBERG, N. & KATADA, T. 2002. A novel role of the mammalian GSPT/eRF3 associating with poly(A)-binding protein in Cap/Poly(A)-dependent translation. *J Biol Chem,* 277**,** 50286-92.

VAN DAMME, P., VELDINK, J. H., VAN BLITTERSWIJK, M., CORVELEYN, A., VAN VUGHT, P. W., THIJS, V., DUBOIS, B., MATTHIJS, G., VAN DEN BERG, L. H. & ROBBERECHT, W. 2011. Expanded ATXN2 CAG repeat size in ALS identifies genetic overlap between ALS and SCA2. *Neurology,* 76**,** 2066-72.

VASUDEVAN, S., SELI, E. & STEITZ, J. A. 2006. Metazoan oocyte and early embryo development program: a progression through translation regulatory cascades. *Genes Dev,* 20**,** 138-46.

VOELTZ, G. K., ONGKASUWAN, J., STANDART, N. & STEITZ, J. A. 2001. A novel embryonic poly(A) binding protein, ePAB, regulates mRNA deadenylation in Xenopus egg extracts. *Genes Dev,* 15**,** 774-88.

W. BURCHARD, M. S., AND W. H.STOCKMAYER 1980. Information on Polydispersity and Branching from Combined Quasi-Elastic and Integrated Scattering. *Macromolecules,* 13**,** 1265-1272.

WALTERS, R. W., BRADRICK, S. S. & GROMEIER, M. 2010. Poly(A)-binding protein modulates mRNA susceptibility to cap-dependent miRNA-mediated repression. *RNA,* 16**,** 239-50.

WINN, M. D., MURSHUDOV, G. N. & PAPIZ, M. Z. 2003. Macromolecular TLS refinement in REFMAC at moderate resolutions. *Macromolecular Crystallography, Pt D,* 374**,** 300-321.

WU, J. & BAG, J. 1998. Negative control of the poly(A)-binding protein mRNA translation is mediated by the adenine-rich region of its 5'-untranslated region. *J Biol Chem,* 273**,** 34535-42.

XIE, J., KOZLOV, G. & GEHRING, K. 2014. The "tale" of poly(A) binding protein: the MLLE domain and PAM2-containing proteins. *Biochim Biophys Acta,* 1839**,** 1062-8.

YAMASHITA, A., CHANG, T. C., YAMASHITA, Y., ZHU, W., ZHONG, Z., CHEN, C. Y. & SHYU, A. B. 2005. Concerted action of poly(A) nucleases and decapping enzyme in mammalian mRNA turnover. *Nat Struct Mol Biol,* 12**,** 1054-63.

YANAGIYA, A., DELBES, G., SVITKIN, Y. V., ROBAIRE, B. & SONENBERG, N. 2010. The poly(A)-binding protein partner Paip2a controls translation during late spermiogenesis in mice. *J Clin Invest,* 120**,** 3389-400.

YANG, H., DUCKETT, C. S. & LINDSTEN, T. 1995. iPABP, an inducible poly(A)-binding protein detected in activated human T cells. *Mol Cell Biol,* 15**,** 6770-6.

YANG, R., GAIDAMAKOV, S. A., XIE, J., LEE, J., MARTINO, L., KOZLOV, G., CRAWFORD, A. K., RUSSO, A. N., CONTE, M. R., GEHRING, K. & MARAIA, R. J. 2011. La-related protein 4 binds poly(A), interacts with the poly(A)-binding protein MLLE domain via a variant PAM2w motif, and can promote mRNA stability. *Mol Cell Biol,* 31**,** 542-56.

YOO, C. J. & WOLIN, S. L. 1994. La proteins from *Drosophila melanogaster* and *Saccharomyces cerevisiae*: a yeast homolog of the La autoantigen is dispensable for growth. *Mol. Cell Biol.,* 14**,** 5412-5424.

YOSHIDA, M., YOSHIDA, K., KOZLOV, G., LIM, N. S., DE CRESCENZO, G., PANG, Z., BERLANGA, J. J., KAHVEJIAN, A., GEHRING, K., WING, S. S. & SONENBERG, N. 2006. Poly(A) binding protein (PABP) homeostasis is mediated by the stability of its inhibitor, Paip2. *EMBO J,* 25**,** 1934-44.

YOSHIKAWA, T., WU, J., OTSUKA, M., KISHIKAWA, T., OHNO, M., SHIBATA, C., TAKATA, A., HAN, F., KANG, Y. J., CHEN, C. Y., SHYU, A. B., HAN, J. & KOIKE, K. 2015. ROCK inhibition enhances microRNA function by promoting deadenylation of targeted mRNAs via increasing PAIP2 expression. *Nucleic Acids Res,* 43**,** 7577-89.

YSLA, R. M., WILSON, G. M. & BREWER, G. 2008. Chapter 3. Assays of adenylate uridylate-rich element-mediated mRNA decay in cells. *Methods Enzymol,* 449**,** 47-71.

YU, J. H., YANG, W. H., GULICK, T., BLOCH, K. D. & BLOCH, D. B. 2005. Ge-1 is a central component of the mammalian cytoplasmic mRNA processing body. *RNA,* 11**,** 1795-802.

ZEKRI, L., KUZUOGLU-OZTURK, D. & IZAURRALDE, E. 2013. GW182 proteins cause PABP dissociation from silenced miRNA targets in the absence of deadenylation. *EMBO J,* 32**,** 1052-65.

ZHANG, Y., LING, J., YUAN, C., DUBRUILLE, R. & EMERY, P. 2013. A role for Drosophila ATX2 in activation of PER translation and circadian behavior. *Science,* 340**,** 879-82.

ZHENG, D., EZZEDDINE, N., CHEN, C. Y., ZHU, W., HE, X. & SHYU, A. B. 2008. Deadenylation is prerequisite for P-body formation and mRNA decay in mammalian cells. *J Cell Biol,* 182**,** 89-101.